

CHARACTERIZATION OF BAX PORE FORMATION

**CHARACTERIZATION OF BAX PORE FORMATION
USING FLUORESCENCE METHODS**

By

JONATHAN LOVELL, BAsC

A Thesis

Submitted to the School of Graduate Studies

in Partial Fulfilment of the Requirements for the Degree

Master of Science

McMaster University

© Copyright by Jonathan Lovell, July 2007

MASTER OF SCIENCE (2007)
(Biochemistry and Biomedical Sciences)

McMaster University
Hamilton, Ontario

TITLE: Characterization of Bax Pore Formation Using Fluorescence Techniques

AUTHOR: Jonathan Franklin Lovell, B.A.Sc. (University of Waterloo)

SUPERVISOR: Professor D.W. Andrews

NUMBER OF PAGES: xiii, 136

Abstract

Bax is a pro-apoptotic protein believed to permeabilize mitochondria during apoptosis. The mechanism Bax uses is not well understood. In this work, we use fluorescence techniques to shed light on how tBid activates Bax and we examine the topology of the pore-forming domain of Bax.

The manner in which tBid promotes apoptosis via Bax activation is not known. Study of tBid and Bax interaction using a new FRET pair showed that the proteins only interacted in the presence of membranes. The Bax pore was shown to have a variable size distribution. A fluorescence technique of simultaneously measuring pore formation, Bax insertion and FRET showed that tBid interaction with Bax occurred before all the Bax inserted or formed pores in the liposomes. A chronological order is proposed for Bax pore formation. tBid first binds to liposomes. tBid proceeds to interact with Bax, and Bax inserts into the membrane. After insertion, Bax oligomerizes and forms small pores. More Bax is recruited and the pores become larger.

The two central hairpin helices of Bax, helices 5 and 6, are known as the pore-forming domain. We used cysteine scanning with the environment sensitive fluorophore NBD to gain insight into the topology of these helices. Fluorescence intensity changes and emission blue shifts showed that residues in these helices undergo conformational reorganization during pore formation. In the activated oligomeric conformation, fluorescence lifetimes showed that helix 5 was more inaccessible to water than helix 6. Cobalt, a cationic NBD quencher, effectively quenched residues in the pore-forming

domain, consistent with a pore that is lined with anionic lipid head groups. Quenching with nitroxide groups at various lipid depths showed that residues on helix 6 were most quenched by a shallow quencher, while residues on helix 5 were quenched by deeper quenchers. Compared to beta sheet pore-forming proteins, the data obtained suggests that Bax and possibly other alpha helical pore-forming proteins form a lipidic pore in a dynamic environment. Combined together, the data suggest a model for Bax in which helix 5 spans the bilayer, and helix 6 is buried just below the lipid headgroups of a toroidal pore.

Acknowledgements

Thanks to everybody who made this research possible, especially my supervisor, Dr. David Andrews. I am inspired by the ingenious explorers who have blazed the trail and the smiling souls who remind others about the joy of life.

Table of Contents

1	Introduction.....	1
1.1	Apoptosis	1
1.2	The Bcl-2 family.....	4
1.3	Pore formation by Bax.....	12
1.4	Other pore-forming proteins.....	17
1.5	Investigations presented in this thesis	21
2	Materials and methods	23
2.1	General materials and methods.....	23
2.2	Cloning of Bax single cysteine mutants	23
2.3	Cloning of Bid G94E.....	28
2.4	Bax purification and labeling	28
2.5	tBid purification and labeling.....	31
2.6	Liposome preparation	33
2.7	Determining suitable wavelengths for the ANTS / DPX assay.....	34
2.8	Bax and tBid functional assay	34
2.9	Pore size assay	36

2.10	Bax-NBD steady state measurements and CL2B and CHAPS gel filtration	38
2.11	Calculation of Forster distance for DACM and IANBD	40
2.12	tBid to Bax FRET and Bax to Bax FRET	41
2.13	3 fluorophore simultaneous analysis	42
2.14	Blueshift and fluorescence increase assays	43
2.15	Lifetime assays	44
2.16	Quenching Analysis.....	45
3	Results.....	48
3.1	Cloning, protein purification and labeling.....	48
3.2	Functional assay	54
3.3	A novel pore sizing assay	59
3.4	Bax pore size is not homogeneous	60
3.5	Behaviour of NBD-labeled Bax	62
3.6	DACM and IANBD FRET pair.....	64
3.7	tBid-Bax and Bax-Bax interactions only occur in the presence of liposomes. ..	65
3.8	Ordering of pore formation steps using a 3 fluorophore simultaneous assay	68
3.9	Conformational change of Bax may be monitored with NBD fluorescence.....	74
3.10	Lifetimes show three populations and subtle lifetime changes	78
3.11	Quenching reveals dynamic lipid interaction and suggests membrane	

topology	81
3.12 Doxyl quenching suggests a distinct dynamic membrane spanning topology ...	86
4 Discussion and conclusions	89
4.1 Behaviour of Bax.....	89
4.2 Characterization of Bax activation by tBid	93
4.3 Conformational change of Bax.....	99
4.4 A model for the Bax pore-forming domain	104
4.5 Future Direction.....	107
5 References.....	110
6 Supplementary material	125
6.1 Cleavage by hydroxylamine is preferred over betamercaptoethanol	125
6.2 Absorbance spectra of NBD labeled mutants.....	126
6.3 Ionic quenching titrations	128
6.4 Tb-DPA liposomes can be lysed with 0.5% CHAPS	134
6.5 Data fitting for lifetimes	135

List of Figures

Figure 1.1: Sequence alignment for some members of the Bcl-2 family.....	7
Figure 1.2: Structures of Bax, Bcl-xL and diphtheria toxin transmembrane domain.	11
Figure 1.3: Space filling model of Bax showing some mutant locations.....	16
Figure 3.1: Cloning Bax single cysteine mutants.....	49
Figure 3.2: Purified and labeled Bax and tBid	52
Figure 3.3: Most Bax and Bid mutants behave similarly to wildtype Bax and tBid.....	57
Figure 3.4: Fluorophores used to estimate pore size.....	60
Figure 3.5: Bax pores vary in size.....	61
Figure 3.6: Effect of tBid on Bax.....	63
Figure 3.7: DACM and IANBD: a new FRET pair	65
Figure 3.8: Interactions between tBid and Bax are only observed in the presence of membranes	67
Figure 3.9: A simultaneous 3 fluorophore assay.....	69
Figure 3.10: Ordering the steps of Bax activation	72
Figure 3.11: NBD emission intensity and wavelength suggest Bax conformational reorganization.....	77
Figure 3.12: Lifetimes suggest distinct environments for different areas of Bax.	80
Figure 3.13: Differential ionic quenching of Bax residues	85
Figure 3.14: Lipid quenching.....	87
Figure 4.1: Steps in Bax pore formation	98

Figure 4.2: Model for topology of the Bax pore-forming domain	107
Figure 6.1: Cleavage by hydroxyl amine can reduce non-specific labeling of Bax.....	125
Figure 6.2: Absorbance spectra of labeled Bax mutants	127
Figure 6.3: Quenching titrations for KI and CoCl ₂	133
Figure 6.4: 0.5% CHAPS is suitable for lysing Tb-DPA containing liposomes.....	134

List of Tables

Table 2.1: Silent sites for cysteine scanning helix 5 and 6.....	24
Table 2.2: Oligonucleotides used to generate cysteine mutants.....	25
Table 3.1: List of mutant plasmids generated	49
Table 3.2: Bax yields and NBD labeling efficiencies for mutants used in this study.....	52
Table 3.3: Bax yields and NBD labeling efficiencies for mutants that were not used in this study	54
Table 3.4: Two and three component lifetime fits for Bax	81
Table 3.5: Quenching of different Bax residues	88
Table 6.1: Three component fit parameters for lifetimes.....	135

List of abbreviations

ANTS: 8-aminonaphthalene-1,3,6-trisulfonic acid

BSA: Bovine serum albumin

CHAPS: 3-[(3-Cholamidopropyl)dimethylammonio]-1-propanesulfonate

DAC: Dimethylamino - 4 - methylcoumarin - 3 yl

DACM: 7 - Dimethylamino - 4 - methylcoumarin - 3 yl maleimide

DMACA-SE: 7 - Dimethylaminocoumarin - 4 - acetic acid, succinimidyl ester

DPX: p-xylene-bis-pyridinium bromide

DPA: Dipicolinic acid

DTT: Dithiothreitol

EDTA: Ethylenediamine tetraacetic acid

ER: Endoplasmic reticulum

FRET: Fluorescence resonance energy transfer

FPLC: Fast Protein Liquid Chromatography

HEPES: 4-(2-hydroxyethyl)-1-piperazineethanesulfonic acid

IANBD: *N,N*-dimethyl-*N*-(iodoacetyl)-*N*-(7-nitrobenz-2-oxa-1,3-diazol-4-yl) ethylenediamine

IMS: Intermembrane space

LB-ON: Luria-Bertani broth, no salt

MPTS: 8-Methoxypyrene - 1,3,6 - trisulfonic acid, trisodium salt

MOM: mitochondrial outer membrane

NBD: *N*-(7-nitrobenz-2-oxa-1,3-diazol-4-yl)

PDB: Protein Data Bank

PTI: Photon Technology International

RPM: Rotations per minute

SDS PAGE: Sodium dodecyl sulphate polyacrylamide gel electrophoresis

TBS-T: Tris Buffered Saline with Tween

TNF: Tumor necrosis factor

VDAC: Voltage dependent anion channel

1 Introduction

1.1 Apoptosis

Apoptosis is a form of programmed cell death that multicellular organisms employ to dispose of unwanted cells in the most efficient manner. By using apoptosis, organisms can avoid evoking an immune response while recycling cellular building blocks. Apoptosis is used by higher organisms for sculpting organ morphology, regulating cell numbers, or removing cells that have served their roles or are harmful. Given these crucial functions, it is not surprising that misregulated apoptosis is at the root of many human diseases. When cells undergo apoptosis too quickly, as brain cells do during a stroke, unwanted induction of apoptosis may result in a permanent loss of brain function. Other neurodegenerative diseases such as Alzheimer's, Parkinson's and Huntington's are also caused by the premature loss of neurons brought about by apoptosis. Conversely, when cells become resistant to apoptosis, the resulting proliferation leads to cancers.

Cells that are dying have long been observed to be different from other cells (Hacker, 2000). Cells shrink; plasma membranes pinch off, or bleb; nuclei condense; apoptotic cells round up and detach from neighbouring cells. Other changes such as the externalization of phosphatidyl serine and the degradation of DNA and proteins also occur. Eventually, apoptotic cells are taken up by macrophages. Protein degradation is carried out by the caspases, the so-called executioners of cell death (Cohen, 1997). Caspases are a family of proteases that have a cysteine active site and the ability to cleave

proteins next to aspartic acid residues. Synthesized as inactive proenzymes, caspases are cleaved during apoptosis and proceed to degrade a variety of important cellular protein targets. Caspase activation is the endpoint of the two major apoptotic pathways known as the extrinsic and intrinsic pathways (Boatright and Salvesen, 2003). In general, the extrinsic pathway is used to get rid of unwanted cells during immune responses, while the intrinsic pathway is used to get rid of unwanted cells that have suffered damage. The extrinsic pathway makes use of death receptors – plasma membrane proteins that bind an extracellular ligand and transduce the apoptotic signal. The intrinsic pathway is regulated by internal mechanisms that sense cellular damage. Both extrinsic and intrinsic apoptotic pathways make use of the mitochondria for committing to apoptosis.

Mitochondria are central to apoptosis. Once the mitochondrial outer membrane (MOM) has been permeabilized, the cell is destined to carry out its death program. The mitochondria intermembrane space (IMS) contains several factors that, while harmless or essential for cellular function when confined to the mitochondria, initiate irreversible motions leading to apoptosis when unleashed into the cytosol. A major insight was gained with the discovery that cytochrome C, normally an electron carrier in oxidative phosphorylation, moves into the cytosol and activates caspases during apoptosis (Liu et al., 1996). By forming a complex with Apaf-1 and dATP known as the apoptosome, cytochrome C is able to initiate cleavage of procaspase-9 into activated caspase-9 (Zou et al., 1999). Activated caspase-9 then can go on to cleave downstream targets such as caspase-3, initiating a caspase cascade leading to protein degradation. Although it has been known for a long time that cytochrome C redistributes to the cytosol from the

mitochondria in cells that have been irradiated (Zhivotovsky et al., 1998), the explanation for this observation was not known. The unexpected role for a well characterized IMS protein clarifies how cells initiate apoptosis. Several other IMS proteins have been discovered that also have a role in the apoptosis program. Caspase activity is normally kept in check by the cytosolic IAP (Inhibitor of Apoptosis Protein) family. Smac/DIABLO is an IMS protein that antagonizes IAPs after MOMP (Du et al., 2000). By binding to IAPs, caspase activation is further magnified during apoptosis. Like Smac/DIABLO, Omi/HtrA2 is another inhibitor of IAPs located in the IMS. This serine protease was identified as a protein that binds to XIAP, a prominent member of the IAP family (Suzuki et al., 2001). Although caspase activation is a hallmark of apoptosis linked to IMS proteins, it was noted that caspase activity is not essential for cell death to occur (Xiang et al., 1996). Other mitochondria IMS proteins were identified that contribute to apoptosis in a caspase independent manner. AIF is an IMS protein that has an important role in apoptosis (Susin et al., 1999). During apoptosis, AIF translocates to the nucleus, and overexpression of the protein induces chromatin condensation. Even in the presence of caspase inhibitors, AIF can induce apoptosis. Endonuclease G was identified as another mitochondria IMS protein involved in apoptosis (Li et al., 2001). This protein was isolated through an in vitro screen that identified a mitochondrial factor that could degrade DNA.

1.2 *The Bcl-2 family*

Bcl-2 was discovered at the breakpoint of a (14:18) chromosomal translocation found in B cells lymphomas (Tsujimoto et al, 1984). This translocation places the *bcl-2* gene downstream to the enhancer of the highly expressed immunoglobulin G heavy chain, resulting in deregulated expression of Bcl-2 (Bakhshi et al., 1985). A critical realization of the importance of apoptosis came when Bcl-2 overexpression was shown to promote cell proliferation by preventing cells from dying, and not by simply increasing the rate of cell division (Vaux, 1988). Expression of Bcl-2 shields cells from death by growth factor deprivation, UV and gamma radiation, heat shock, TNF, chemotherapeutic drugs and other cellular insults that would otherwise initiate apoptosis (Reed, 1994). A functional role was established for Bcl-2 when it was shown that Bcl-2 could prevent cytochrome C release from mitochondria and the resulting caspase activation (Yang et al., 1997; Kluck et al., 1997).

Bax, named as Bcl-2 Associated X protein, was identified as a pro-apoptotic protein that heavily co-immunoprecipitated with Bcl-2 in a cancerous human B cell line (Oltvai et al., 1993). Overexpression of this protein led to accelerated cell death, which prompted the proposal of the “rheostat” model, which postulates that the ratio of Bax to Bcl-2 determines whether or not the cell lives or dies. Supporting this theory, Bax transcription is upregulated during apoptosis by p53 (Miyashita and Reed, 1995). However, the rheostatic model falls short on some levels, since many other important Bcl-2 family members have since been discovered and furthermore, Bax and Bcl-2 have different

subcellular localization in healthy cells. It was also noted that Bax and Bcl-2 shared short stretches of sequence homology, referred to as Bcl-2 homology BH1 and BH2 regions (Oltvai et al., 1993). At the same time Bax was discovered, another Bcl-2 family member, Bcl-xL was identified and was shown to have some of the same sequence similarity to Bcl-2 and Bax (Boise et al., 1993). The major splice variant of this protein, like Bcl-2, prevented apoptosis.

Subsequently, many related proteins have been discovered, some anti-apoptotic and some pro-apoptotic, which are classified as Bcl-2 family proteins. Two other regions of conserved sequence were discovered in Bcl-2 family members; the BH3 region and the BH4 region (Hanada et al., 1995; Zha and Reed, 1996). The Bcl-2 family members fit into three categories based on the BH regions they contain. The pro-apoptotic Bcl-2 proteins contain either all the BH1, BH2 and BH3 regions of BH homology, or only the BH3 region. The Bcl-2 members that contain three regions, such as Bax and Bak are called the multi BH region pro-apoptotic proteins. The members that contain only the BH3 region, such as Bid, are called the BH3-only pro-apoptotic proteins. The anti-apoptotic proteins, such as Bcl-xL and Bcl-2, contain the BH1, BH2 and BH3 regions, as well as a conserved BH4 region near the N terminus. Figure 1.1 shows an amino acid sequence alignment for several Bcl-2 family members. Highlighted in blue is the BH4 region that only the anti-apoptotic Bcl-xL and Bcl-2 share. Evidence exists that if this region is cleaved, these anti-apoptotic proteins become pro-apoptotic (Cheng et al., 1997; Basanez et al., 2001). This is not entirely unexpected since the anti-apoptotic proteins also contain the other conserved BH regions. The BH1 (red) and BH2 (green) regions flank

the pore-forming domain of Bax. The bold text for Bax shows the location in the primary sequence for the residues that make the pore-forming domain. The sequence for Bid is shown in both human and murine forms, since this study used murine Bid. Despite a comparable structure, the only conserved region shared by Bid is the BH3 region, shown in orange. This short amphipathic region has only a few residues that are identical in all the proteins. Evidence exists that suggests the BH3-only proteins are sensors for various apoptotic stimuli, while the multidomain pro-apoptotic proteins integrate the signals from the BH3-only proteins. For example, the BH3-only proteins Bim, Bad and Bid have been reported to be sensors for loss of cytoskeleton integrity, growth factor withdrawal, and death domain receptor signaling, respectively (van Gurp et al., 2003). Interestingly, many different viruses have been shown to encode Bcl-2 family proteins, in order to prevent the host cell from killing itself and destroying the virus (Hay and Kannourakis, 2002).

```

BCL2_HUMAN 1 MAHAGRTGYD-NREIVMKYIHYKLSQRGYEWDA-GDV----GAAPPGAAP---APGIFSS 51
BCLX_HUMAN 1 MSQS-----NRELVDFLSYKLSQKGYSWSQFSDVEENRTEAPEGTESEMETPSAING 53
BAXA_HUMAN 1 MD-----GSGEQPRGGGPTSSEQIMKTGALL-- 26
BAK_HUMAN 1 MASGQGPGRP-RQEC-----GEP---ALPSASEEQVAQDTEEV-- 34
BID_HUMAN 1 MDCEVNNGSSLRDECITNLLVFGFLQ-----SCSDNSFRRELDALGHELP 45
BID_MOUSE 1 MDSEVSNSSGLGAEHITDLLVFGFLQ-----SSGTRQEEVLGREL 43

BCL2_HUMAN 52 QPG-HT-----PHPAASRDVPARTSPLQTPAAPGAAAGPALSVPVPPVHLLTLRQAGDD 103
BCLX_HUMAN 54 NPSWHL-----ADSPAVNGATGHSSSLDAREVI PMAA-----VKQALREAGDE 96
BAXA_HUMAN 27 -LQGFI-----QDRAGRMGGEAPELALDP---VPQDA-----STKKLSECLKRIGDE 69
BAK_HUMAN 35 -FRSYVFPYRHQQEQEAEGVAAAPADPEMVTLP---LQPSS-----TMGQVGRQLAIIGDD 84
BID_HUMAN 46 VLAPQWEG--YDELQTDGNNRSSHS-RLGRIEADSESQED-----IIRNIARHLAQVGD 96
BID_MOUSE 44 VQA-YWEADLEDELQTDGSSQASRSFNQRIEPPDESQEE-----IIRNIARHLAQIGDE 96

BCL2_HUMAN 104 FSRRYRRDFAE-MSSQLHLTPFTARGRFATVVEELERDG-VNWGRIV---AFFEFGGVMC 158
BCLX_HUMAN 97 FELRYRRAFSD-LTSQLHITPGTAYQSFEQVNVNELERDG-VNWGRIV---AFFSFGGALC 151
BAXA_HUMAN 70 LDSNM--ELQR-MIAAVD--TDSPREVFRVAADMESDGNFNWGRVV---ALFYFASKLV 121
BAK_HUMAN 85 INRRYDSEFQT-MLQHLQPTAENAYEYFTKIATSLFESG-INWGRVV---ALLGFGYRLA 139
BID_HUMAN 97 MDRSIPPLVNLGLALQLRNTSRSEEDRNRDLATALEQLL-QAYPRDMEKEKTMVLVALLL 155
BID_MOUSE 97 MDHNIQPTLVRQLAAQFMNGSLSEEDKRNCLAKALDEVK-TAFPRDMENDKAMLIMTMLL 155

BCL2_HUMAN 159 VESVNREMSPLVDNIALWMT EYLNRRH-LHTWIQDNGGWD AFV ELYG PSM-----RPLF 210
BCLX_HUMAN 152 VESVDKEMQVLVSRIA AAWMATYLNDRH-LEPWIQENGGWDT FV ELYG NNA A A ESRKQ QERF 210
BAXA_HUMAN 122 LKALCTKVP E L I R T I M G W T L D F L R E R - L L G W I Q D Q G G W D G L L S Y P G T P T ----- 169
BAK_HUMAN 140 LHVYQHGLTGFLGQVTRFVVDFMLHHC IARWIAQRGGWVAALNLNGNPI----- 188
BID_HUMAN 156 AKKVASHTPSLLRDVFHTTVNFINQN-LRTYVRSL----- 189
BID_MOUSE 156 AKKVASHAPSLLRDVFHTTVNFINQN-LFSYVRNL----- 189

BCL2_HUMAN 211 DFSWLSLKTLLSLALVGCITL GAYLGHK 239
BCLX_HUMAN 211 NRWFLTGMTVAGVLLGSLFS-----RK 233
BAXA_HUMAN 170 ----WQTVTIFVAGVLTASLTIWKK--MG 192
BAK_HUMAN 189 ----LNVLVVLGVVLLGQFVV--RRFFKS 211
BID_HUMAN 190 -----APNGMD 195
BID_MOUSE 190 -----VRNEMD 195

```

Figure 1.1: Sequence alignment for some members of the Bcl-2 family.

Alignment was performed with Jalview software (available online at <http://www.jalview.org>) using the MAFFT algorithm (Kato et al., 2005). The numbers indicate residue numbers and the dashes show gaps in the alignment. The red highlighted region shows the BH1 region, green shows the BH2 region, orange shows the BH3 region and blue shows the BH4 region. The bold font of Bax shows the pore-forming domain. The darker highlighted residues are absolutely conserved between all proteins shown.

While Bcl-2 family proteins localize to the mitochondria either constitutively or during apoptosis, it should be noted that the mitochondria is not their only destination. Bcl-2 and some other Bcl-2 family members are localized at the ER and nuclear envelope (Annis et al., 2003). There are some members that do exclusively reside on the

mitochondria, such as Bcl-w (Hinds et al, 2003). ER permeability is also connected to MOMP, since if the ER calcium stores are released into the cytosol, swelling and rupture of the mitochondria follow, leading to the release of apoptogenic IMS proteins.

A characterized apoptotic pathway is initiated by the Fas ligand and involves the cleavage and targeting of BH3-only protein Bid to the mitochondria. Part of the extrinsic pathway, upon binding to an extracellular ligand, the Fas receptor forms a complex that proceeds to cleave procaspase-8 into active caspase-8. A major discovery found that a main target of caspase-8 is Bid (Luo et al., 1998; Li et al., 1998). Upon cleavage by caspase-8, the larger C terminal fragment of Bid, known as tBid, translocates to the mitochondria and initiates MOMP. It was further demonstrated that tBid is able to induce Bax and Bak oligomerization during MOMP (Wei et al., 2000). Cardiolipin, a lipid found only in mitochondria was shown to play a role in tBid targeting to mitochondria (Lutter et al., 2000). Cardiolipin was also identified as a lipid present in Bax and tBid permeable mitochondrial reconstituted vesicles but absent from Bax and tBid impermeable reconstituted ER vesicles (Kuwana et al., 2002). Yeast cells with the cardiolipin producing gene knocked out display no effect when tBid is expressed, while wildtype yeast demonstrate abnormal mitochondrial respiration when tBid is expressed (Gonzalvez et al., 2005). However, the role of cardiolipin remains controversial since only the mitochondrial inner membrane, and not the outer membrane, contains cardiolipin (de Kroon et al., 1997) and human cells with the cardiolipin gene knocked down actually displayed an increased sensitivity to tBid mediated apoptosis (Choi et al., 2007).

A key finding came when it was shown that Bak or Bax knockout mice and mouse embryonic fibroblasts can still respond to apoptotic signals, but the double Bax and Bak knockout are extremely resistant to all forms of apoptosis induction (Wei et al., 2001). This study cemented the paradigm of the multi BH-region Bax or Bak proteins being activated to cause apoptosis by BH3-only proteins like tBid. The connection of Bid to the Fas pathway was further validated since injection of Fas had no effect on mice that had the Bid gene knocked out.

Recently, much attention has been given to the interactions between the multidomain pro-apoptotic members, the BH3-only members, and the anti-apoptotic members that regulate MOMP. Besides activation by BH3-only proteins, some evidence exists that Bax or Bak can be directly activated by exposure to heat of 43° C (Pagliari et al., 2005), as well as by the tumor suppressor protein p53 (Chipuk et al., 2004). At least three models exist to explain how the anti-apoptotic proteins and BH3-only proteins interact to regulate apoptosis with Bak and Bax. One model is known as the direct activation model. In this model, specific BH3-only proteins activate Bak or Bax, and the anti-apoptotic proteins function by binding to these BH3-only proteins before they can activate Bax or Bak. Other BH3-only proteins serve to bind the anti-apoptotic proteins. When the anti-apoptotic proteins become bound by these so-called sensitizer BH3-only proteins, the cell becomes “primed for death”, and ready for an activator BH3-only protein to initiate apoptosis (Certo et al., 2006). Supporting the direct activation model, when proteins are mutated so Bax and Bak do not bind anti-apoptotic Bcl-2 members, cells do not undergo apoptosis spontaneously (Kim et al., 2006). A second model is the

indirect activation model. In this model, Bax and Bak are inherently active, but in non-dying cells are neutralized by anti-apoptotic proteins. A BH3-only protein may proceed to bind to an anti-apoptotic protein, freeing Bax or Bak to permeabilize membranes (Willis et al., 2007). Finally, a third model proposed by our lab, is called “embedding together”. This model proposes that the pro- and anti- Bcl-2 family members engage in related interactions and conformational changes and that relevant interactions only occur within the membrane (Leber et al., 2007).

The pro- and anti- apoptotic Bcl-2 members share a remarkably similar fold. Figure 2 shows the structures of both Bax and Bcl-xL. Like all the Bcl-2 family members, they only contain alpha helical secondary structure, being composed of nine helices. Two of the helices comprise a hydrophobic hairpin that is central to the protein (shown in blue). These helices are known as the pore-forming domain. Some of the Bax residue numbers are indicated in Figure 1.2 to show the location of some of the mutations that were used in this study. Bax and Bcl-xL also have a hydrophobic C terminus, although the structure of Bcl-xL was solved with this tail truncated. The structures of Bcl-2 proteins show that the BH 1, 2 and 3 regions form a hydrophobic groove where other BH3 peptides can bind (Petros et al., 2004).

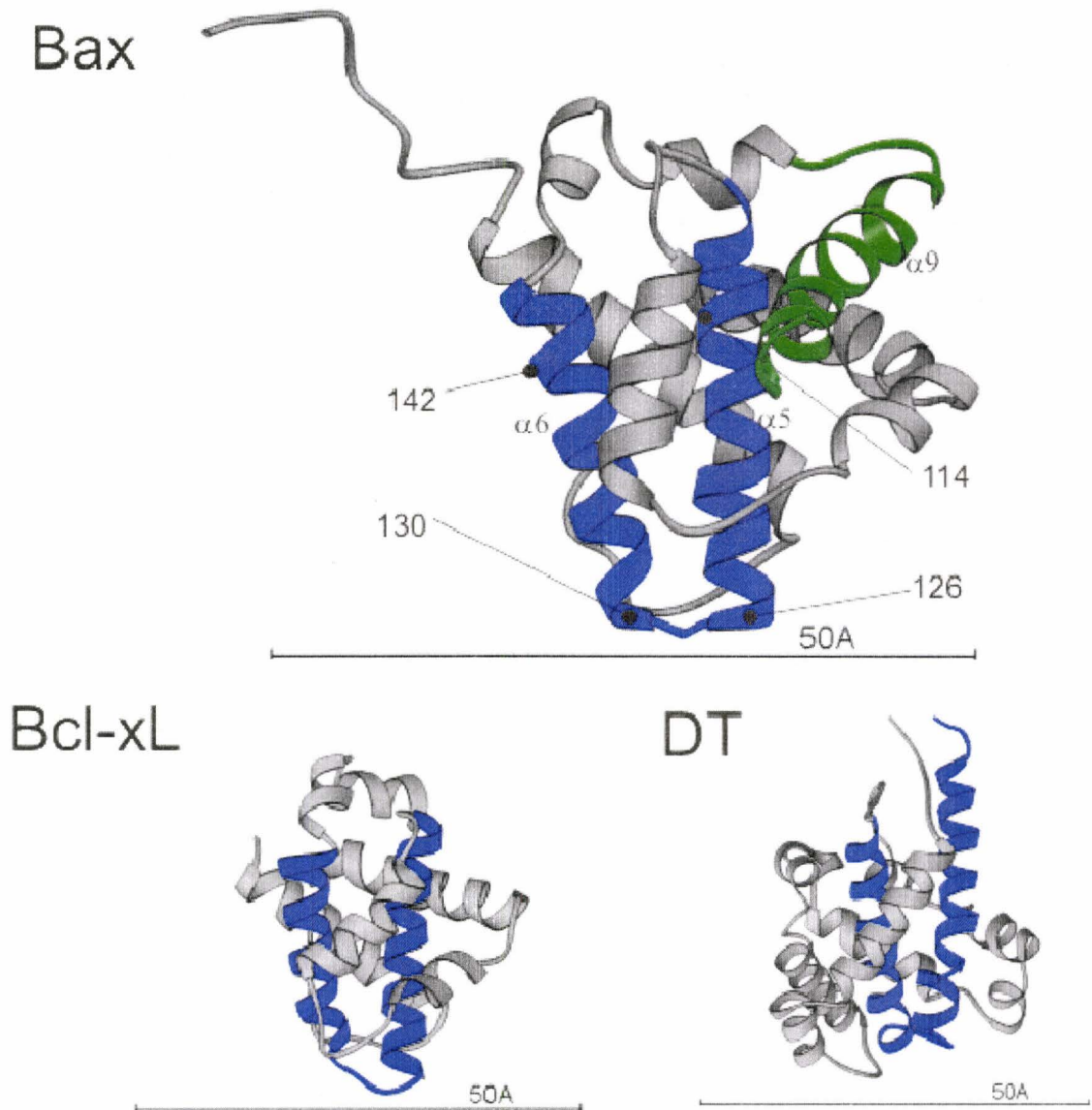


Figure 1.2: Structures of Bax, Bcl-xL and diphtheria toxin transmembrane domain.

Figures prepared with the Ribbons program (available online at <http://torus.cbse.uab.edu/ribbons>). The PDB files used were 1F16 for Bax, 1R2D for Bcl-xL and 1SGK for the diphtheria translocation domain. The suspected pore-forming helices are coloured in blue. Residue numbers are shown on the pore-forming domain of Bax. The location of helix 5,6 and 9 is indicated for Bax. The Bax hydrophobic C terminus is highlighted in green. A 50 angstrom scale bar is shown at the bottom of the each structure for comparison.

When the first member of the Bcl-2 family, Bcl-xL, had its structure solved, a strong similarity in appearance with the diphtheria toxin translocation domain was noted (Muchmore et al., 1996). As seen in Figure 1.2, Bcl-xL and diphtheria have the same number of helices organized around two central hairpin hydrophobic helices, although these helices of diphtheria are the C terminal two helices. The hairpin helices for Bcl-xL and Bax are numbers 5 and 6. Since the diphtheria toxin has been shown to form pores, this possible mechanism was put forth to explain how the Bcl-2 family regulates apoptosis. Investigations confirmed that Bcl-xL could form pores in acidic, non physiological pH environments (Minn et al., 1997).

1.3 Pore formation by Bax

The role of Bax in apoptosis has been the focus of extensive research. Clinically, it has been shown that more than 50 percent of a type of colon adenocarcinoma carries Bax frameshift mutations (Rampino et al., 1997). Another study found that over 20 different human hematopoietic malignancy lines, especially acute lymphoblastic leukemia cells, carry a frameshift mutation or point mutations to the BH1 or BH3 region of Bax (Meijerink et al., 1998).

Investigation of Bax led to the important observation that in healthy cells, Bax is a cytosolic protein, but during apoptosis, Bax translocates to the mitochondria (Hsu et al., 1997; Wolter et al., 1997). In human tissue culture cells, mitochondria from cells

undergoing apoptosis contain oligomers of Bax that remain stable in CHAPS detergent that have shifted from a non-apoptotic monomeric molecular weight of 21,000 kDa to an apparent oligomeric mass of 96,000 kDa and 260,000 kDa, as determined by gel filtration (Antonsson et al., 2001). This leads to a general model for Bax where the protein translocates and oligomerizes at the mitochondria, in the process causing cytochrome C release. In simplified in vitro systems, Bax can permeabilize isolated mitochondria, causing cytochrome C release and this process occurs with the formation of higher order Bax oligomers (Jurgensmeier et al., 1998; Antonsson et al., 2000). Bax can cause liposomes formed from lipids mimicking the MOM to release very large 1 MDa dextrans (Kuwana et al., 2002). Pores formed by detergent-activated, C terminally truncated Bax have been directly visualized using AFM (Epanand et al., 2002). These pores had exceptionally large diameters ranging from 100 to 200 nm. Bax has been shown to promote transbilayer diffusion, suggesting a lipidic pore model where the pore is lined by lipid headgroups and not just protein (Terrones et al., 2004).

Some work has suggested that the outer membrane complex VDAC forms part of the Bax pore (Shimizu et al., 2000). However, this role is not certain because VDAC is not required for liposome permeabilization by Bax and VDAC does not oligomerize with Bax (Antonsson et al., 2001).

Several mutagenesis and deletion studies have shed light on certain aspects of Bax function, although the picture is far from clear. The N terminus of Bax contains a mitochondrial targeting sequence (Cartron et al., 2003). When the first 37 amino acids of

Bax are deleted, Bax loses its ability to localize to mitochondria. However, when only the first 19 amino acids are deleted, which leaves helix 1 intact, Bax demonstrates enhanced mitochondria targeting. This implies that the first helix of Bax is critical in directing the protein to the MOM, while the first 19 amino acids help regulate the first helix. Further work showed that specific point mutations in the first alpha helix of Bax can prevent Bax targeting to mitochondria (Cartron et al., 2005), as well as interfering with binding to BH3-only proteins (Cartron et al., 2004). Consistent with these results, another study found that truncating the first 29 amino acids of Bax resulted in constitutive mitochondrial localization and high levels of apoptosis (Parikh, et al., 2007). The same work found that while truncating the C terminus tail did not affect targeting or apoptosis, eliminating helix 5 and 6 completely destroyed Bax function. This corroborates many works finding that the Bax pore-forming domain, helices 5 and 6, is absolutely essential for Bax activity. The pore-forming domain of Bax is shown in blue in Figure 1.2. As can be seen in amino acid sequence of Bax shown in Figure 1.1, the conserved BH1 and BH2 regions lie directly before and after the pore-forming domain. It was demonstrated using low pH activation and a yeast lethality assay that Bax pore formation depends on the pore-forming domain, and that helix 5 and 6 from Bcl-2 cannot substitute for helix 5 and 6 of Bax (Matsuyama et al., 1998). The importance of these helices was emphasized in another study that showed that Bax lacking the C terminus or residues in the BH3 region could still release cytochrome C from isolated mitochondria, but deletion of the pore-forming domain abrogated Bax function (Heimlich et al., 2004). Interestingly, mutations of up to five charged residues in the pore-forming domain did not remove Bax pore-

forming ability, although once the eight charged residues were mutated, pore-forming ability was lost (Nouraini et al., 2000). Peptides corresponding to helices 5 or 6 of Bax are sufficient to permeabilize liposomes (Garcia-Saez et al., 2005; Garcia-Saez et al., 2006). The conserved BH3 region of Bax, shown in yellow in Figure 1.1 is important for oligomerization. The BH3 region of Bax comprises helix 2 of the protein. Specific mutagenesis in the conserved IGDE sequence of the Bax BH3 region can selectively remove Bax-Bcl-2 binding and deletion of this sequence destroys Bax homobinding (Zha and Reed, 1997). Mutations to other residues in the BH3 region can also selectively destroy homobinding or Bcl-2 binding (Wang et al., 1998).

The structure of Bax, the first full length Bcl-2 family member to be solved, showed that the hydrophobic C terminal helix of Bax (shown in green in Fig 1.2) lies in a hydrophobic pocket created by the other BH regions (Suzuki et al., 2000). This is the same pocket where BH3 peptides bind the similar Bcl-xL. Bcl-xL structures have been solved with both the Bak and Bid peptides bound into the hydrophobic groove. This structure suggested a model in which, during apoptosis, the tail of Bax moves out of the hydrophobic pocket to allow BH3 regions of other proteins entry and thereby causing oligomerization to proceed. However, many earlier reports using Bax have shown that Bax lacking the C-terminus is still capable of forming pores, demonstrating that this helix is not required for pore formation. Mutagenesis studies have shown that the C terminus of Bcl-xL is essential for formation of cytosolic homodimers (Jeong et al., 2004). Although Bax does not form cytosolic homodimers, studies have shown that the tail is not a membrane anchoring signal and that the C terminal is involved in the Bax

oligomerization process (Er et al., 2007). The C terminus has also been shown to play an important regulatory role for Bax. Mutation of the serine at position 184 to a lysine inactivated GFP tagged Bax while deletion of this residue or mutation to alanine caused Bax to become constitutively active (Nechushtan et al., 1999). This work also showed that the C terminal tail alone could direct GFP to the mitochondria, although it has been also shown Bax does not require the tail for targeting to mitochondria (Tremblais et al., 1999).

The space filling model of Bax is shown in figure 1.3. The blue atoms, representing the pore domain, are mostly from helix 6 since the residues of helix 5 tend to be buried in the core of the protein. Some of the residues at the bottom of helix 5 are visible; residue 126, at the bottom of helix 5, is marked. The locations of other accessible residues are indicated in the figure.

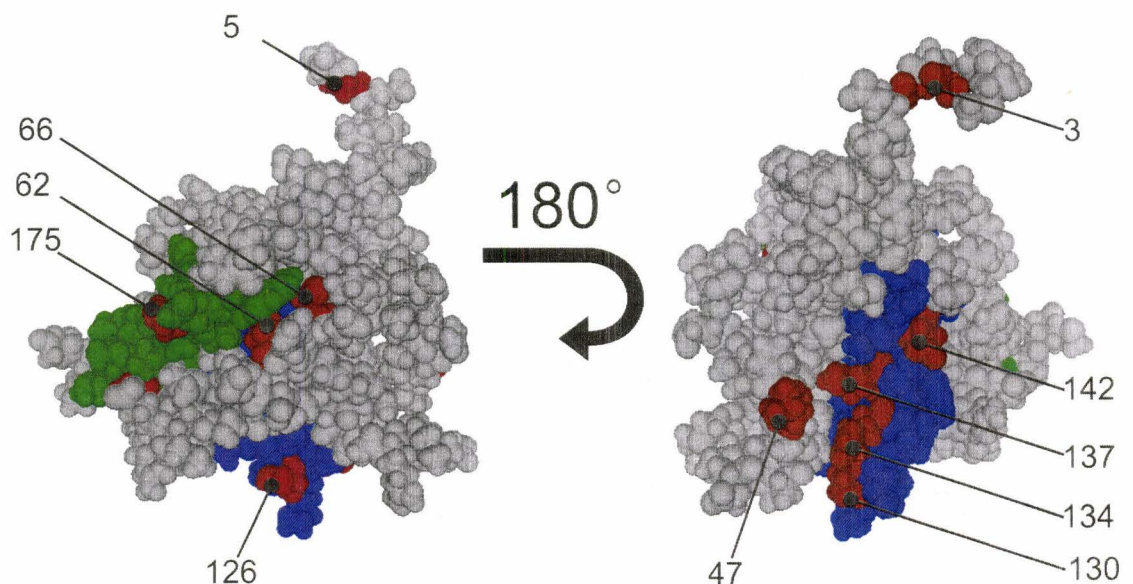


Figure 1.3: Space filling model of Bax showing some mutant locations

A space filling model was created with Pymol software (available online at <http://pymol.sourceforge.net>) and PDB file 1F16. Helix 9 of Bax is shown in green and the poreforming domain is shown in blue. The red atoms mark the indicated residue numbers. The model on the right is Bax rotated 180° relative to the model on the left. Residues in red have numbers indicating the residue number.

1.4 Other pore-forming proteins

Pore-forming toxins are commonly used by bacteria to kill the other cells by either rupturing the cell membrane or by permeabilizing an endosomal membrane to release toxic components into the cytosol after being uptaken through endocytosis. Pore-forming toxins may be divided into two broad groups; those with alpha helical structure and those with beta barrel structure (Tilley et. al, 2006). The membrane topology and pore structure of the alpha helical toxins is not well understood. Like Bax, pore-forming proteins change from a monomeric soluble form, to a membrane inserted oligomer. Remarkably, like members of the Bcl-2 family, the monomeric form of alpha helical toxins all usually contain about ten alpha helices with two central hydrophobic helices that form a hairpin turn. As can be seen in Figure 1.2, Bax, Bcl-xL and the transmembrane domain of diphtheria toxin bear a strong similarity to the central hydrophobic hairpin helices of the proteins shown in blue.

The diphtheria toxin is produced by *Corynebacterium diphtheriae* that has been infected by a specific bacteriophage (Zalman and Wisnieski, 1984). The toxin consists of three domains: one for receptor binding, one for pore formation (referred to as the transmembrane domain) and one for catalytically halting protein translation. After receptor binding and endocytosis, the transmembrane domain undergoes a pH dependent

conformational change as the endosome acidifies, causing pore formation and releasing the catalytic domain. The catalytic domain then kills the cell by inactivating elongation factor 2, halting all protein translation. When the structure of the diphtheria toxin was solved, helices 8 and 9 of the transmembrane domain were suspected of being “membrane-soluble daggers” due to their hydrophobic nature and central location buried within the protein (Choe et al., 1992). These helices were shown to be protected from proteases when the protein inserts into membranes (Quertenmont et al., 1996). They were also shown to adopt a membrane spanning conformation as determined by biotinylation accessibility studies (Senzel et al., 2000). Earlier studies estimated the diphtheria toxin pore diameter at 2.4 nm (Zalman and Wisnieski, 1984). More recently, the protein was shown to form variable size pores, depending on the concentration of toxin in the membrane. At the highest concentration, the pores were able to release dextrans of up to 10 kDa, but not 70 kDa. (Sharpe and London, 1999). Light scattering and sedimentation velocities showed that a 45 kDa fragment of the toxin forms oligomers composed of 20 to 24 subunits (Bell et al., 1997). The mechanism of the diphtheria toxin has been described as poorly understood and a challenging target for topography experiments due to flexibility in its structure (Rosconi et al., 2004)

The colicins are also alpha helical pore-forming toxins. Like the diphtheria toxin, colicins consist of three domains. The translocation domain brings the toxin across the outer cell wall, the middle domain mediates receptor binding and the C terminal domain is responsible for pore formation. It is also known that different colicins exert action by depolarizing membrane potential, inhibiting protein or peptidoglycan synthesis, or by

exerting nuclease activity (Musse and Merrill, 2003). The structures determined for the pore-forming domains of colicins A, E1, Ia, B and N show they are made of 10 alpha helices. The structure of the colicins also reveals the presence of two hydrophobic hairpin helices that are proposed to be essential for anchoring the channel (Elkins et al., 1997). The knowledge of the structure and function of membrane-bound colicins is described as “modest at best” (Tory and Merrill, 1999). Some evidence based on the helix topology exists to support a model that colicin forms a toroidal pore (Musse et al., 2006). Colicins form pores much smaller than Bax and diphtheria toxin, and do not allow the passage of molecules bigger than 1 kDa. Some colicins may be able to permeabilize membranes without oligomerization (Tory and Merrill, 1999), while other colicins have been shown to oligomerize during activation (Cavard et al., 1998).

Another pore-forming toxin is the botulinum neurotoxin, which is secreted by *Clostridium botulinum* and is responsible for botulism. Like the other alpha helical toxins, this protein consists of three domains. The receptor binding domain binds to a pre-synaptic nerve ending. The function of the translocation domain is poorly understood, as it has a similar alpha helical fold to the other alpha helical pore-forming toxins. The toxin is activated by a pH change in endosomes. The catalytic domain consists of a highly specific zinc protease that degrades SNAP 25, an important protein in neurons (Lacy et al., 1998).

Connexin, the protein that forms gap junctions, facilitates intercellular communication by allowing the passage of signaling factors, metabolites and other

molecules up to 1 kDa in size, between adjacent cells. Although not a pore-forming toxin, this protein does form pores. The structure of the gap junction, solved by electron crystallography, revealed that the large 2 nm junction pore was lined by the alpha helices. The pore was made of a large oligomer composed of 12 subunits (Unger et al., 1999). Since the connexin pore is lined with helices, gap junctions may be generated by a similar pore-forming action as Bax.

Compared to alpha helical toxins, the mechanism and structure for beta barrel pore-forming toxins is better understood. Beta barrel pore-forming toxins are released as soluble monomers that oligomerize before they form pores. A subfamily of the beta barrel pore-forming toxins is the cholesterol dependent cytolysin toxins. This family forms large pores of about 25 nm in diameter, composed of 30 to 50 subunits (Geny and Popoff, 2006). Pneumonolysin, a cholesterol dependent cytolysin which affects millions of people every year and is secreted by *Streptococcus pneumonia*, was shown to form large pores of 26 nm in diameter and is composed of 44 subunits (Tilley et al., 2005).

Equinatoxin, secreted by certain sea anemones, and eiseniapore, secreted by certain earthworms, are both sphingomyelin dependent toxins produced by eukaryotes. The proteins share structural similarity to cholesterol dependent cytolysin Perfringolysin O. The tetrameric equinatoxin pores and the hexameric eiseniapore pores are only a few nanometers in diameter, much smaller than the pores formed by Perfringolysin O (Lange et al., 1997; Hong et al., 2002).

Unfortunately, since no structure is yet available for oligomeric Bax or any alpha helical pore-forming toxin, our knowledge of the topology of activated Bax is limited. Very little information is known about the conformational changes leading to Bax activation. It has been shown that interaction with a lipid membrane causes Bax to change conformation so that a specific epitope near the N terminus becomes exposed (Yethon et al., 2003). In tissue culture cells, Bax that has inserted into mitochondria contains residues on helix 5,6 and 9 that are protected from chemical labeling (Annis et al., 2005). This suggests a topographical model in which these helices are inserted into the bilayer. However, the orientation of these helices is not known. Other indirect studies using hydrophobicity analysis and glycosylation mapping have suggested that helix 5 and 9 are transmembrane helices (Garcia-Saez et al., 2004).

1.5 Investigations presented in this thesis

An in vitro system comprising liposomes and recombinant tBid and Bax will result in Bax targeting, Bax oligomerization and liposome permeabilization, but there are few known details besides these ones. In this thesis, we make use of some established and some new techniques to make discoveries about how Bax is activated and how Bax forms pores.

A fluorescence pore sizing assay was developed and used to show that Bax forms pores that vary in size. A unique FRET pair was created and was used to show that Bax

and tBid only interact in the presence of liposomes. A simultaneous 3 fluorophore kinetic assay was developed to study the order in which Bax is activated, interacts with tBid and forms pores. Finally, a new approach to ionic quenching in the presence of membranes suggests that the Bax pore-forming domain lines a lipidic pore.

Most work done through the course of this thesis builds on existing fluorescence methods. Bax single cysteine mutants were cloned, purified and labeled with NBD to determine the environment of the pore-forming domain, imitating a technique used to study the Perfringolysin O beta barrel toxin (Shepard et al., 1998). Although the results of the fluorescence measurements were drastically different from the Perfringolysin O results, this work represents the most thorough study of Bax pore-forming domain topology.

The mysteries of Bax are far from being solved but the conclusions of this thesis shed much needed new light on how this important protein functions.

2 Materials and methods

2.1 *General materials and methods*

General chemical reagents were obtained from Sigma or BioShop.

LB-ON used to culture *Escherichia Coli* was made with 5 g yeast extract (BD) and 10 g trypticase (BD) per litre of water. SB used to grow *Escherichia Coli* for plasmid purification was made with 32 g trypticase, 20 g yeast extract and 5 g NaCl per liter of water.

SDS PAGE electrophoresis was performed using 10% acrylamide tricine gels (Shagger and von Jagow, 1987). Protein samples were denatured in loading buffer containing 0.1 M Tris, pH 8.9, 2 mM EDTA, 10% SDS, 20% glycerol, 0.1% bromphenol blue, and 0.25 M DTT. The prestained molecular weight ladder used was PageRuler Prestained Protein Ladder (#SM0671, Fermentas).

2.2 *Cloning of Bax single cysteine mutants*

All Bax clones were based on the IMPACT purification system (New England Biolabs). This is a recombinant protein expression system that uses a self cleaving intein fused with a chitin binding domain. Site directed mutagenesis was performed to create a Bax plasmid in which oligonucleotides encoding single cysteine mutants could be directly ordered and ligated to rapidly generate clones. The starting material was a Bax mutant

previously created that had the two endogenous cysteines mutated to alanine to yield a cysteine negative Bax (plasmid #1730). The cysteine negative backbone was mutated to yield two additional silent restriction sites around the pore-forming domain. Locations for the silent sites were determined by the silent site mutation program (available online at http://www.dwalab.ca/silent_sites.htm). Using this program, a MluI site and a BsiWI site were introduced as shown in Table 2.1.

Table 2.1: Silent sites for cysteine scanning helix 5 and 6		
	MluI site	BsiWI site
Wild type sequence	GGC CGG GTT encoding Gly ₁₀₈ Ala ₁₀₉ Val ₁₁₀	AGA ACC encoding Arg ₁₃₄ Thr ₁₃₅
Enzyme recognition	A [^] CGCGT	C [^] GTACG
Silent site sequence (changes in bold)	GGA CGC GTT encoding Gly ₁₀₈ Ala ₁₀₉ Val ₁₁₀	CGT ACG encoding Arg ₁₃₄ Thr ₁₃₅

The primers were designed using the PrimerX program (available online at <http://www.bioinformatics.org/primerx>) and were 5' GGC AAC TTC AAC TGG GGA CGC GTT GTC GCC CTT TTC TAC 3' (forward) and 5'GTA GAA AAG GGC GAC AAC GCG TCC CCA GTT GAA GTT GCC 3' (reverse) for the MluI site, and 5' CCA AGG TGC CGG AAC TGA TCC GTA CGA TCA TGG GCT GGA CAT 3' (forward) and 5'CCA ATG TCC AGC CCA TGA TCG TAC GGA TCA GTT CCG GCA CCT TGG 3' (reverse) for the BsiWI site. Site-directed mutagenesis was performed as per the Quikchange (Stratagene) guidelines.

After generating the new silent sites, mutants were created by ordering forward and backward oligonucleotides (Sigma) with the appropriate overhang. To generate the backbone plasmid, the cysteine negative Bax plasmid was cut with the appropriate enzymes and the backbone was isolated from a 1% agarose gel using a gel extraction kit (#28704, Qiagen). Oligonucleotides were designed to code for the wildtype sequence with an alanine replacing the endogenous cysteine at position 126, and with a single cysteine mutation located at a specific location. The oligonucleotides used for the various mutants created are shown in Table 2.2. The underlined sequences in the oligonucleotides show the location of the introduced cysteine.

Table 2.2: Oligonucleotides used to generate cysteine mutants				
Plasmid ID	Mutation	Enzymes to cut backbone	Forward oligonucleotide	Reverse oligonucleotide
2013	V111C	MluI, BsiWI	5'CGCGTT <u>TGT</u> GCCCTTT CTACTTTGCCAGCAAAC TGGTGCTCAAGGCCCTG GCCACCAAGGTGCCGGA ACTGATCC3'	5'GTACGGATCAGTTCCGG CACCTTGGTGGCCAGGGC CTTGAGCACCAGTTTGCT GGCAAAGTAGAAAAGGG <u>CACA</u> AA3'
2014	L113C	MluI, BsiWI	5'CGCGTTGTCGCC <u>TGTT</u> TCTACTTTGCCAGCAA CTGGTGCTCAAGGCCCT GGCCACCAAGGTGCCGG AACTGATCC3'	5'GTACGGATCAGTTCCGG CACCTTGGTGGCCAGGGC CTTGAGCACCAGTTTGCT GGCAAAGTAGAA <u>ACAGG</u> CGACAA3'
2015	F114C	MluI, BsiWI	5'CGCGTTGTCGCCCT <u>T</u> <u>GTT</u> ACTTTGCCAGCAA CTGGTGCTCAAGGCCCT GGCCACCAAGGTGCCGG AACTGATCC3'	5'GTACGGATCAGTTCCGG CACCTTGGTGGCCAGGGC CTTGAGCACCAGTTTGCT GGCAAAGTA <u>ACA</u> AAGGG CGACAA3'
2016	Y115	MluI, BsiWI	5'CGCGTTGTCGCCCTTT <u>TC</u> <u>TGT</u> TTTGCCAGCAA CTGGTGCTCAAGGCCCT GGCCACCAAGGTGCCGG AACTGATCC3'	5'GTACGGATCAGTTCCGG CACCTTGGTGGCCAGGGC CTTGAGCACCAGTTTGCT GGCAA <u>ACA</u> GAAAAGGG CGACAA3'

2017	F116C	MluI, BsiWI	5'CGCGTTGTCGCCCTTT TCTACT <u>TGT</u> GCCAGCAAA CTGGTGCTCAAGGCCCT GGCCACCAAGGTGCCGG AACTGATCC3'	5'GTACGGATCAGTTCGG CACCTTGGTGGCCAGGGC CTTGAGCACCAGTTTGCT GGC <u>ACA</u> GTAGAAAAGGG CGACAA3'
2018	A117C	MluI, BsiWI	5'CGCGTTGTCGCCCTTT TCTACTTT <u>TGT</u> AGCAAAC TGGTGCTCAAGGCCCTG GCCACCAAGGTGCCGGA ACTGATCC3'	5'GTACGGATCAGTTCGG CACCTTGGTGGCCAGGGC CTTGAGCACCAGTTTGCT <u>ACA</u> AAAAGTAGAAAAGGG CGACAA3'
2019	K119C	MluI, BsiWI	5'CGCGTTGTCGCCCTTT TCTACTTTGCCAGC <u>TGTC</u> TGGTGCTCAAGGCCCTG GCCACCAAGGTGCCGGA ACTGATCC3'	5'GTACGGATCAGTTCGG CACCTTGGTGGCCAGGGC CTTGAGCACCAG <u>ACA</u> GCT GGCAAAGTAGAAAAGGG CGACAA3'
2020	L120C	MluI, BsiWI	5'CGCGTTGTCGCCCTTT TCTACTTTGCCAGCAAA <u>TGT</u> TGCTCAAGGCCCT GGCCACCAAGGTGCCGG AACTGATCC3'	5'GTACGGATCAGTTCGG CACCTTGGTGGCCAGGGC CTTGAGCAC <u>ACA</u> TTTGCT GGCAAAGTAGAAAAGGG CGACAA3'
2021	P130C	MluI, BsiWI	5'CGCGTTGTCGCCCTTT TCTACTTTGCCAGCAAA CTGGTGCTCAAGGCCCT GGCCACCAAGGT <u>TGTG</u> AACTGATCC3'	5'GTACGGATCAGTTC <u>ACA</u> CACCTTGGTGGCCAGGGC CTTGAGCACCAGTTTGCT GGCAAAGTAGAAAAGGG CGACAA3'
2022	M137C	BsiWI, BseRI	5'GTACGATC <u>TGTGG</u> CTG GACATTGGACTTCCTCC GGGAGCGGCTGTTGGGC TGGATCCAAGACCAGGG TGTT3'	5'CCACCCTGGTCTTGGAT CCAGCCCAACAGCCGCTC CCGGAGGAAGTCCAATGT CCAGCC <u>ACA</u> GATC3'
2023	W139C	BsiWI, BseRI	5'GTACGATCATGGGCTG <u>TAC</u> ATTGGACTTCCTCC GGGAGCGGCTGTTGGGC TGGATCCAAGACCAGGG TGTT3'	5'CCACCCTGGTCTTGGAT CCAGCCCAACAGCCGCTC CCGGAGGAAGTCCAATGT <u>ACA</u> GCCCATGATC3'
2024	T140C	BsiWI, BseRI	5'GTACGATCATGGGCTG <u>GTT</u> TTGGACTTCCTCCG GGAGCGGCTGTTGGGCT GGATCCAAGACCAGGGT GGTT3'	5'CCACCCTGGTCTTGGAT CCAGCCCAACAGCCGCTC CCGGAGGAAGTCCA <u>ACA</u> CCAGCCCATGATC3'
2025	L141C	BsiWI, BseRI	5'GTACGATCATGGGCTG GACA <u>TGT</u> ACTTCCTCC GGGAGCGGCTGTTGGGC TGGATCCAAGACCAGGG TGTT3'	5'CCACCCTGGTCTTGGAT CCAGCCCAACAGCCGCTC CCGGAGGAAGT <u>ACA</u> TGT CCAGCCCATGATC3'
2120	F143C	BsiWI,	5'GTACGATCATGGGCTG GACATTGGACTGTCTCC	5'CCACCCTGGTCTTGGAT CCAGCCCAACAGCCGCTC

		BseRI	GGGAGCGGCTGTTGGGC TGGATCCAAGACCAGG TGGTT3'	CCGGAGACAGTCCAATGT CCAGCCCATGATC3'
--	--	-------	--	---------------------------------------

Before ligation, the oligonucleotides were phosphorylated by incubating 300 pmol of oligonucleotides at 37° C for one hour in a 10 µL reaction with 1 mM ATP, and 1 µL T4 polynucleotide kinase (#EK0031, Fermentas). 100 pmol of forward and reverse oligonucleotides were heated to 95° C for 10 minutes and then cooled to anneal properly. The oligonucleotides were then ligated into the backbone in 20 mM Tris pH 8, 10 mM MgCl₂, 50 mM NaCl and 1 mM DTT using T4 ligase as per the T4 ligase manufacturer protocol (#EL004, Fermentas). Ligation proceeded at room temperature for 1 hour. The mixture was then heat inactivated at 65° C for 10 minutes. 5 µL of ligation reaction was then used to transform 50 µL chemically competent DH5α cells by heat shock. A single colony was selected and grown in SB medium. The plasmid DNA was purified using the lab alkaline lysis with phenol chloroform extraction protocol (available online at <http://www.dwalab.ca>). The plasmid was verified by restriction digest and sequencing.

For cloning of Bax 124C, 127C, 136C, 144C and 128C, the existing pUTK plasmids (plasmid numbers 1674, 1838, 1676, 1678 and 1839 respectively) were cut using NcoI and BseRI according to the enzyme manufacturer protocol (New England Biolabs), yielding a fragment containing the desired mutation. The dropout was gel purified. This fragment was ligated using T4 ligase (#EL004, Fermentas), as per the manufacturer protocol into the pBS cysteine negative vector backbone (plasmid #1730) cut with the same enzymes and gel purified. After ligation and transformation, a single

colony was picked, grown in SB medium, and the plasmid was isolated according to the lab protocol. The plasmid was verified by restriction digestion and DNA sequencing.

2.3 *Cloning of Bid G94E*

Murine Bid (plasmid #1446) was subjected to Quikchange mutagenesis according to the Stratagene guidelines using the forward primer 5'GAC ATC TCG CCC AAA TAG AAG ATG AGA TGG ACC3' and the reverse primer GGT CCA TCT CAT CTT CTA TTT GGG CGA GAT GTC. The primers were designed using the PrimerX program (available online at <http://www.bioinformatics.org/primerx>).

2.4 *Bax purification and labeling*

50 μ L of *Escherichia Coli* T7 polymerase salt inducible electrocompetent cells were transformed with 1 μ g of plasmid encoding Bax intein fusion mutants. Transformation was performed with an electroporator (Electroporator 2510, Eppendorf) set at 2500 volts. After letting the cells recover in 1 mL of LB for 15 minutes at 37° C, 50 μ L of cells were plated overnight on a 1.5% agar LB-ON plate with 0.1 mg/mL ampicillin. The next day, a single colony was grown overnight in 100 mL LB-ON with 0.1 mg/mL ampicillin at 37° C in an incubator with shaking. This culture was used to inoculate 3 L of LB-ON containing 0.1 mg/mL ampicillin. The cultures were grown at

37° C with shaking until reaching an OD between 0.6 - 0.9, and the cells were induced with 0.3 M NaCl for 3 hours at 37° C. Cells were spun down at 5000 g for 10 minutes at 4° C. Typically, the cell pellet weighed 5-10 g. The cell pellet was then frozen at -20° C overnight. The pellet was thawed and resuspended in a lysis buffer of 0.1% CHAPS, 10 mM HEPES pH 7, 1 mM PMSF, 0.1M NaCl, 0.2 mM EDTA, 1 ug/mL DNase and 1 ug/mL RNase. Clumps of bacteria were broken by repeatedly drawing the cells through a 16 gage needle (#305198, BD) before being lysed with two passes through a French press. Debris was removed from the lysate by centrifugation at 20,000 g. The supernatant was incubated with 1.5 mL of chitin bead resin (#S6551L, New England Biolabs) for 1 hour at 4° C before being passed through a 20 mL disposable column with a filter that retained the resin (Biorad). The flowthrough was passed through the column one additional time. The column was then washed with 50 mL of 0.5 M NaCl, 0.2% CHAPS, and 10 mM HEPES pH 7. After the wash, the column was flushed with 3 bed volumes of cleavage buffer containing 0.2 M NaCl, 10 mM HEPES pH 7, 0.2 mM EDTA, and 0.1% CHAPS. Unless otherwise stated, the cleavage buffer also contained 100 mM hydroxylamine (adjusted to pH 7 with NaOH). The protein was left to cleave for 16-24 hours at 4° C before being eluted with 0.2 M NaCl, 0.2 mM EDTA, 10 mM HEPES pH 7, and 10% glycerol. Typically, 2 mL of protein was eluted. The hydroxylamine was removed by dialysis in a buffer of 0.2 M NaCl, 0.2 mM EDTA, 10 mM HEPES pH 7, and 10% glycerol. 3500 Da cutoff tubing (#21-152-10, Fisher) was used and the 1 L dialysis buffer was changed 3 times with the sample having at least 4 hours to equilibrate each time the buffer was replaced.

Bax concentration was determined by using the molar extinction coefficient $37,000 \text{ M}^{-1}\text{cm}^{-1}$ at 280 nm. IANBD (#D2004, Invitrogen) was prepared in DMSO and the IANBD concentration determined by absorption at 478 nm of a 1 in 1000 or 1 in 5000 dilution in methanol using the molar extinction coefficient $25,000 \text{ M}^{-1}\text{cm}^{-1}$. Bax was labeled by adding a 10 fold molar excess of IANBD in a labeling buffer of 0.5% CHAPS 0.2 M NaCl, 0.2 mM EDTA, 10 mM HEPES pH 7, and 10% glycerol. The reaction was incubated on a rotator at room temperature for 2 hours in the dark. 1 mM DTT was then added and incubated for 10 minutes to quench the unreacted dye. Free dye was removed from the sample by gel filtration over a 15 mL G-25 Fine Sephadex (GE Health) column with a running buffer of 0.2 M NaCl, 0.2 mM EDTA, 10% glycerol and 10 mM HEPES pH 7. Protein containing fractions were identified by NBD fluorescence. An absorption scan was measured on the Tecan (SAFIRE) between 250 and 500 nm, using the Sephadex column running buffer as a blank. NBD and Bax concentrations were calculated using the extinction coefficients of $25,000 \text{ M}^{-1}\text{cm}^{-1}$ for the NBD peak around 475 nm and $37,000 \text{ M}^{-1}\text{cm}^{-1}$ for the Bax protein absorption peak at 280 nm with a path length of 0.8 cm. Labeling efficiency was determined by the concentration of NBD divided by the concentration of Bax. Protein was aliquoted and flash frozen in liquid nitrogen before being stored at -80°C . 10 μL of Bax was subjected to SDS PAGE. For 126C-Bax-NBD, before Coomassie staining, a fluorescence scan was performed of the gel on a Typhoon 9200 variable mode imager (Molecular Dynamics). The Typhoon scan was performed using a broad 532 nm laser and a 526 nm shortpass emission filter recommended for AlexaFluor 488. DAC labeled Bax mutants were prepared in the same way, except that

DACM (#81403, Anaspec) was used to label the Bax instead of IANBD. DAC concentration was determined by using an extinction coefficient of $27,000 \text{ M}^{-1}\text{cm}^{-1}$ at 380 nm.

2.5 *tBid purification and labeling*

N terminal polyhistidine tagged murine Bid plasmid (plasmid #1446) was transformed in BL21 arabinose inducible *Escherichia Coli* cells by electroporation. After recovery and overnight plating on LB agar plates with 0.1 mg/mL ampicillin, a colony was selected and grown in 100 mL LB media with 0.1 mg/mL ampicillin. Cells were then grown in 2 L of LB with 0.1 mg/mL ampicillin at 37° C with shaking. Cells were induced at an optical density at 600 nm of 0.6 for 3 hours with 0.2% arabinose. After induction, cells were spun down for 10 min at 5000 g and approximately 5-10 g of cells were obtained. Cells were resuspended in 25 mL of 0.3 M NaCl, 10 mM imidazole, 1 mM PMSF, 10 mM HEPES pH 7, 1 ug/mL DNase and 1 ug/mL RNase. Cells were lysed with two passes through a French press. Debris was cleared by spinning the lysate 20,000 g for 10 minutes. The supernatant was then passed over a 1 mL bed volume of Ni-NTA (#1018240, Qiagen) 5 times. The column was washed with 50 mL 1% CHAPS, 0.5 M NaCl, 10 mM HEPES pH 7 and eluted with 0.1 M NaCl, HEPES pH 7, 0.2 M imidazole, 0.1% CHAPS, 1 mM DTT and 10% glycerol. Concentration was determined by the absorbance at 280 nm, using an extinction coefficient of $8,500 \text{ M}^{-1}\text{cm}^{-1}$.

tBid was generated by cleaving 0.2-0.5 mg of Bid with 500 units of recombinant caspase-8 (#SE172-5000, Biomol) in the Bid storage buffer for 20 hours at room temperature. The cleaved Bid was then rebound to 0.5 mL Ni-NTA by first diluting the sample 10 times (in order to reduce the concentration of imidazole) and then passing the solution over the nickel column. After washing with a 1 mL of 0.3 M NaCl, and 10 mM HEPES pH 7, tBid was eluted from the column with 3 mL of 0.5 M NaCl, 1.2% octyl-glucoside and 10 mM HEPES pH 7. The protein was concentrated to less than 0.5 mL by ultrafiltration using a 10 kDa cutoff protein concentrator (Amicon Ultra #UFC901008, Millipore) and spinning at 2000 g for 30 to 60 minutes. To reduce the amount of octyl-glucoside present in the tBid, the sample was then diluted with 10 mL of 10% glycerol, 0.1 M NaCl, 0.2 mM EDTA, 1mM DTT and 10 mM HEPES pH 7 and reconcentrated to approximately 1 mL. tBid concentration was determined using Bradford Reagent (#500-0006, Biorad) as per manufacturer instructions.

For the DAC labeled tBid, Bid that had been eluted without DTT was labeled with a 10 fold excess of DACM dissolved in DMSO for 2 hours at room temperature. The total DMSO concentration in the labeling reaction was less than 3%. After labeling, Bid was diluted ten fold in 0.2 M KCl and 10 mM HEPES pH 7 to dilute the imidazole concentration and facilitate binding the protein to the nickel column. The labeled Bid was washed with at least 20 column volumes of 0.5% CHAPS, 0.2 M NaCl and 10 mM HEPES pH 7. Bid-DAC was then eluted with 0.1M NaCl, 1 mM DTT, 0.2 M imidazole, 0.1% CHAPS and 10% glycerol. The concentration was determined by absorption using an extinction coefficient of $8,500 \text{ M}^{-1}\text{cm}^{-1}$ at 280 nm for the Bid and $27,000 \text{ M}^{-1}\text{cm}^{-1}$ at

380 nm for the DAC. tBid-DAC was prepared the same way as tBid, and the tBid concentration was determined by the Bradford assay and the DAC concentration was determined spectrophotometrically.

2.6 *Liposome preparation*

Unless otherwise stated, liposomes were prepared as follows: Lipids dissolved in chloroform were combined to create 1 mg of lipid composed of 0.46 mg of egg phosphatidylcholine (#840051C, Avanti), 0.25 mg of egg phosphatidylethanolamine (#84118C, Avanti), 0.11 mg of bovine liver phosphatidylinositol (#840042C, Avanti), 0.10 mg of 18:1 phosphatidylserine (#840035C, Avanti), and 0.08 mg of cardiolipin (#710335C, Avanti). This composition is based on an existing protocol and is referred to as mitochondrial like lipid composition (Yethon et al., 2003; Kuwana et al., 2002). The chloroform was mostly removed by evaporation under a stream of nitrogen in a fume hood. The lipid films were then further dried for two hours in a vacuum dryer. Lipid films were stored under argon gas, stored at -20° C, and used within one week. The lipid film was hydrated with 1 mL of 0.2 M KCl, 1 mM MgCl₂ and 10 mM HEPES pH 7. The hydrated lipid film was then frozen and thawed 5 times before creating large unilamellar vesicles by extruding through a 100 nm polycarbonate membrane (#610005, Avanti) with 11 passes using a liposome extruder (#610020, Avanti). Liposomes were kept on ice and used within two days.

2.7 *Determining suitable wavelengths for the ANTS / DPX assay*

The spectra shown in Figure 3.3A were measured on the double excitation monochromator PTI fluorometer. Samples were measured in 300 μ L of 0.2 M KCl, 1 mM MgCl₂ and 10 mM HEPES pH 7. 100 μ M ANTS emission was measured between 400 and 650 nm with 340 nm excitation and 2 nm bandpass for excitation and emission. ANTS excitation spectra was measured from 300 to 450 nm using 565 nm emission. No blank subtraction was necessary due to high fluorescence of the sample. DAC spectra were measured for 200 nM tBid-DAC, with 2 nm bandpass for excitation and emission. Emission was measured from 375 to 550 nm exciting at 360 nm; excitation was measured from 250 to 450 nm while measuring the emission at 470 nm. A buffer blank was subtracted from the spectra. NBD spectra were obtained for 500 nM 126C-Bax-NBD using 5 nm bandpass. NBD emission scan was measured from 485 to 650 nm, while exciting at 470 nm. NBD excitation was measured from 300 to 550 nm, while measuring emission at 565 nm.

2.8 *Bax and tBid functional assay*

For the functional ANTS/DPX release assay, 1 mg of mitochondrial lipids was hydrated with 1 mL 45 mM DPX (#X1525, Invitrogen) and 12.5 mM ANTS (#A350, Invitrogen) with 135 mM KCl, 1 mM MgCl₂ and 10 mM HEPES pH 7 in a 10 mL

borosilicate glass test tube. This molarity of KCl was used in order to maintain an isotonic concentration for the liposomes with the entrapped ANTS and DPX, since all assays were performed in 200 mM KCl. The lipid mixture was frozen and thawed 5 times, then extruded 11 times through a 0.1 μm polycarbonate membrane. After extrusion, liposomes were isolated from the unentrapped ANTS and DPX by gel filtration over a 12 mL CL2B column equilibrated with 0.2 M KCl, 1 mM MgCl_2 , and 10 mM HEPES pH 7. Liposome containing fractions were distinguished by eye and usually eluted in a 2 mL volume in the 4th and 5th fractions. Since the original 1 mL volume of liposomes was collected in 2 mL after removing the unentrapped ANTS and DPX, the liposome concentration was assumed to be half of what it was before gel filtration. ANTS/DPX release measurements were made using a SAFIRE platereader (TECAN) in a 96 well quartz plate (#730.009-QG, Hellma). 25 μL of ANTS/DPX containing liposomes (50 μM lipid) was added to 275 μL buffer of 0.2 M KCl, 1 mM MgCl_2 , 10 mM HEPES pH 7. Initial liposome fluorescence was measured exciting the ANTS at 355 nm and reading the emission at 490 nm from the bottom of the plate using 12 nm bandwidths. If proteins were labeled with NBD, the wavelengths used to measure ANTS were 355 nm excitation and 490 nm emission with 12 nm bandpass. If proteins were labeled with DAC, the wavelengths used to measure ANTS were 340 nm excitation and 550 nm emission with 12 nm bandpass. Proteins were added (100 nM Bax and 20 nM tBid unless noted otherwise) and release was measured over two hours before lysing the liposomes with 0.5% Triton X-100. Release was calculated based on fluorescence emission using the formula:

$$\text{Release} = (F - F_{\text{init}}) / (F_{\text{lysed}} - F_{\text{init}}) * 100\%$$

For determining the relative activity of the mutants, the following formula was used:

$$\text{Activity} = (\text{Release}_{\text{mutant}} - \text{Release}_{\text{lipos}}) / (\text{Release}_{\text{wildtype}} - \text{Release}_{\text{lipos}}) * 100\%$$

where $\text{Release}_{\text{lipos}}$ was the average release of the liposomes alone in that particular experiment and $\text{Release}_{\text{wildtype}}$ was the release caused by 100 nM wildtype Bax and 20 nM wildtype tBid in that particular experiment.

2.9 Pore size assay

1 mg mitochondrial like lipid was hydrated with 1 mL 0.2 M KCl, 1 mM MgCl₂, 10 mM HEPES pH 7, as well as 0.4 mg Betaphycoerythrin (#100301, Cyanotech), 0.4 mg Allophycocyanin (#100300, Cyanotech), 0.5 mg 3000 Da Fluorescein-dextran (#D3305, Invitrogen) and 0.75 mM MPTS (#85725, Anaspec). MPTS concentration determined by using an extinction coefficient of 29,000 M⁻¹cm⁻¹ at 404 nm. Liposomes were frozen and thawed 3 times and extruded through a 0.1 μm polycarbonate membrane 10 times. Only 3 freeze thaw cycles were used in order to minimize loss of Allophycocyanin fluorescence, which is sensitive to freezing and thawing. Unencapsulated fluorophores were removed by gel filtration over a 12 mL CL2B column equilibrated with 0.6 M KCl, 1 mM MgCl₂ and 10 mM HEPES pH 7. Liposomes were then diluted so the assay buffer was 300 μL 0.2 M KCl, 1mM MgCl₂ and 10 mM HEPES pH 7. The indicated amounts of Bax and tBid were added and incubated at 37° C for 3 hours. After incubation, the extent of

fluorophores release was determined by gel filtration over a 4 mL CL2B column. 24 350 μ L fractions were collected in a 96 well plate (Costar #3370, Corning) and Triton X-100 was added to 0.5% from a 10% stock solution to all fractions in order to remove a high local concentration quenching effect observed in the liposome fractions. Fluorescence was measured on the TECAN from the bottom with 12 nm slit widths for emission and excitation. MPTS was excited at 405 nm and measured at 435 nm; the fluorescein-dextran was excited at 495 nm and measured at 522 nm; the Betaphycoerythrin was excited at 545 nm and measured at 575 nm; and the Allophycocyanin was excited at 610 nm and measured at 660 nm. After background subtraction, the fraction release was calculated as:

$$[1 - (\Sigma \text{Fluorescence}_{\text{first 7 fractions}} / \Sigma(\text{Fluorescence}_{\text{first 22 fractions}}))]]$$

The release was expressed taking into account the amount of release caused by the liposomes alone using the formula:

$$(\text{Release} - \text{Release}_{\text{liposomes}}) / (1 - \text{Release}_{\text{liposomes}}) * 100\%$$

Where *Release* represents the fraction release for each fluorescence channel at the particular protein concentration and *Release_{liposomes}* represents the fraction release of liposomes alone for the same fluorescence channel.

When developing this assay, several different fluorophores were assessed for suitability. One strategy was to label proteins with FITC and verify their release from liposomes. In this procedure, several milligrams of protein were labeled at room

temperature for two hours in 1 mL at pH 9.5 with 200 μ M FITC (from a DMSO solution, assuming FITC extinction coefficient of 75,000 in 0.1 M NaOH). The reaction was then quenched with 10 mM Tris pH 8. The sample was then extensively dialyzed in 0.3 M KCl, 10 mM HEPES pH 7 and 1 mM DTT to remove free dye. BSA, trypsin inhibitor, cytochrome C and thyroglobulin were labeled in this manner. These labeled proteins, as well as the small ANTS and NADH fluorophores were determined to be unsuitable for the assay. NADH was not bright enough and ANTS precipitated the other proteins coencapsulated in the liposomes. The FITC labeled proteins were also not ideal since they were not bright enough (cytochrome C, thyroglobulin) or they did not display favourable CL2B gel filtration profiles (BSA, trypsin inhibitor).

2.10 Bax-NBD steady state measurements and CL2B and CHAPS gel filtration

100 nM 126C-Bax-NBD was incubated at 37° C with or without 20 nM tBid and liposomes (125 μ M lipid) in a buffer of 0.2 M KCl, 1 mM MgCl₂ and 10 mM HEPES pH 7. NBD emission was monitored on the PTI fluorometer using 5 nm excitation bandwidth at 475 nm and 10 nm emission bandwidth at 530 nm. The liposome background was subtracted from the data before it was normalized to the initial Bax-NBD emission.

To test targeting, a 300 μ L reaction was subjected to gel filtration over a 400 μ L CL2B column. 300 μ L fractions were collected and 10 μ L of each fraction was subjected to SDS PAGE. The proteins in the gel were then transferred to a nitrocellulose membrane

by applying 50 mA current for 1 hour per gel. Following transfer, the nitrocellulose membrane was blocked for 30 minutes in blocking buffer (140 mM NaCl, 10 mM KPO₄ pH 7.4, 0.02% azide, 5 g/L skim milk powder). The membrane was then incubated with a 1 in 10,000 dilution of mouse monoclonal anti Bax antibody, 2D2, in a monoclonal antibody buffer (140 mM NaCl, 10 mM KPO₄ pH 7.4, 0.02% azide, 0.1% Triton X-100, and 1% BSA) overnight at 4° C. The antibody was then collected for reuse and the membrane was washed three times with TBS-T (10 mM Tris-CL pH 7.4, 0.5 M NaCl, 0.2% Tween-20) for at least 10 minutes per wash. A secondary horseradish peroxidase donkey anti mouse antibody was then incubated with the membrane for two hours at room temperature at a 1 in 5000 dilution in TBS-T with 1% BSA. The secondary antibody was discarded and the membrane was again washed three times in TBS-T for 10 minutes per wash. Enhanced chemical luminescent reagents (Western Lightning, PerkinElmer) were added as per the manufacturer recommendation and the membrane was exposed to film (#CLEC810, Clonex) in a dark room. The film was developed and scanned.

For determining the status of Bax oligomerization, 100 nM 126C-Bax-NBD and liposomes (125 µM lipid) were lysed with 2% CHAPS after being incubated at 37° C with or without 20 nM tBid in a buffer of 0.2 M KCl, 1 mM MgCl₂ and 10 mM HEPES pH 7. 250 µL of sample was then subjected to FPLC (AKTA FPLC unit, GE Health) using a Superdex 200 column (GE Health) equilibrated with 2% CHAPS, 0.3 M KCl, 10 mM HEPES pH 7 as the running buffer. The sample loading loop was emptied with 7.5

mL of running buffer and 800 μ L fractions were then collected. Immunoblots of the fractions were prepared as described above, with the first sample of the blot starting at the third eluted fraction from the FPLC.

2.11 Calculation of Forster distance for DACM and IANBD

Forster distance was calculated using the formula:

$$R_0 = 0.211 [k^2 n^{-4} Q_D J(\lambda)]^{1/6} \quad (\text{Lakowicz, 1999, pp. 369})$$

R_0 is the Forster distance in angstroms, k^2 is the orientation factor and is assumed to be 2/3, n is the refractive index of the medium, assumed to be 1.4, and Q_D is the quantum yield of the donor, reported as 0.82 (Ogawa et al., 1979). $J(\lambda)$, the overlap integral was calculated as:

$$J(\lambda) = \frac{\int_0^\infty F_D(\lambda) \epsilon_A(\lambda) \lambda^4 d\lambda}{\int_0^\infty F_D(\lambda) d\lambda}$$

$F_D(\lambda)$ is the emission spectra of the donor as a function of wavelength and $\epsilon_A(\lambda)$ is the extinction coefficient of the acceptor, as a function of wavelength. The overlap integral was calculated from 350 nm to 550 nm.

2.12 *tBid to Bax FRET and Bax to Bax FRET*

Where FRET was measured over time, background was collected for liposomes (125 μ M lipid) alone at 37° C in 1 mL 0.2 M KCl, 1 mM MgCl₂, 10 mM HEPES pH 7 in the PTI fluorometer with stirring at 300 RPM. 20 nM DAC labeled tBid was then added and equilibrated before 100 nM 126C-NBD Bax was added. Emission was monitored at 460 nm, exciting at 380 nm using 5 nm slitwidths. The FRET signal was corrected for background and normalized to the starting point as soon as Bax was added. Bax to Bax FRET was measured in a similar manner, except that 20 nM 134C-Bax-DAC or 20 nM 126C-Bax-NBD was initially added to the liposomes and equilibrated before 100 nM 126C-Bax-NBD and 20 nM tBid were added and measurement was started immediately.

For endpoint tBid to Bax FRET measurements, Bax was preinserted by incubating either 100 nM 126C-Bax-NBD or 100 nM wildtype Bax with 50 μ M Bid BH3 peptide (Dalton Chemical Laboratories) in a 300 μ L reaction for two hours at 37° C with liposomes (125 μ M lipid). The amino acid sequence of the peptide was acetyl-EDIIRNIARHLAQVGDSMDR-amide, corresponding to the BH3 region, from residue 80 to 99 of human Bid. Background fluorescence emission was recorded and then 20 nM tBid-DAC or 20 nM G94E-tBid-DAC was added to either the preinserted 126C-Bax-NBD, the preinserted wildtype Bax, 100 nM wildtype Bax or 100 nM 126C-Bax-NBD and incubated for 30 minutes at 37° C. DAC emission was then measured and FRET efficiency was calculated as:

$$\left[1 - \frac{F_{tBid \text{ with labeled Bax}}}{F_{tBid \text{ with unlabeled Bax}}}\right] * 100\%$$

2.13 3 fluorophore simultaneous analysis

The emission and excitation spectra for tBid-DAC and 126C-Bax-NBD were obtained as described earlier. The Tb-DPA emission and excitation spectra were obtained from 50 μM Tb and 150 μM DPA in 0.2 M KCl, 1 mM MgCl_2 and 10 mM HEPES pH 7 using 2 nm bandwidths. The emission scan was obtained using 280 nm excitation and the excitation scan was generated using emission at 490 nm.

A 1 mg mitochondrial lipid film was hydrated with 0.2 M KCl, 1 mM MgCl_2 , 10 mM HEPES pH 7, as well as 1 mM TbCl_3 and 3 mM DPA. Liposomes were frozen and thawed 5 times, extruded 10 times and then unencapsulated Tb and DPA was removed by gel filtration over a 12 mL column.

Fluorescence measurements were made on the double excitation PTI fluorometer using multidye setting at 37° C with stirring. In this configuration, each of the 3 fluorophores channels was periodically measured at the shortest possible interval. Each cycle took approximately 15 seconds to measure all 3 fluorophores. The Tb channel was monitored at 280 nm excitation and 490 nm emission; the DAC channel was monitored at 380 nm excitation and 460 nm emission; and the NBD channel was monitored at 475 nm excitation and 530 nm emission. 5 nm excitation and emission bandwidths were used with 1 second integration time and no pause between collecting the data points. 200 μL liposomes (125 μM lipid) were added to 800 μL of 0.2 M KCl, 1 mM MgCl_2 and 10 mM

HEPES pH 7 along with 2 mM EDTA (to quench the Tb upon liposome permeabilization) After collecting the liposome background for the different channels, 20 nM tBid-DAC or 20 nM ¹³⁴C-Bax-DAC was added and allowed to equilibrate. After equilibration of the DAC labeled protein, 100 nM NBD labeled Bax was added and the 3 channel measurement was started immediately. After the reaction was completed, CHAPS was added to 0.5% to lyse the liposomes. Data were normalized to their initial values, taking the liposome only background into consideration, except for the Tb channel, which used the fluorescence of the CHAPS lysed liposomes for the background (effectively showing the amount of Tb release).

2.14 Blueshift and fluorescence increase assays

A background emission spectrum was measured at room temperature on the dual excitation monochromator PTI fluorometer of a 250 μ L sample with liposomes (125 μ M lipid) 0.2 M KCl, 1 mM MgCl₂, and 10 mM HEPES pH 7, from 500 to 600 nm using 475 nm excitation and 10 nm excitation and emission bandwidths. The fluorescence of a 100 nM NBD labeled Bax mutant was then measured at room temperature either without tBid, or with 2 hours incubation with 20 nM tBid at 37° C. Liposome background was subtracted from all emission spectra. Increase was calculated as F_{tBid}/F_0 , where F_{tBid} was the maximum value in the emission spectra after incubation with tBid, and F_0 was the maximum value in the emission spectra without incubation with tBid. ΔF was calculated as $(F_{\text{tBid}} - F_0)/(\text{fraction labeling})$, where the fraction labeling is shown in Table 3.2. The

change was divided by the fraction labeling to compensate for a change in residues that were not labeled equally. The blueshift was calculated as $\lambda_{\text{no tBid}} - \lambda_{\text{tBid}}$, where λ_{tBid} was the wavelength of the maximum emission value after incubation with 20 nM tBid and liposomes for 2 hours and $\lambda_{\text{no tBid}}$ was the wavelength of the maximum emission value for Bax with liposomes, but without incubation with tBid.

2.15 Lifetime assays

Lifetimes were measured on a frequency domain lifetime fluorometer (Chronos, ISS). Before measuring NBD labeled Bax mutants, the lifetime of Coumarin-6 (#546283, Sigma) in absolute ethanol was measured using fluorescein in 0.1 M NaOH as a reference standard with a 4 ns lifetime. The Coumarin-6 lifetime was verified to have a single exponential lifetime of 2.5 ns using the Vinci analysis software. A 450 +/- 32.5 nm bandpass filter (#25750, Chroma) was used to isolate the 473 nm laser diode emission, and a 525 +/- 20 nm bandpass filter (Brightline, Semrock) was used for the emission filter. The emission polarizer was set at the magic angle (54.7°). For Bax measurements, 100 nM labeled Bax was assayed in 250 μL 0.2 M KCl, 1 mM MgCl_2 and 10 mM HEPES pH 7 with liposomes (125 μM lipid) with or without 2 hour incubation with 20 nM tBid at 37° C. 20 frequencies were collected between 1 and 300 MHz and the data was analyzed with the Vinci software (ISS). The data shown is the mean of three experiments, with the

values representing the intensity weighted means of a three component fit. See Supplementary Table 1 for detailed fitting parameters.

2.16 Quenching Analysis

For cobalt and iodide quenching, quenching was analyzed in a buffer of 0.2 M KCl, 1 mM MgCl₂, 10 mM HEPES pH 7, liposomes (125 μM lipid) and 100 nM labeled Bax with or without 2 hour incubation with 20 nM tBid at 37° C. Bax-NBD emission was monitored as cobalt or iodide was titrated on the PTI double excitation monochromator with 10 nm bandpass excitation at 475 nm and 10 nm bandpass emission at 530 nm at room temperature. For cobalt quenching, cobalt chloride was titrated in 0.5 mM increments ranging from 0 to 2.5 mM, from a 125 mM stock solution. For iodide quenching, potassium iodide was titrated in 20 mM increments from 0 to 100 mM, using a 2 M stock solution supplemented with 2 mM sodium thiosulfate to prevent oxidation. Fluorescence emission values of the NBD labeled Bax mutant at varying quencher concentrations were then expressed as F_0 / F , where F_0 is the initial intensity, and F is the decreased emission of Bax-NBD with the quencher. Bimolecular quenching constants were calculated dividing the slope of the quenching of 20 mM KI by the intensity weighted mean lifetime. See supplementary Figure 3 for representative quenching curves for the mutants. The bimolecular cobalt quenching constants were calculated by the slope of only the first 0.5 mM cobalt added divided by the same average lifetimes. The graph depicting the fold efficiency of cobalt quenching was determined by dividing the

bimolecular quenching constant of cobalt by the bimolecular quenching constant of iodide. This is a lifetime independent calculation and equivalent to dividing $F_{0.5\text{mMCo}}/F_0/c_{\text{Co}}$ by $F_{20\text{mMKI}}/F_0/c_{\text{KI}}$, where F_0 was the initial emission, $F_{0.5\text{mMCo}}$ was the emission at 0.5 mM cobalt, and $F_{20\text{mMKI}}$ was the emission at 20 mM KI, C_{Co} was 0.5 mM and C_{KI} was 20 mM. For the cobalt quenching graph showing the quenching for the initial and subsequent cobalt titration after incubation with tBid, the bimolecular quenching constants were determined by the slope of the entire quenching plots in the case of the Bax mutants without incubation with tBid. In the case where tBid was added, the bimolecular quenching constants were calculated from the slope of the first titration point, from 0 to 0.5 mM cobalt, or from the slope of the titration between 1 to 2.5 mM cobalt where indicated.

For lipid quenchers, lipid films were made in the same manner as mitochondrial like liposomes, except that 0.15 mg of egg phosphatidylcholine was replaced with 0.15 mg of either 16:0 phosphatidylcholine (#850355C, Avanti), 16:0 phosphatidylcholine-TEMPO (#810606C, Avanti), 16:0 phosphatidylcholine-5 DOXYL (#810601C, Avanti), 16:0 phosphatidylcholine-12 DOXYL (#810600C, Avanti), or 16:0 phosphatidylcholine-16 DOXYL (#810604, Avanti). 100 nM Bax-NBD was then incubated with 20 nM tBid and each of the different quenching liposomes (125 μM lipid) in 0.2 M KCl, 1 mM MgCl_2 and 10 mM HEPES pH 7 for 2 hours at 37° C. Fluorescence was measured in a quartz plate, exciting on the SAFIRE at 475 nm, and measuring at 530 nm with 12 nm bandwidths. Quenching was calculated as:

$$[1 - (F_{dox} - F_{lipos}) / (F_{no\ dox} - F_{lipos})],$$

where F_{lipos} was the fluorescence emission of liposomes alone, F_{dox} was the fluorescence of the labeled Bax mutant in the presence of the lipidic quencher, and $F_{no\ dox}$ was the fluorescence in the absence of the lipidic quencher.

3 Results

3.1 Cloning, protein purification and labeling

20 Bax mutants and one Bid mutant were cloned. To generate most Bax mutants, restriction enzyme sites were used as shown in Figure 3.1A. By introducing silent sites, oligonucleotides could be ordered and directly ligated into the Bax expression backbone. The pBS vector used for expressing the intein fusion protein for Bax mutants is shown in Figure 3.1B.

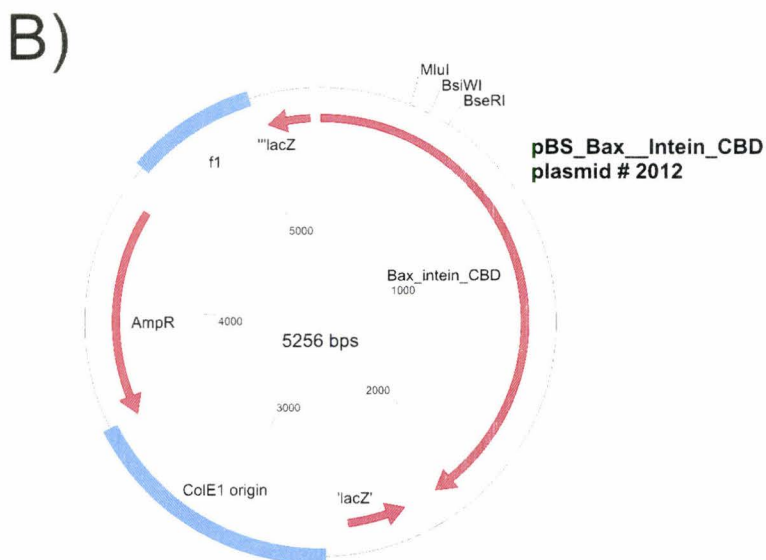
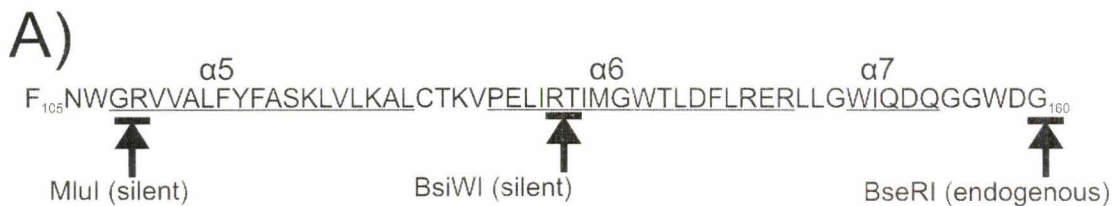


Figure 3.1: Cloning Bax single cysteine mutants

A: Amino acid sequence of the sequence around the Bax pore-forming domain showing the location of the introduced silent sites or the endogenous restriction site. The helix numbers are indicated above the sequence and are underlined. The numbers at the ends of the sequence show the residue number.

B: pBS plasmid map for Bax mutants. This mutant was used for cloning and contained the indicated silent sites and no cysteines.

Some other Bax mutants were subcloned into the pBS bacterial expression vector from existing plasmids. The list of mutants created and how they were generated is shown in Table 3.1.

Table 3.1: List of mutant plasmids generated		
Plasmid ID	Mutation	Method used to create plasmid
2012	Bax, Cys neg, new silent sites	Quikchange
2013	Bax V111C	Ligated oligos directly using MluI and BsiWI sites
2014	Bax L113C	Ligated oligos directly using MluI and BsiWI sites
2015	Bax F114C	Ligated oligos directly using MluI and BsiWI sites
2016	Bax Y115	Ligated oligos directly using MluI and BsiWI sites
2017	Bax F116C	Ligated oligos directly using MluI and BsiWI sites
2018	Bax A117C	Ligated oligos directly using MluI and BsiWI sites
2019	Bax K119C	Ligated oligos directly using MluI and BsiWI sites
2020	Bax L120C	Ligated oligos directly using MluI and BsiWI sites
2021	Bax P130C	Ligated oligos directly using BsiWI and BseRI sites
2022	Bax M137C	Ligated oligos directly using BsiWI and BseRI sites
2023	Bax W139C	Ligated oligos directly using BsiWI and BseRI sites

2024	Bax T140C	Ligated oligos directly using BsiWI and BseRI sites
2025	Bax L141C	Ligated oligos directly using BsiWI and BseRI sites
2120	Bax F143C	Ligated oligos directly using BsiWI and BseRI sites
1989	Bax A124C	Subcloned from plasmid 1674
1991	Bax T127C	Subcloned from plasmid 1838
1990	Bax K128C	Subcloned from plasmid 1839
1993	Bax I136C	Subcloned from plasmid 1676
1992	Bax L144C	Subcloned from plasmid 1678
2121	Bid 94E	Quikchange

Bax mutants were expressed in a similar manner as described previously (Yethon et al., 2003). Cleaving was induced with hydroxylamine instead of betamercaptoethanol, since it was discovered that this could greatly reduce nonspecific IANBD labeling (Supplementary Figure 1). Figure 3.2Ai shows a typical Coomassie stain for one of the purified and labeled mutants, 126C-Bax-NBD. The molecular size ladder shows that the purified Bax was the correct size for a 21 kDa protein, as it is close to the 22.7 kDa lactoglobulin marker (lactoglobulin is actually 18.4 kDa, but we have found that if the marker is prestained, it migrates as a 22.7 kDa protein). Figure 3.2Aii shows a NBD fluorescence scan for the same gel shown in Figure Ai. As expected, the molecular markers did not appear since they are not fluorescent at the wavelengths of NBD. The single band in the fluorescence scan of the gel shows the Bax was highly pure and was the only source of NBD fluorescence. An absorbance scan for this protein is shown in Figure 3.2Aiii. The absorption peak at 280 nm is from absorption of tryptophan and

tyrosine residues in Bax, while the peaks at 350 nm and 475 nm are from the covalently attached NBD. Supplementary Figure 2 shows the absorption spectra for all the NBD labeled Bax mutants used in this study. Figure 3.2Bi shows the purification for G94E-tBid-DAC. This tBid was labeled at its endogenous cysteine at residue 126. After the molecular weight marker, the first lane shows labeled Bid, before cleavage with caspase-8. The second lane shows the cleaved Bid, with the higher fragment being tBid, or the p15 fragment. The final lane shows the purified, labeled tBid. The absorption scan for the purified DAC labeled tBid is shown in figure 2Bii. The DAC peak is apparent at 375 nm. Note that tBid does not contain any tryptophan residues to create an absorption peak at 280 nm.

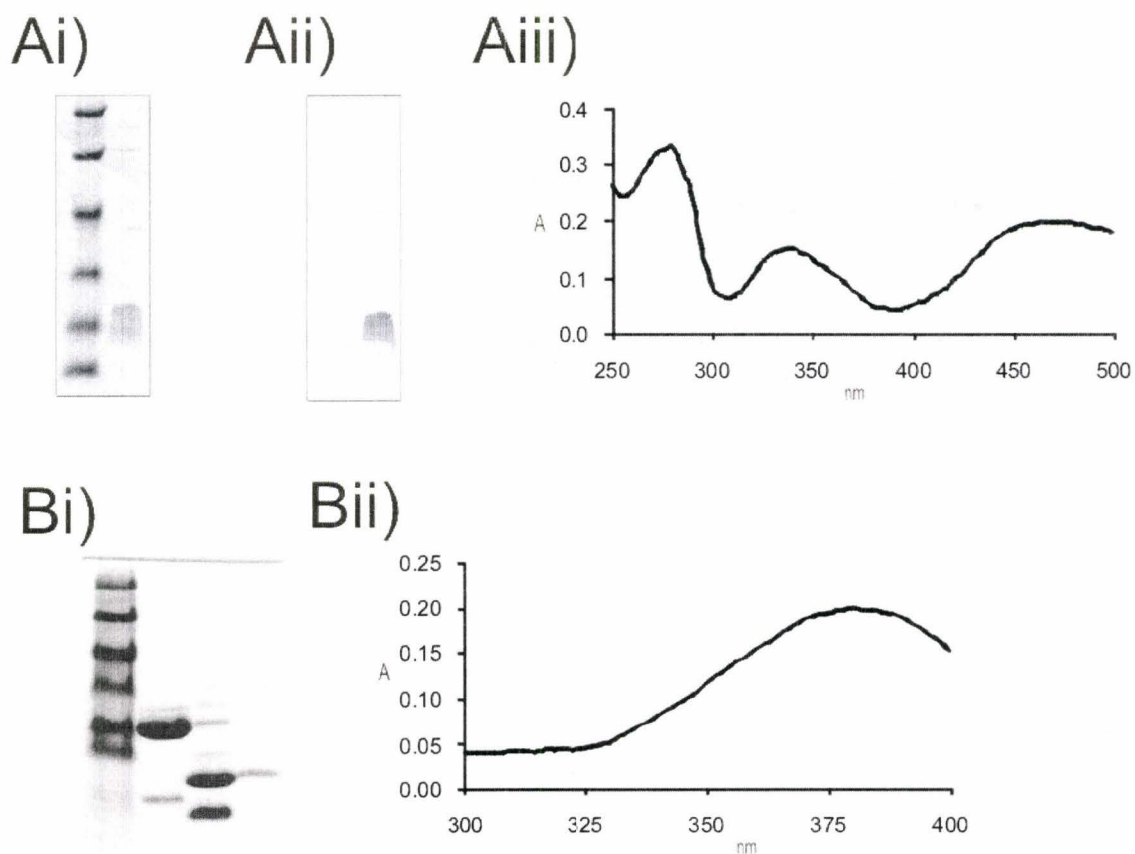


Figure 3.2: Purified and labeled Bax and tBid

Ai) Coomassie stain of SDS PAGE loading 10 μ L (~150 pmol) of purified and labeled Bax C126-NBD. The first lane shows molecular weight markers. When Bax purifications were subjected to SDS PAGE, Bax typically did not appear as a sharp band, but as a slightly smeared band.

Aii) Typhoon fluorescence scan of the same SDS PAGE gel prior to Coomassie staining showing NBD emission of labeled Bax.

Aiii) Absorption scan for purified and labeled Bax C126-NBD. This scan was performed after labeling with NBD.

Bi) Coomassie stain of purified and labeled tBid-G94E-DAC. The first lane is the molecular weight marker, the second lane is Bid-G94E-DAC before caspase 8 cleavage (~300 pmol), the third lane is the cleaved Bid-G94E-DAC and the fourth lane is the purified tBid-G94E-DAC. The final purified tBid lane (~40 pmol) appears much lighter since this sample was more dilute being stored in a larger volume and due to nonspecific losses.

Bii) Absorption scan for purified and labeled tBid-G94E-DAC.

Table 3.2 shows the concentrations and labeling efficiencies for the proteins used in this study. Only proteins that were greater than 60% labeled were used for further experiments.

Table 3.2: Bax yields and NBD labeling efficiencies for mutants used in this study			
Plasmid number	Mutation	Labeled Bax concentration	Labeling efficiency
1997	3	4.5 μ M	62%
1999	5	8.4 μ M	70%
2035	47	2 μ M	98%
1732	62	8.2 μ M	98%
1868	66	7.8 μ M	80%
1869	79	6.7 μ M	97%
2015	114	8.4 μ M	71%

2016	115	3.4 μ M	74%
2017	116	3.9 μ M	80%
1734	118	3.4	74%
2020	120	4.1 μ M	99%
1735	122	5.7 μ M	84%
1989	124	4.5 μ M	99%
1731	126	11 μ M	89%
2021	130	4.5 μ M	100%
1736	134	4.3 μ M	75%
1993	136	6.4 μ M	78%
2022	137	7.1 μ M	72%
1737	138	5.7 μ M	71%
2023	139	4.3 μ M	63%
2024	140	5.7 μ M	84%
2025	141	8.8 μ M	74%
1738	142	6.4 μ M	90%
2120	143	4.2 μ M	96%
1992	144	4.2 μ M	96%
1739	175	5.9 μ M	88%

Table 3.3 shows the labeling efficiency of mutants that were purified, but since NBD labeling efficiency was below 50%, these mutants were not used in the study due to complexity in interpreting functional data. It would be difficult to determine whether or not the unlabeled protein retained function if the labeled protein did not.

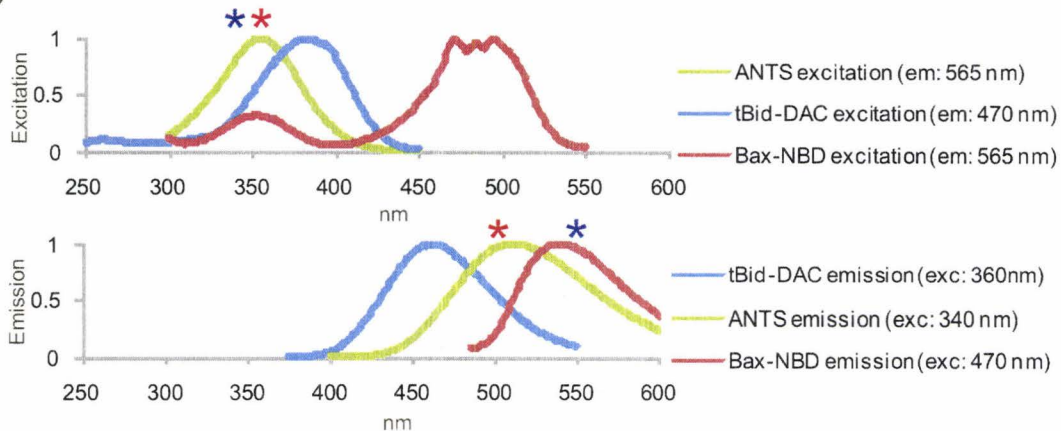
Table 3.3: Bax yields and NBD labeling efficiencies for mutants that were not used in this study

Plasmid number	Mutation	Labeled Bax concentration	Labeling efficiency
2013	111	2.7 μM	37%
2014	113	2.6 μM	57%
2018	117	3.4 μM	39%
2019	119	7.2 μM	35%

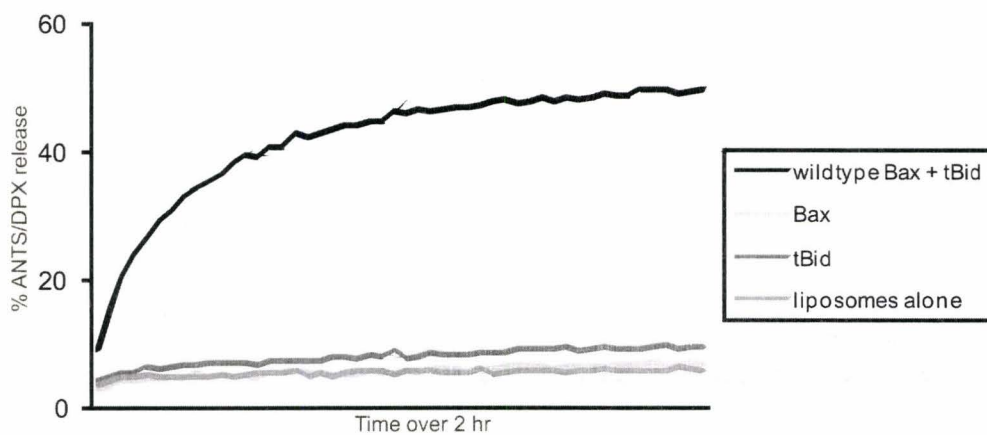
3.2 Functional assay

Slight modifications in the measurement parameters for the ANTS/DPX release assay had to be made to avoid interference from the fluorescently labeled proteins. As seen in Figure 3.3A top panel, the normalized excitation spectra for ANTS (green), DAC (blue) and NBD (red) lie close together, especially ANTS and DAC. The bottom panel shows the normalized emission spectra for these fluorophores. By choosing the appropriate ANTS wavelength of 340 nm excitation and 550 nm emission, DAC labeled proteins could be used in the ANTS/DPX release assay without interfering with the ANTS signal. The ANTS fluorescence was resolved from NBD labeled proteins by measuring ANTS emission below 500 nm, where there was no emission from NBD.

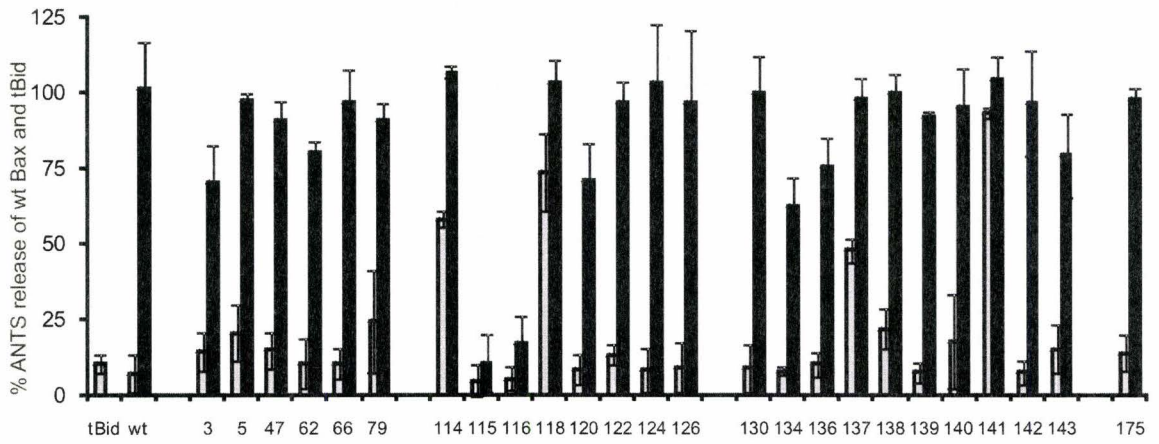
A)



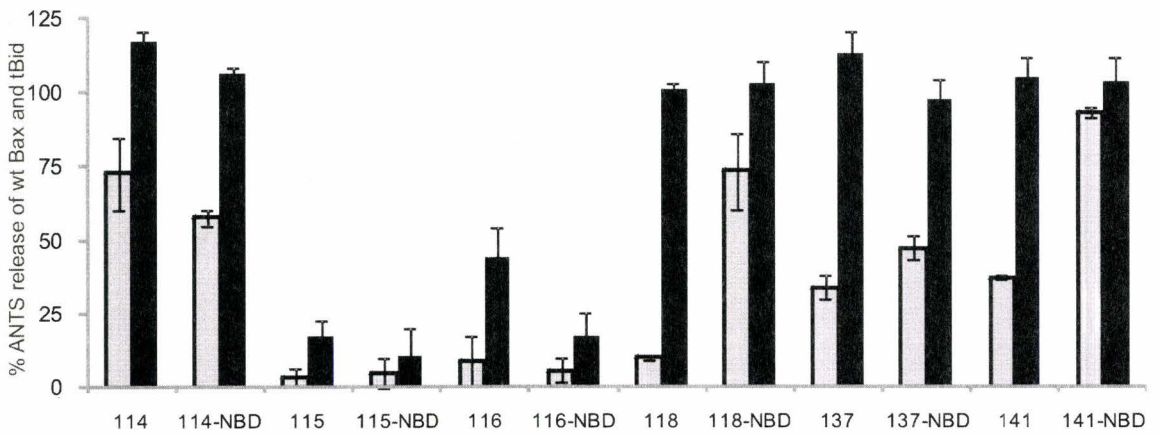
B)



C)



D)



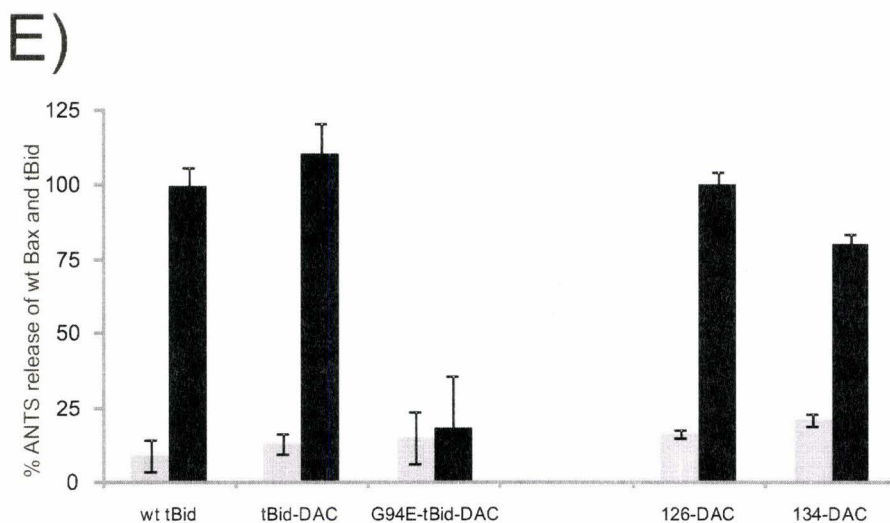


Figure 3.3: Most Bax and Bid mutants behave similarly to wildtype Bax and tBid

A: NBD, ANTS and DAC could be resolved at appropriate wavelengths. Emission and excitation spectra of 500 nM Bax 126C-NBD (red), 1 mM ANTS (green), and 100 nM tBid-DAC (blue). The top panel shows the normalized excitation spectra and the bottom panel shows the normalized emission spectra. Spectra were normalized to maximum peak height. The blue and red asterisks mark where DAC and NBD labeled proteins, respectively, may be excited and emitted without interfering with the fluorescence of the ANTS/DPX assay.

B: Bax and tBid acted synergistically to permeabilize liposomes. Time course of a typical ANTS/DPX release assay. 20 nM tBid and 100 nM Bax, both wildtype and unlabeled proteins were added to ANTS/DPX containing mitochondria like liposomes (50 μ M lipid) and incubated for 2 hours at 37° C.

C: Most, but not all NBD labeled Bax mutants behaved similarly to wild type Bax. Activity of NBD-labeled mutants is shown, normalized to the release of wildtype Bax and tBid over a 2 hour period. Grey bars show 100 nM Bax activity without tBid, black show 100 nM Bax activity with 20 nM tBid. Error bars represent +/- S.D. with n = 3.

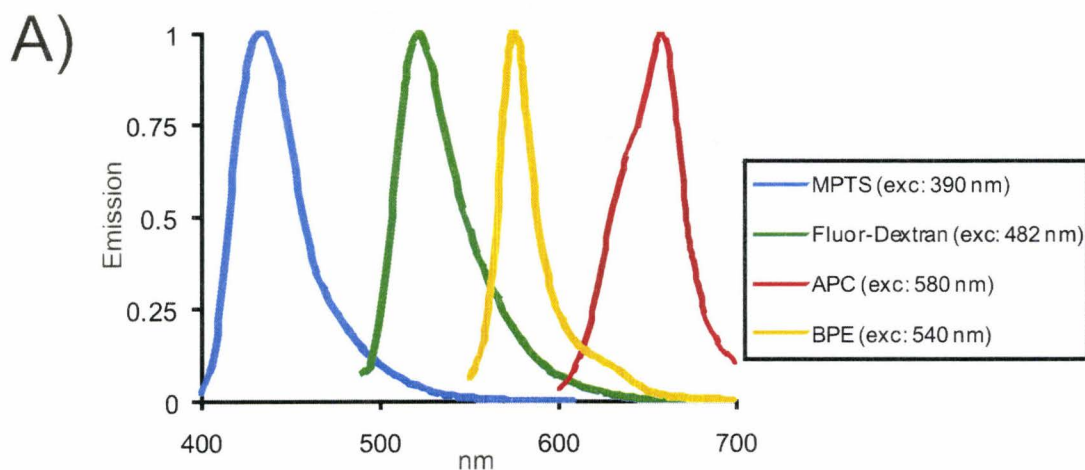
D: Previously unknown mutations altered Bax behaviour. Activity for NBD labeled mutants that displayed altered functionality for labeled and unlabeled proteins. Grey bars show 100 nM Bax activity without tBid, black show 100 nM Bax activity with 20 nM tBid. Activity is normalized to wildtype Bax and tBid activity. Error bars represent +/- S.D. with n = 3.

E: DAC-labeled mutants behaved similarly to wildtype proteins. Activity of DAC labeled proteins compared to wildtype Bax and tBid is shown. Grey bars show 100 nM Bax activity without tBid, black show 100 nM Bax activity with 20 nM tBid. As expected, the BH3 mutated G94E-DAC tBid did not cause much liposome permeabilization with Bax compared to the wt tBid-DAC. Error bars represent +/- S.D. with n = 3.

Figure 3.3B shows the results for a typical ANTS/DPX release assay. 20 nM tBid and 100 nM Bax synergistically combined to permeabilize liposomes. However individually, tBid and Bax did not release much more ANTS/DPX than liposomes alone. Most, but not all of the proteins were not affected by the cysteine mutation or the fluorescent NBD label. Figure 3C shows the release for the NBD labeled mutants described in Table 3.2, relative to the release of wildtype 20 nM tBid and 100 nM Bax. The divisions in the layout of the graph separate residues located towards the N terminus before the pore-forming domain, residues on helix 5, residues on helix 6, and the single Bax mutant with the NBD label on helix 9, 175C-Bax-NBD. Some residues such as 115C-Bax-NBD and 116C-Bax-NBD displayed much less activity compared to wildtype Bax and the other labeled mutants. Figure 3D shows the activity, relative to wildtype Bax and tBid, for these mutants that displayed decreased or increased activity. The activity is shown for both the mutants labeled with NBD and the mutants without NBD labeling. For example, 114C-Bax-NBD without tBid addition (grey bar) caused much more release than wildtype Bax without tBid. Conversely, 115C-Bax-NBD with tBid addition (black bar) resulted in only a fraction of the ANTS/DPX release of wildtype Bax and tBid. Note that with the exception of 118C-Bax-NBD, these misregulated mutants behaved similarly with or without the NBD label. Figure 3E shows the activity for DAC labeled mutants. As can be seen in the figure, the DAC labeled tBid behaved similarly to unlabeled tBid, and labeled 134C-Bax-DAC and 126C-Bax-DAC behaved similarly to wildtype Bax. As expected, the BH3 mutant G94E-tBid-DAC did not cause much release.

3.3 *A novel pore sizing assay*

To estimate the size of the Bax pores, a pore sizing assay was developed. Four fluorophores of different sizes were encapsulated in liposomes. Several fluorophores were evaluated for their suitability for this assay. For a smaller fluorophore, concentrations as low as 1 mM ANTS precipitated coentrapped proteins, and NADH was not a bright enough fluorophore to be detected after liposome isolation. Several proteins were labeled with FITC including BSA, cytochrome C, trypsin inhibitor and Thyroglobulin. Unfortunately, all these proteins either were too dim to be detected (even when hydrating the liposomes with several milligrams per mL) or did not separate from the liposomes over the CL2B column. Eventually, four suitable fluorophores were discovered. Figure 3.4A shows the emission spectra of the suitable fluorophores. The emissions of the fluorophores did not overlap spectrally. Part B shows the approximate sizes of the encapsulated fluorophores.



B)

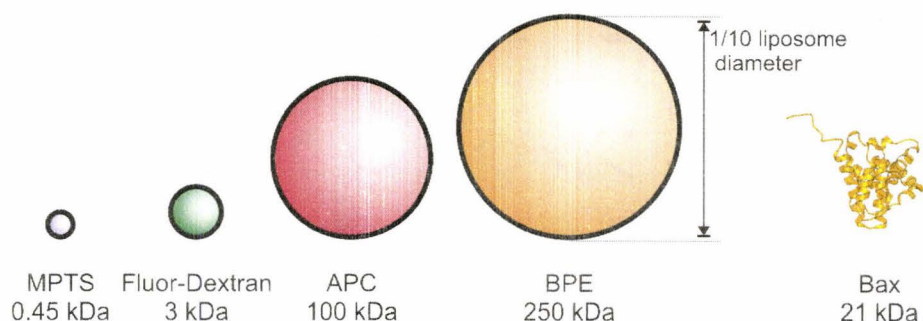


Figure 3.4: Fluorophores used to estimate pore size

A: Emission spectra of the four fluorophores of different sizes used in this assay – MPTS, fluorescein labeled dextran (Fluor-Dextran), Allophycocyanin (APC) and Betaphycoerythrin (BPE). Spectra were normalized to maximum peak height and measured individually for each fluorophore. The excitation wavelength used is indicated in the legend.

B: Relative diameters of fluorophores based on their molecular mass. This is an approximation based on the relationship that the diameter cubed is proportional to the molecular weight. The spheres do not represent the actual shapes of the fluorophores. Bax is shown as well at the same relative scale. The BPE was calculated as having a 10 nm diameter, 1/10th the length of the 100 nm liposome diameter.

3.4 *Bax pore size is not homogeneous*

Figure 3.5Ai shows the gel filtration profile for the different fluorescent channels for liposomes containing the four fluorophores, after incubation with 200 nM Bax. The peak in fraction 5, 6 and 7 corresponds to the encapsulated protein that had not been released by Bax. Figure 3.5Aii shows the gel filtration profile for the liposomes when 20 nM tBid was added to activate the Bax. The reduced peak in fractions 5, 6 and 7 still corresponds to the signal from liposomes that have not released their contents, while the increased signal from the later fractions came from the released fluorophores. Part B shows the quantified release for various Bax concentrations. The gradient of increasing release for smaller fluorophores demonstrates that Bax formed pores that varied in size.

Some liposomes had pores big enough to release large 250 kDa proteins, while others had pores large enough to only release 3 kDa fluorophores.

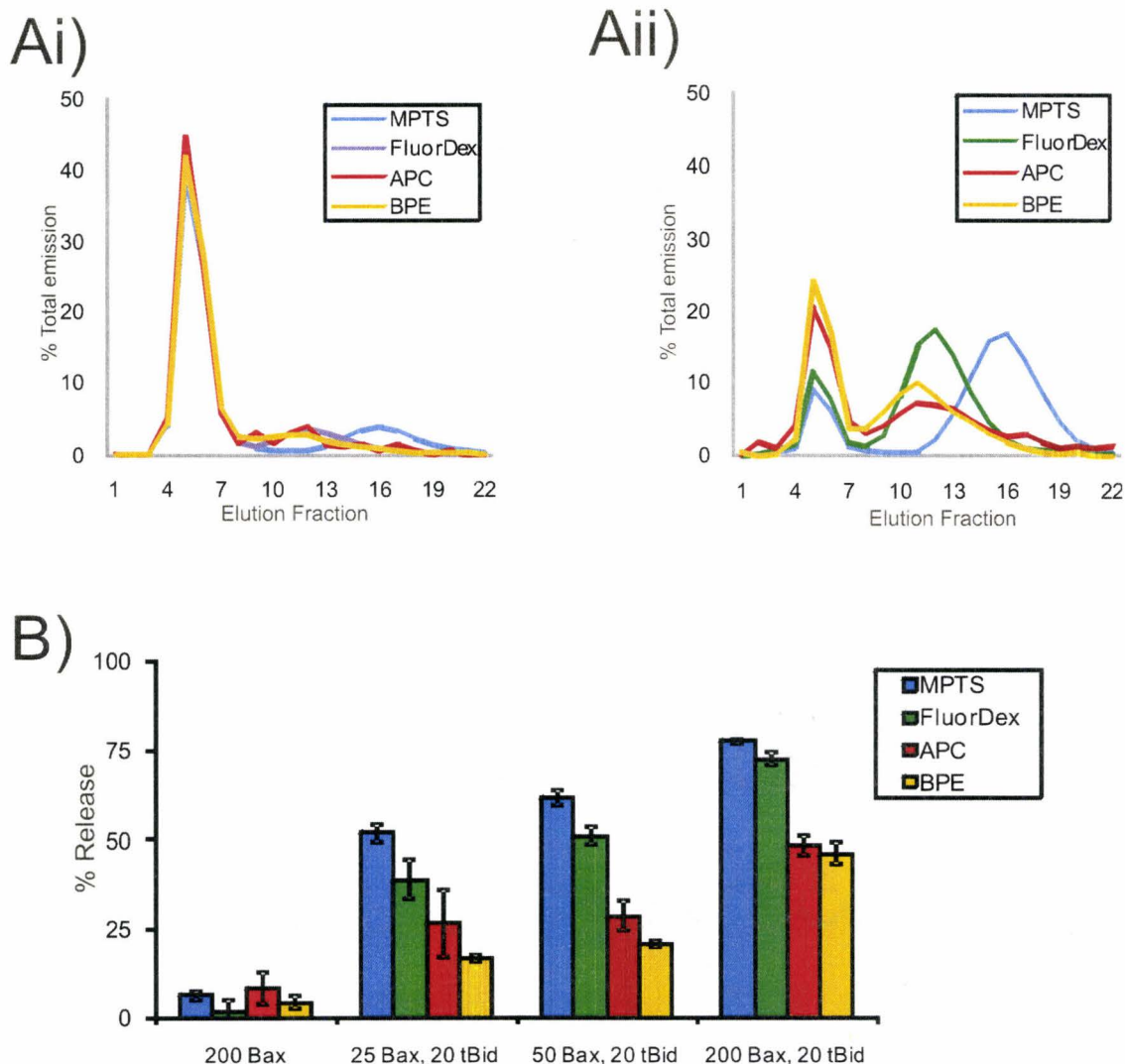


Figure 3.5: Bax pores vary in size

Ai: Mitochondria like liposomes containing the four fluorophores were incubated with 200 nM Bax for 3 hours. The mixture was subjected to gel filtration and the fluorescence of the different fluorophores was recorded. Liposome fractions correspond to fractions 1-7.

Aii : Liposomes containing the four fluorophores were incubated with 200 nM Bax with the addition 20 nM tBid for 3 hours. The mixture was subjected to gel filtration and the fluorescence of the different fluorophores was recorded. Liposome fractions correspond to fractions 1-7 and the later fractions correspond to the released fluorophores.

B: Quantification for release experiments after 3 hours of incubation with the liposomes and the indicated proteins. Release was corrected for the amount of release of liposomes alone in a separate experiment. Error bars represent +/- S.D. with n = 3.

3.5 Behaviour of NBD-labeled Bax

Figure 3.6A shows the fluorescence increase for 126C-Bax-NBD when tBid was added (dark line) in the presence of liposomes. The increase in NBD emission for this residue increased over 2.5 fold in 15 minutes. Without the addition of tBid, the NBD emission did increase, but by a relatively small amount. This is consistent with the small amount of ANTS/DPX release observed by Bax alone. The increase was due to the labeled residue moving into a more hydrophobic environment.

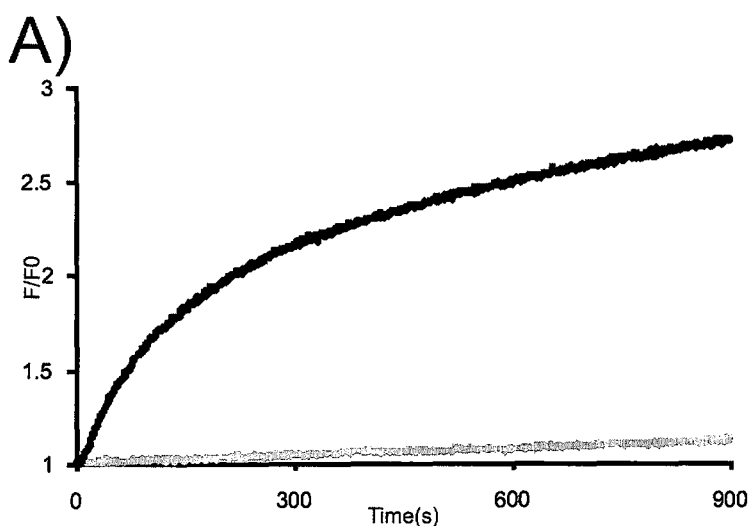




Figure 3.6 Effect of tBid on Bax

A: tBid caused 126C-Bax-NBD emission to increase in the presence of liposomes. 100 nM 126-NBD Bax was incubated with mitochondria like liposomes (125 μ M lipid) at 37° C with stirring. The dark line shows NBD emission with the addition of 20 nM tBid. The grey line shows the emission in the presence of liposomes alone. The emission was normalized to its initial value after tBid was added.

B: tBid caused Bax to migrate to liposomes. Immunoblot using the 2D2 antibody for 100 nM 126C-NBD-Bax after CL2B gel filtration after incubation with mitochondria like liposomes (125 μ M lipid) with or without 20 nM tBid. The line at the left of the blot shows the migration of a 22.7 kDa marker protein.

C: tBid caused Bax to form CHAPS resistant oligomers. Immunoblot using the 2D2 antibody for 126-NBD Bax after solubilization with 2% CHAPS and FPLC gel filtration over a Superdex 200 column with 2% CHAPS in the running buffer. The line at the left of the blot shows the migration of a 22.7 kDa marker protein.

The increase in 126C-Bax-NBD fluorescence occurred as Bax migrated to liposomes. Figure 3.6B shows Bax immunoblots for the NBD labeled protein after CL2B gel filtration. CL2B gel filtration separates liposomes from free protein. The liposomes eluted in the earlier fractions 5 and 6, and this is where the 100 nM Bax eluted when 20 nM tBid was added (top panel). The unbound protein eluted in fractions 9-12, which is where the Bax eluted when tBid was not added (bottom panel).

Along with translocation to liposomes, tBid induced Bax to form CHAPS resistant oligomers. Figure 3.6C shows 3 immunoblots showing an FPLC gel filtration profile performed using 2% CHAPS. The top panel shows that without tBid addition, 126C-Bax-NBD eluted in the later fractions. The middle panel shows that after 15 minutes, Bax that had tBid added formed some higher order oligomers. The bottom panel shows the formation of higher order oligomers continued after 15 minutes and that by 2 hours most of the Bax formed CHAPS resistant oligomers.

3.6 *DACM and IANBD FRET pair*

Since we had verified that many Bax mutants could be labeled without significant change in function, a suitable FRET donor or acceptor probe was investigated in order to look at how Bax and tBid interact. DACM, a small non-ionic sulfhydryl specific probe was selected as a potential FRET donor. Figure 3.7A shows the structures of IANBD and DACM. Part B shows the emission spectra of DAC-tBid and the absorption spectra of 126C-Bax-NBD. These spectra were used to calculate the Forster distance, R_0 , using the following formula:

$$R_0 = 0.211 [\kappa^2 n^{-4} Q_D J(\lambda)]^{1/6} \quad (\text{Lakowicz, 1999, pp. 369})$$

A Forster radius of 4.8 nm was obtained. See materials and methods section for an explanation of this calculation.

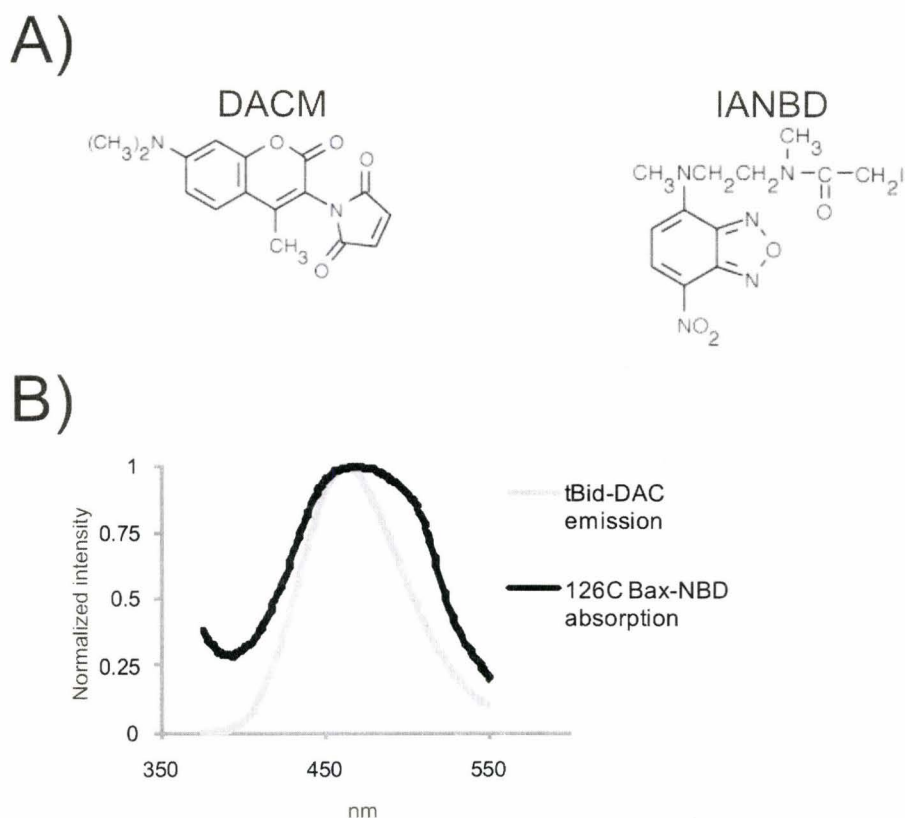


Figure 3.7: DACM and IANBD: a new FRET pair

Ai: The structure of sulfhydryl reactive DACM and IANBD (obtained from the Invitrogen Molecular Probes website; <http://probes.invitrogen.com>).

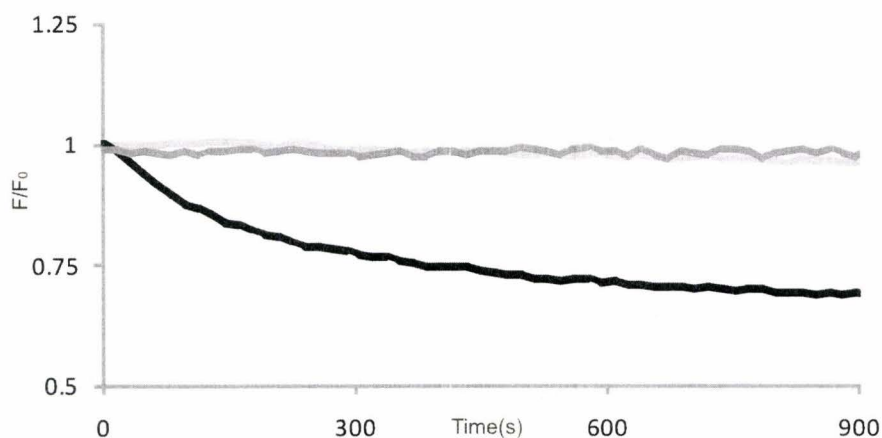
B: Overlap of tBid-DAC emission and 126C-Bax-NBD absorbance. tBid-DAC spectrum was recorded in a buffer of 0.2 M KCl, 1 mM MgCl₂, 10 mM HEPES pH 7 and 126C-Bax-NBD spectrum was recorded in a buffer of 0.2 M NaCl, 0.2 mM EDTA, 10 mM HEPES pH 7.

3.7 *tBid-Bax and Bax-Bax interactions only occur in the presence of liposomes.*

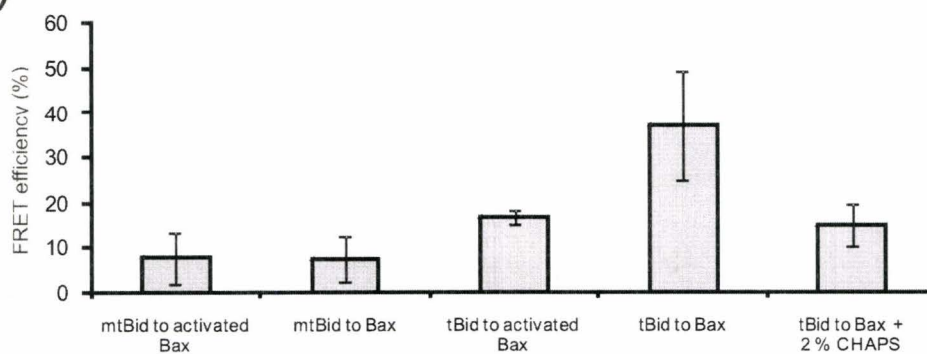
Figure 3.8A shows that tBid to Bax FRET only occurred when liposomes were present. The dark line shows the decrease in FRET donor emission of tBid-DAC in the presence of liposomes and NBD labeled Bax acceptor. The decrease in DAC emission did not occur when unlabeled wildtype Bax was used (light grey line), demonstrating the loss

in DAC fluorescence was specifically due to FRET. In the absence of liposomes, there was no interaction between Bax and tBid based on the absence of a decrease in donor emission in the presence of NBD labeled Bax (medium grey line).

A)



B)



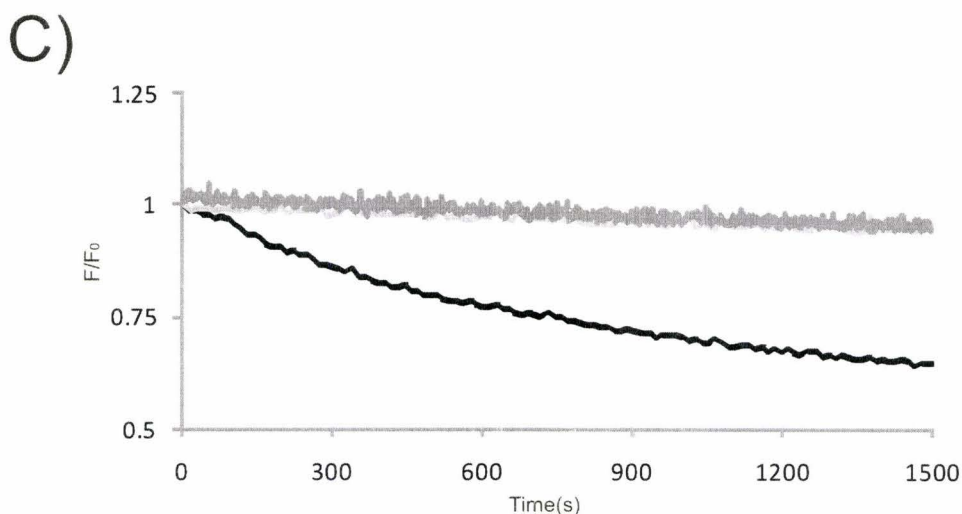


Figure 3.8: Interactions between tBid and Bax are only observed in the presence of membranes

A: tBid to Bax FRET is only observed in the presence of membranes. The black line shows FRET as the loss of 20 nM tBid-DAC donor signal with 100 nM Bax-126-NBD as the acceptor in the presence of liposomes (125 μ M lipid). The light grey line is the tBid-DAC signal using 100 nM wildtype unlabeled Bax in the presence of liposomes (125 μ M lipid). The medium grey line shows the tBid-DAC signal using 100 nM Bax-126-NBD in the absence of liposomes. tBid and Bax were incubated with stirring at 37° C in a buffer of 0.2 M KCl, 1 mM MgCl₂ and 10 mM HEPES pH 7. tBid-DAC excitation was 380 nm and emission was 460 nm.

B: End point FRET efficiency. 100 nM 126C-Bax-NBD was used as the FRET acceptor, using unlabeled 100 nM wildtype Bax as a control to calculate the amount of FRET. 20 nM tBid was used. mtBid is G94E-tBid-DAC that has been reported not to bind with Bax. Activated Bax was obtained by incubating for 2 hours with 50 μ M Bid BH3 peptide. tBid-DAC excitation was 380 nm and emission was 460 nm. Error bars represent +/- S.D. with n = 3.

C: Bax to Bax FRET is only observed in the presence of membranes. FRET is shown in black as the loss of 20 nM Bax-134-DAC donor signal using 100 nM Bax-126-NBD as the acceptor. The light medium grey line is signal using wt Bax and the medium grey line is Bax Bax FRET after adding tBid in the absence of liposomes. 134C-Bax-DAC excitation was 380 nm and emission was 460 nm.

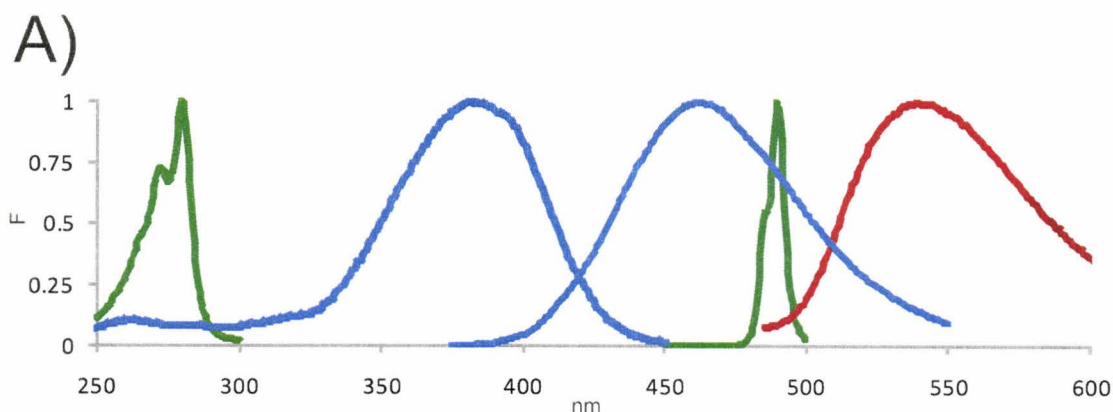
In order to determine whether the tBid to Bax FRET was specific, interaction was tested between peptide inserted Bax and the non Bax binding G94E tBid. Figure 3.8B shows that there was more FRET signal between preinserted Bax and wildtype tBid, compared to Bax binding deficient G94E tBid. This suggests that the observed FRET

between tBid and Bax is not an effect of any two proteins being in the liposome membrane. tBid and Bax do not form a detergent stable complex that can be detected by immunoprecipitation or gel filtration. After adding 2% CHAPS to tBid and Bax, there was a decrease in the amount of FRET, although some FRET remained detectable.

Figure 3.8C shows that Bax to Bax FRET also was only observed if liposomes were present. The dark line shows that intermolecular FRET between Bax molecules occurred when liposomes and tBid were added. The light grey line is the control using wildtype unlabeled Bax as the acceptor. The medium grey line shows that no Bax to Bax FRET occurred after tBid addition if liposomes were not present.

3.8 Ordering of pore formation steps using a 3 fluorophore simultaneous assay

Figure 3.9A shows fluorescence spectra for 3 fluorophores that were used to simultaneously measure pore formation (terbium, green), Bax insertion (NBD emission, red) and protein to protein FRET (loss in DAC signal to NBD labeled acceptor, blue). Since these interactions occur closely together in time, measuring them simultaneously eased interpreting the data from these fluorescent signals. The 3 fluorophores were resolved without any bleed through signal from the other fluorophores.



B)

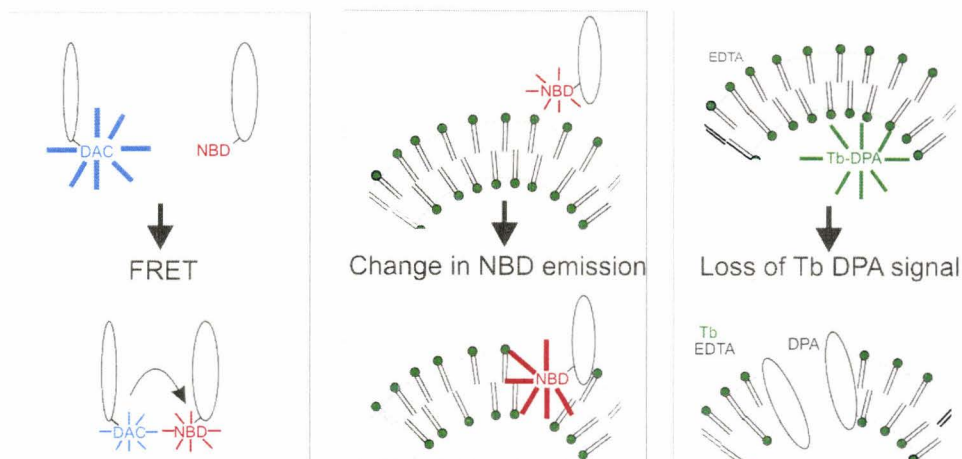


Figure 3.9: A simultaneous 3 fluorophore assay

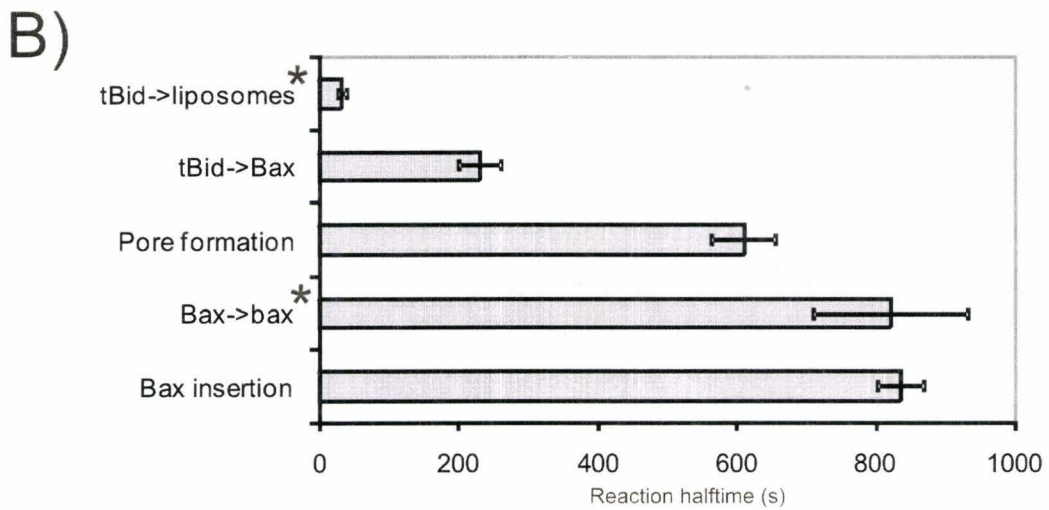
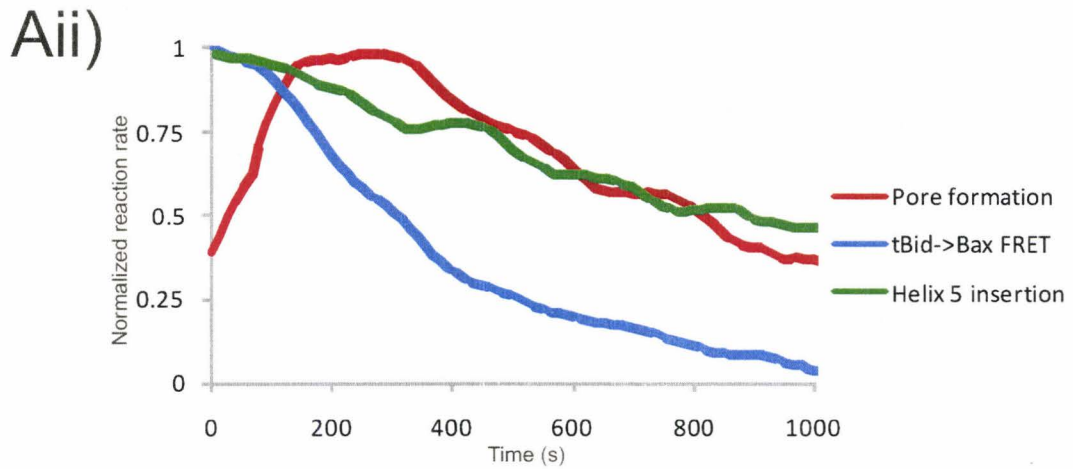
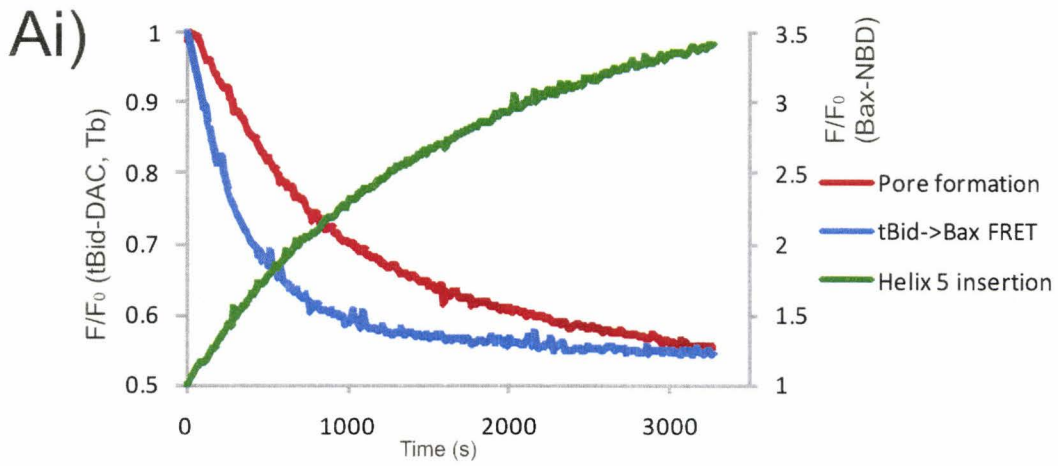
A: NBD, Tb and DAC may be measured simultaneously. Green lines show Tb excitation and emission spectra. Blue lines show tBid-DAC excitation and emission spectra. The red line shows 126C-Bax-NBD emission spectrum. An NBD excitation scan is not shown here for figure clarity, but is shown in Figure 3.3. All the spectra were normalized to their maximum peak values.

B: Description of fluorophore parameters. Relative fluorescence is represented as the weight of the radial lines from the DAC, NBD or Tb-DPA fluorophores. The first panel shows protein protein FRET using DAC and NBD. When the DAC labeled protein moves to the NBD labeled protein, the DAC emission decreases. The second panel shows the increase in NBD emission as the probe moves into a more hydrophobic lipid bilayer. The third panel shows pore formation measured by Tb chelating from EDTA found outside the liposome.

Figure 3.9B shows a schematic diagram of what each fluorophore measured. NBD

fluorescence increased as it moved into a more hydrophobic environment. For 126C-Bax-NBD, this residue increased emission as it migrated to liposomes and oligomerized. As proteins moved close together, FRET was observed from DAC labeled proteins to NBD labeled proteins. FRET was measured as a decrease in DAC emission. Finally, pore formation was measured using the Tb-DPA assay. As liposomes became permeabilized, EDTA outside the liposome chelated the Tb from the Tb-DPA complex, resulting in a loss of fluorescence.

Figure 3.10Ai shows the fluorescence of the 3 fluorophores when tBid-DAC, Bax-NBD, and Tb-DPA containing liposomes were combined. All the fluorescence measurements were observed in one single reaction. The fluorescence was normalized to its initial value after background correction. Note that the Tb pore formation and tBid-DAC FRET signals both decreased over time, while the 126C-Bax-NBD signal increased over time. Figure 3.10Aii shows the rates of the Bax insertion, tBid to Bax FRET and pore formation reactions. These rates represent the slope of the lines from Figure 3.10Ai over time. These units can be thought of as the rate of tBid binding to Bax events, Bax insertion events and liposome permeabilization events.



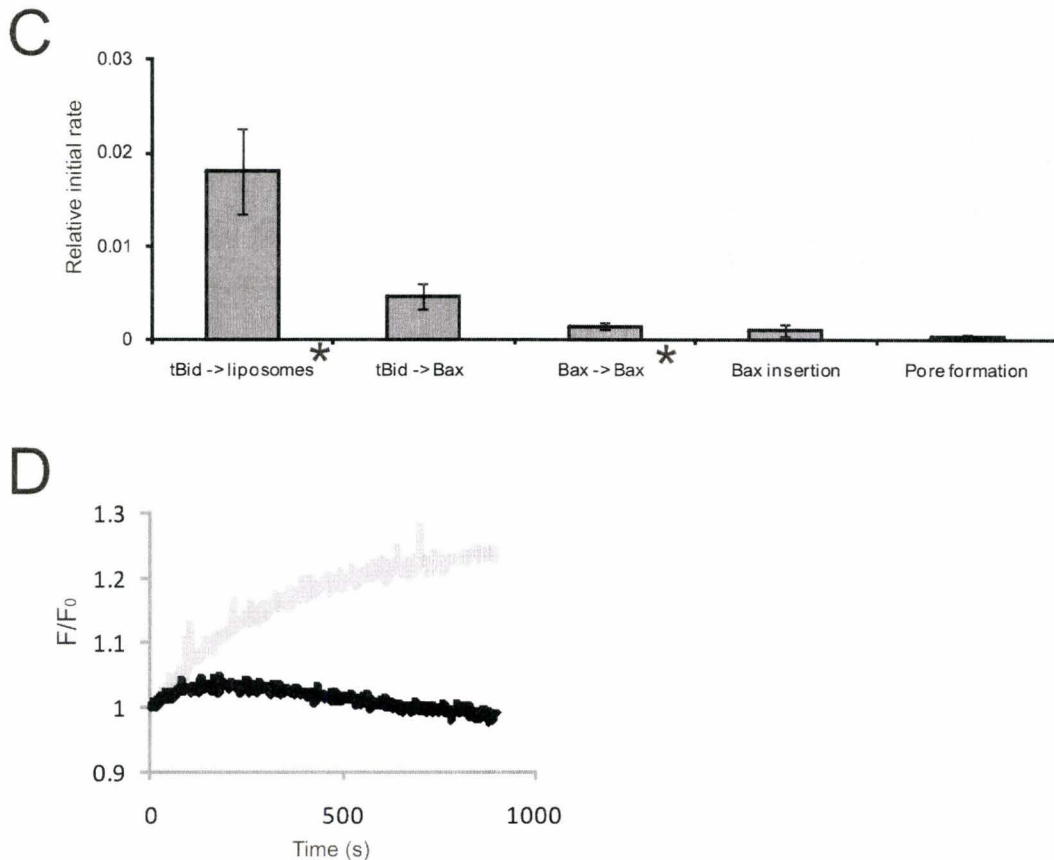


Figure 3.10: Ordering the steps of Bax activation

Ai: Simultaneous 3 fluorophore assay monitoring tBid Bax binding, Bax insertion and pore formation. Normalized fluorescence simultaneously monitoring 20 nM tBid-DAC to 100 nM 126-NBD-Bax FRET, 126-NBD emission increase and pore formation by Tb chelation by EDTA. After tBid-DAC was added to Tb-DPA containing liposomes ($\sim 125 \mu\text{M}$ lipid) at 37°C , Bax was added and fluorescence measurements were normalized to initial values. Aii shows the slope of reactions in Ai. The normalized slope from the data shown in Ai is shown. The data was normalized to the maximum rate.

B: Reaction half times show that tBid binding to liposomes occurs the most rapidly followed by tBid Bax interaction. The approximate half times are shown in seconds. The asterisks indicate the data was taken from a separate experiment. tBid-DAC to liposome containing NBD labeled lipid FRET data was from Scott Bindner, Bax to Bax FRET was from separate experiment using 20 nM ^{134}C -Bax-DAC as the donor and 100 nM ^{126}C -Bax-NBD as the acceptor. Error bars represent \pm S.D. with $n = 3$.

C: Initial rates of reactions. Data was normalized so that all channels began and ended at the same value and the first few data points were used to generate the slope. The rate corresponds to the

fraction of the reaction completed per second. Asterisk marks data from a separate experiment. Error bars represent +/- S.D. with n = 3.

D: Bax to Bax FRET suggests insertion precedes oligomerization. 126C-Bax-DAC to 126C-Bax-NBD FRET is shown in dark line. The line shows the DAC emission, measured at 460 nm and excited at 380 nm. 126C-Bax-DAC emission wt Bax is shown in light grey. Note the initial increase in both lines as this residue moves into the membrane.

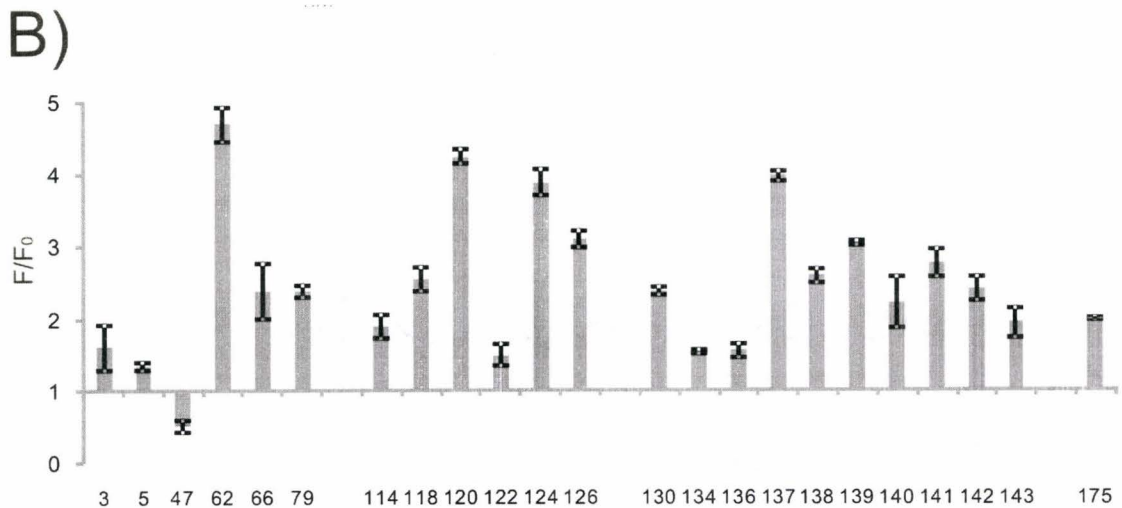
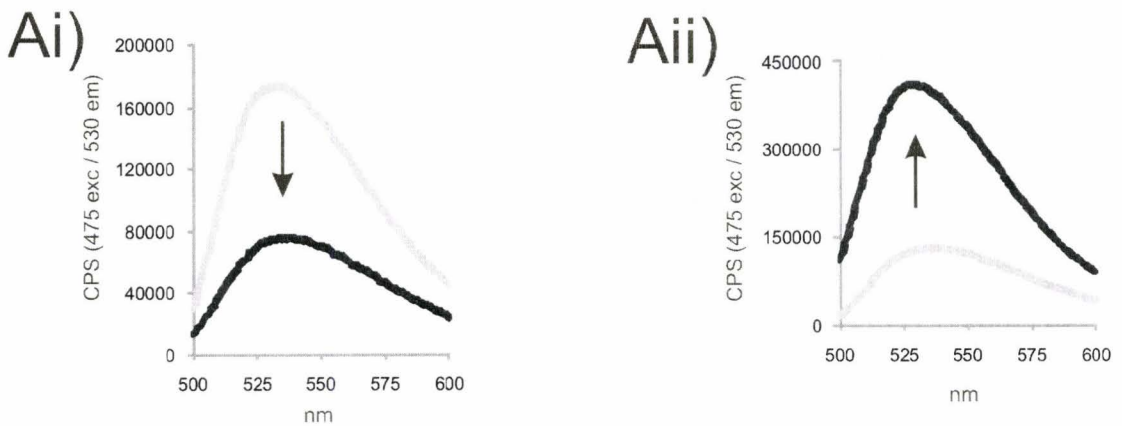
Figure 10B shows the half times for the different reactions leading to Bax pore formation. tBid binding to liposomes FRET occurred the most quickly, with a half time of less than one minute. This data was obtained by Scott Bindner and is not shown. The next chronological half time to occur was tBid-DAC binding to 126C-Bax-NBD. This reaction likely occurred close to the liposome membrane since tBid and Bax only interacted when liposomes were present (Figure 3.8A). Interestingly, the next chronological event based on half times was liposome permeabilization. It is surprising that the half time for liposome permeabilization came before the half time of Bax helix 5 insertion and Bax oligomerization. One explanation for this occurrence is that Bax continued to oligomerize and form larger pores even after small pores had been formed. A major limitation to interpreting the longer half times shown is that the reactions were not completely finished at the one hour mark. This suggests if anything, the halftimes may in fact be slightly greater than the data shown. The reaction half times are in agreement with the initial rates of reaction shown in figure 3.10Ai. The initial rates were calculated from the first few points of the reactions. tBid to liposome interaction occurred quickly, followed by tBid to Bax interaction. Bax to Bax interaction and Bax insertion happened next at approximately the same time, followed lastly by Bax pore formation.

The dark line in Figure 3.10D shows FRET between 20 nM 126C-Bax-DAC and 100 nM 126C-Bax-NBD. The grey line shows the DAC signal using unlabeled acceptor. When using the unlabeled acceptor, although the emission increase was much less than the change in NBD for the same residue (Figure 3.6), the increase was consistent with this residue moving into a more hydrophobic environment. As can be seen in the first seconds of this reaction when the labeled Bax acceptor was present, the DAC emission increased before it then decreased. This suggests the increase was due to Bax first moving to a hydrophobic environment before it found other Bax binding partners to oligomerize with.

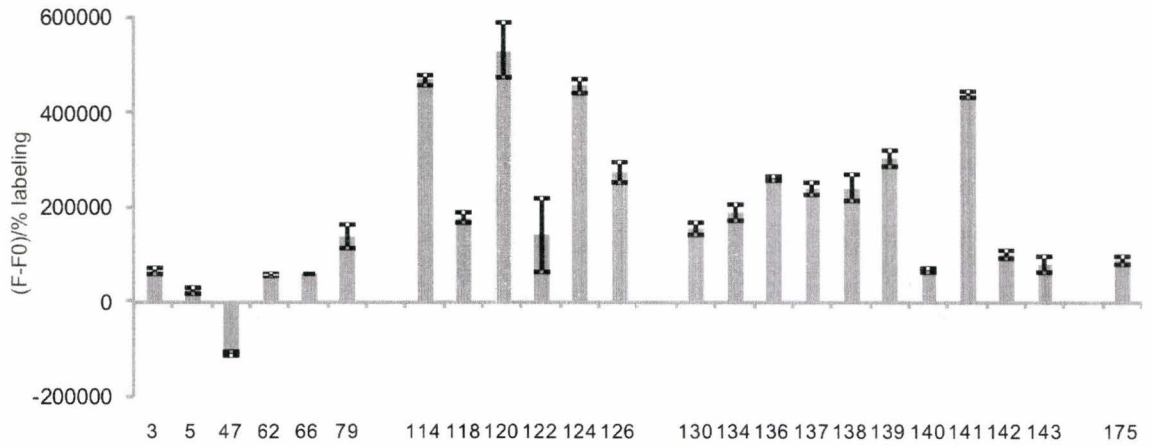
3.9 *Conformational change of Bax may be monitored with NBD fluorescence*

Figure 3.11Ai shows the emission spectra for 47C-Bax-NBD. The dark line shows the NBD emission spectrum after the labeled Bax was incubated with tBid while the grey line shows the emission spectrum without incubation with tBid. As indicated by the arrow, the emission intensity for this residue decreased during Bax activation showing that the probe at this location moved to a less hydrophobic environment. Figure 3.11Aii shows the emission spectra increased for 126C-Bax-NBD. In this case, the emission of the NBD probe located at position 126 increased after incubation with tBid. As shown in Figure 3.11B, all residues except for 47C-Bax-NBD increased emission after tBid incubation. There was no immediately apparent trend as to which parts of the protein had a greater fold increase. Figure 3.11C also shows the additive change in NBD fluorescence, representing the difference in counts rather than the fold increase. The

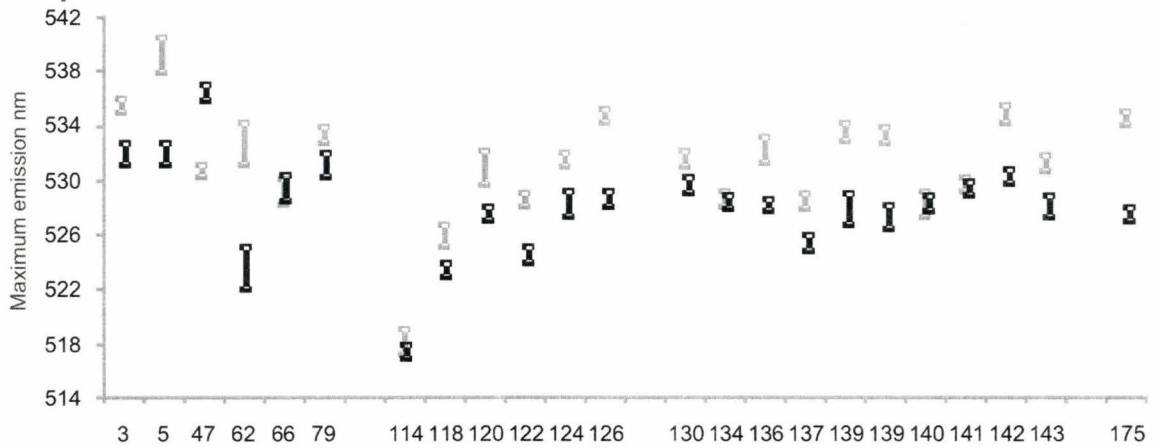
increase was adjusted to take labeling percentage into consideration. There was a general trend that the N terminal residues (3, 5, 47, 62, 66, 79) did not display a large change in intensity relative to the residues on helix 5 and 6. Figure 3.11D shows the emission maximum for the labeled residues with or without incubation with tBid. The difference between these two bars, the blue shift, is summarized in Figure 3.11E. Most residues displayed a blue shift, consistent with the probe moving into a more hydrophobic environment. Unlike the other labeled mutants, 47C-Bax-NBD displayed a red shift of over 5 nm, consistent with this residue moving into a less hydrophobic environment.



C)



D)



E)

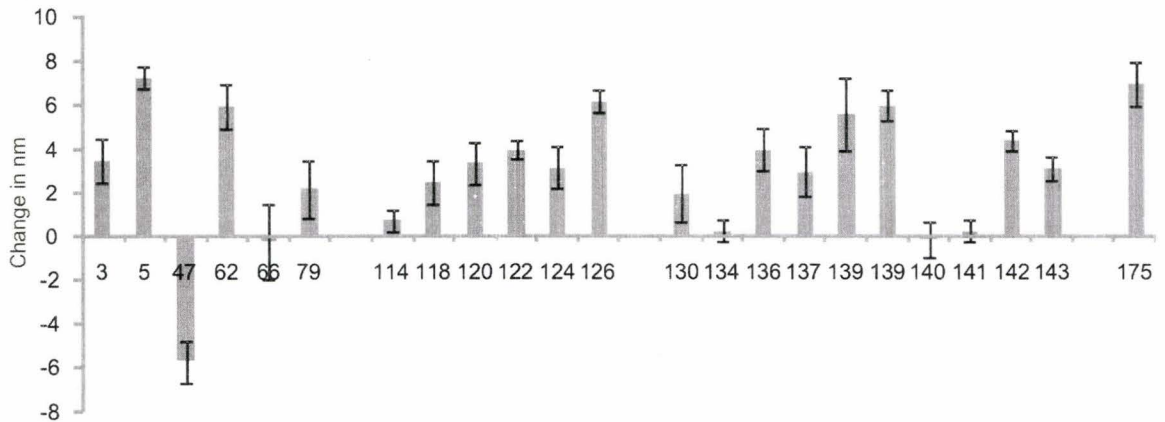


Figure 3.11 NBD emission intensity and wavelength suggest Bax conformational reorganization

Ai: Emission spectra for 100 nM 47C-Bax-NBD in the presence of liposomes (125 μ M lipid) with (black line) or without (grey line) incubation with 20 nM tBid for 2 hours at 37° C. Arrow indicates direction of change with tBid addition. Aii shows the emission spectra for 126C-Bax-NBD in the presence of liposomes (125 μ M lipid) with (black line) or without (grey line) incubation with 20 nM tBid for 2 hours at 37° C. Liposome background spectrum was subtracted from the spectra.

B: Fluorescence increase for 100 nM NBD labeled Bax mutants in the presence of liposomes (125 μ M lipid) after incubation with 20 nM tBid for 2 hours at 37° C. F_0 represents the maximum emission value from the spectra without incubation with tBid, and F represents the maximum emission value from the spectra after incubation with 20 nM tBid. Error bars represent +/- S.D. with $n = 3$.

C: Absolute change in emission value for 100 nM NBD labeled Bax mutants in the presence of liposomes (125 μ M lipid) after incubation with 20 nM tBid for 2 hours at 37° C. F_0 represents the maximum emission value from the spectra without incubation with tBid, and F represents the maximum emission value from the spectra after incubation with 20 nM tBid. The absolute change in counts was measured and divided by the fraction labeling to correct for the variability in the labeling. Error bars represent +/- S.D. with $n = 3$.

D: Emission maximums for 100 nM NBD labeled Bax mutants in the presence of liposomes with or without incubation with 20 nM tBid. Black bars show the wavelength of maximum emission for Bax that has been incubated with tBid and grey bars show maximums for Bax that has not been incubated with tBid. Error bars represent +/- S.D. with $n = 3$.

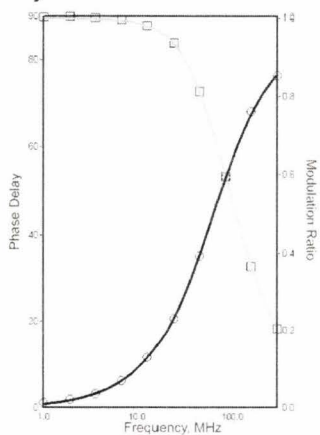
E: Blueshifts for 100 nM Bax mutants in the presence of liposomes after incubation with 20 nM tBid for 2 hours at 37° C. Error bars represent +/- S.D. with $n = 3$.

3.10 Lifetimes show three populations and subtle lifetime changes

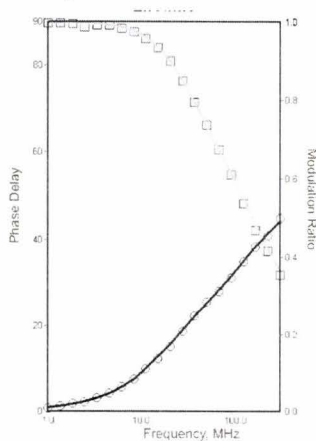
Figure 3.12Ai shows the fitted lifetime model for coumarin-6, a fluorescence standard used to ensure the lifetime fluorometer was functioning properly. These data show a single exponential fit for the coumarin-6, with a lifetime of 2.5 ns, as expected, with a chi square value of 2 between the observed data and the model data. The fit (solid lines) matched well to observed data (square and circle points). Control data are shown because the NBD lifetimes did not fit a single or double exponential. Table 3.4 shows the parameters for fitting the lifetime of 126C-Bax-NBD with two or three components. Figure 3.12Aii shows a three component fit for 47C-Bax-NBD after incubation with tBid and liposomes. The intensity weighted average lifetime for this fit was 2.6 ns. Figure 3.12Aiii shows the lifetime fit for 120-Bax-NBD after incubation with tBid. This residue had a much longer average lifetime of 8.2 ns.

Figure 3.12B shows the lifetimes for all the assayed mutants, either with incubation with tBid (black bars) or without (grey bars). In general, the lifetimes were not drastically different for the NBD labeled Bax mutants with or without incubation with tBid. The lifetimes shown are the intensity weighted average lifetimes of a three component fit. The average lifetime is shown for simplicity in showing the lifetime components. See Table 6.1 for the individual lifetime components, weightings and the chi square values. The chi square values typically were between 1 and 2.5.

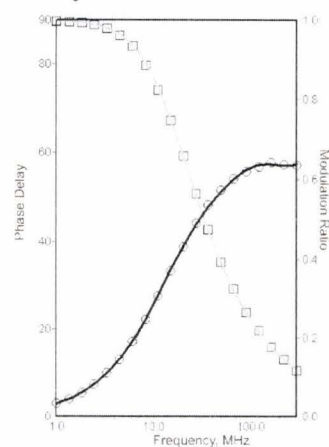
Ai)



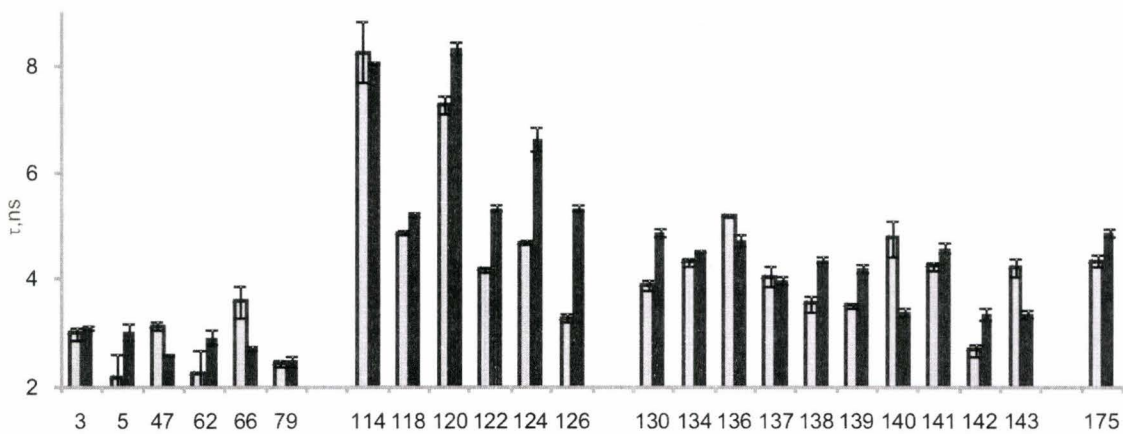
Aii)



Aiii)



B



C

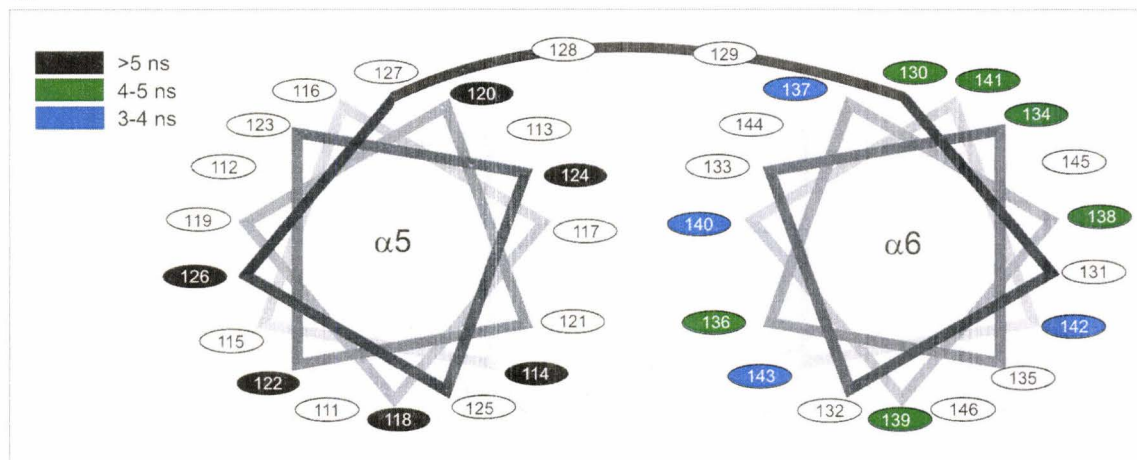


Figure 3.12 Lifetimes suggest distinct environments for different areas of Bax

Ai: Single exponential fit showing a lifetime of 2.5 ns for coumarin-6 in absolute ethanol. Recorded modulation ratio data is shown as squares and recorded phase delay data is shown as circles. The fit is shown as solid lines. **Aii** shows a triple exponential fit with an average lifetime of 2.6 ns for 100 nM 47C-Bax-NBD incubated with 20 nM tBid and liposomes (125 μ M lipid). **Aiii** shows a triple exponential fit with an average lifetime of 8.2 ns for 100 nM 120-NBD incubated with 20 nM tBid and liposomes (125 μ M lipid). Fluorescein in 0.1 M NaOH was used as a reference with a 4 ns lifetime for all measurements.

B: Intensity weighted average lifetimes for a three component fit for 100 nM NBD labeled Bax mutants. Dark bars show the lifetimes for the mutants with incubation with liposomes (125 μ M lipid) and 20 nM tBid, and grey bars show the lifetimes for the mutants in the presence of liposomes, but without tBid incubation. See supplementary data for fitting details. Error bars represent +/- S.D. with $n = 3$.

C: Helical plot showing the lifetimes for the pore-forming domain. Helical wheel was generated with Helical Wheel Projection software (available online at <http://rzlab.ucr.edu/scripts/wheel/wheel.cgi>). As shown in the legend, black residues correspond to lifetimes over 5 ns, green residues correspond to residues between 4 and 5 ns and blue residues 3 to 4 ns. Unfilled circles show residues that were not assayed.

In general, the N terminal residues before the pore-forming domain had lifetimes that varied between 2 and 4 ns. These lifetimes were shorter than the lifetimes of the rest of the assayed mutants. In active form, the residues on helix 6 displayed lifetimes varying between 3 and 5 ns. These lifetimes were longer than the N terminal mutants, but were shorter than those of the mutants on helix 5. After incubation with liposomes and tBid, the helix 5 mutants all had lifetimes greater than 5 ns, ranging from 5 ns to 8 ns. The residue on helix 9, 175C had a lifetime of just under 5 ns, similar to the lifetime of the residues with longer lifetimes on helix 6. Figure 3.12C shows a helical wheel plot for helix 5 and 6, with the lifetimes of the inserted and oligomerized Bax mutants indicated. All the mutants on helix 5 had lifetimes greater than 5 ns, whereas the mutants on helix 6

had lifetimes that ranged from 3 to 5 ns. The helical wheel of helix 5 shows lifetimes for 6 labeled mutants. Some further residues on this helix could not be assayed since they either proved difficult to label (Table 3.3) or were not functional (Figure 3.3). The mutants on helix 6 with a 3 to 4 ns lifetime are shown in blue on the helical wheel and the mutants with a 4 to 5 ns lifetime are shown in green. There was no obvious division in the helix that separated the 3-4 ns lifetime mutants from the 4-5 ns lifetime mutants on helix 6.

Table 3.4 shows fits for two component and three component lifetimes for 126C-Bax-NBD. The chi square value improved about 10 fold when a third component was added. Table 6.1 shows fit parameters for the assayed mutants.

Table 3.4: Two and three component lifetime fits for Bax (asterisk shows data from Bax that was from a separate purification than all the rest of the data presented)					
Sample	Component 1	Component 2	Component 3	χ^2	Average
Coumarin-6	2.5 ns, 100%	-	-	2.0	2.5 ns
126C-Bax-NBD in buffer, no liposomes*	0.7 ns, 48%	4.2, 52%	-	9.4	2.5 ns
126C-Bax-NBD in buffer, no liposomes*	0.5 ns, 26%	1.6, 41%	5.8, 33%	0.9	2.7 ns
126C-Bax-NBD in buffer with liposomes	0.5 ns, 36%	4.4 ns, 64%	-	22.2	3.0 ns
126C-Bax-NBD in buffer with liposomes	0.2 ns, 19%	1.5 ns, 36%	6.0 ns, 45%	1.8	3.3 ns

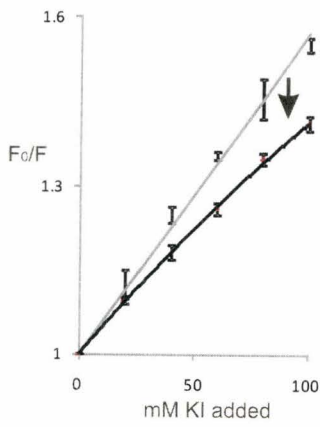
3.11 Quenching reveals dynamic lipid interaction and suggests membrane topology

Figure 3.13Ai shows iodide quenching for 122C-Bax-NBD. The dark line shows

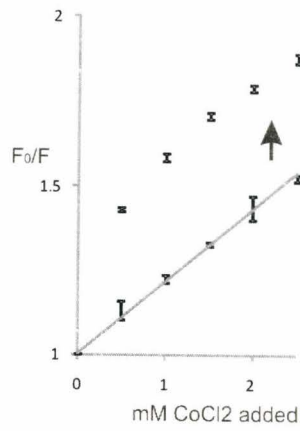
the line of best fit for iodide quenching of 122C-Bax-NBD that had been incubated with tBid, and the grey line shows the line of best fit for the iodide quenching for unactivated 122C-Bax-NBD. The arrow shows the change in quenching caused by the insertion and oligomerization of Bax. The flatter slope for the Bax that had been incubated with tBid indicates this residue became more difficult to quench. Figure 3.13Aii shows cobalt quenching for the same Bax mutant. As indicated by the arrow, in this case, incubation with tBid caused this mutant to become less difficult to quench. A line of best fit is not shown, since a linear fit did not suit the data. It is possible that the large amount of quenching observed from the first addition of 0.5 mM cobalt was due to the cationic cobalt affinity for the anionic lipid headgroups. The strange shape of the quenching curve observed can be explained if the 125 μM lipid concentration was saturated by the 500 μM cobalt that was the first titration point. Figure 3.13B shows the bimolecular quenching constants of iodide for all the Bax mutants. The dark bars show the quenching constants for Bax that had been incubated with tBid and liposomes, while the grey bars show the quenching constants for Bax and liposomes without tBid incubation. The exposed residues towards the N terminus were most prone to iodide quenching, as judged by their higher quenching constants. The residues on helix 5 were most resistant to iodide quenching. In general, labeled mutants became more resistant to iodide quenching after incubation with tBid. Figure 3.13C shows the cobalt bimolecular quenching constants for the labeled Bax mutants. The dark bars show the quenching constants for Bax that had been incubated with tBid and liposomes for 2 hours at 37° C, while the grey bars show the quenching constants for Bax and liposomes without tBid addition. Unlike iodide

quenching, most residues were more quenched by cobalt after incubation with tBid. Residues towards the middle of helix 5, 114C and 118C were resistant to cobalt quenching compared to the other residues of the pore-forming domain. It is informative to note that the residues of the pore-forming domain increased their cobalt quenching upon activation compared to the N terminus residues. This may suggest that these residues were in close proximity to the lipid headgroups. These data are useful for considering whether Bax forms a proteinaceous or lipidic pore (Figure 4.1A). Figure 3.13D shows the cobalt bimolecular quenching constants for both the first and subsequent titrations of cobalt when the NBD labeled Bax mutants were incubated with tBid. The first titration showed several fold greater quenching susceptibility. This is in agreement with the explanation that cobalt saturated the anionic lipids of the liposome. Figure 3.13E demonstrates the high cobalt quenchability of the pore-forming domain for the NBD labeled mutants after incubation with liposomes and tBid. These data are shown as the bimolecular cobalt constant divided by the bimolecular iodide quenching constant. Since these constants both use the same lifetime values, the lifetimes cancel out in the division, and this ratio is independent from the recorded lifetime measurements. These values represent the fold increase in efficiency of cobalt over iodide. After incubation with tBid, several Bax residues in the pore-forming domain were over 200 times more effectively quenched by cobalt than by iodide, more affected than the N terminal residues. This suggests that the pore-forming domain is in close proximity of the lipid head groups.

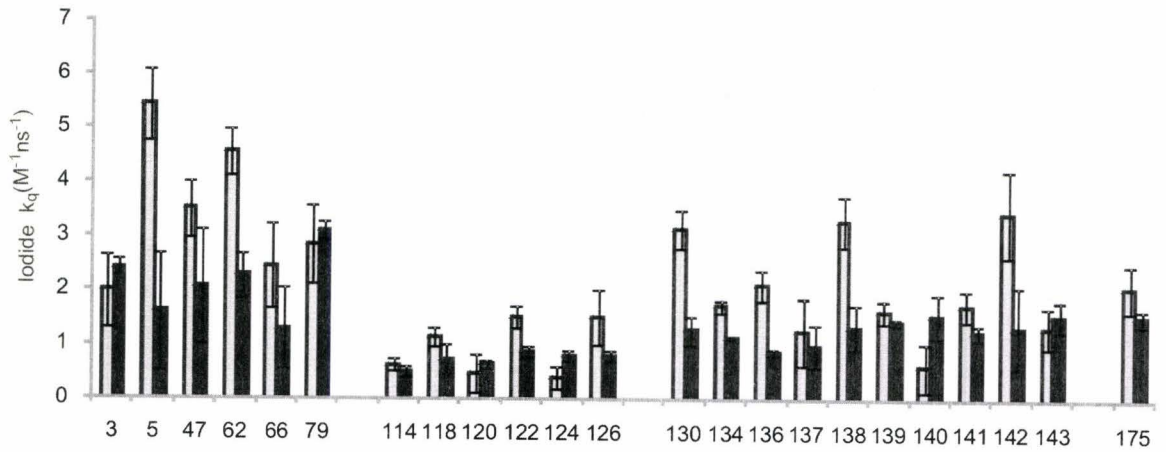
Ai)



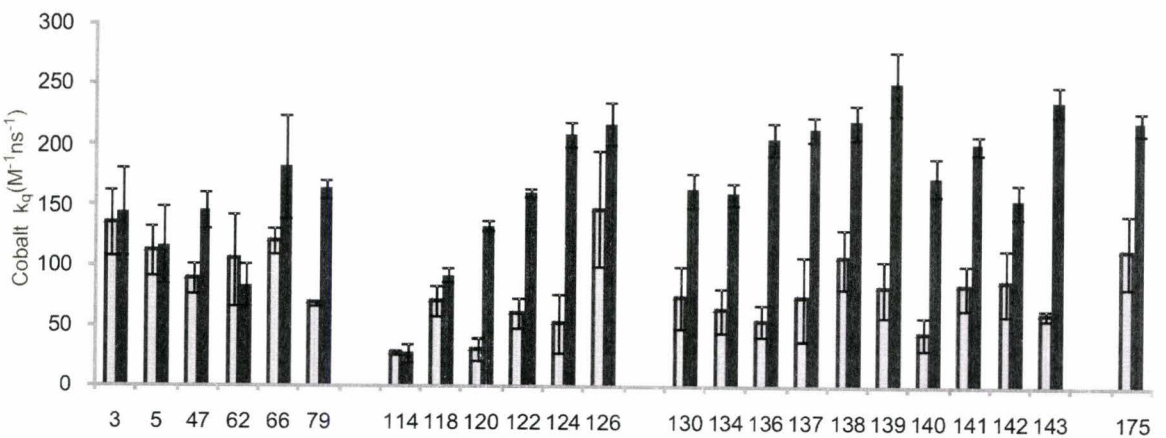
Aii)



B)



C)



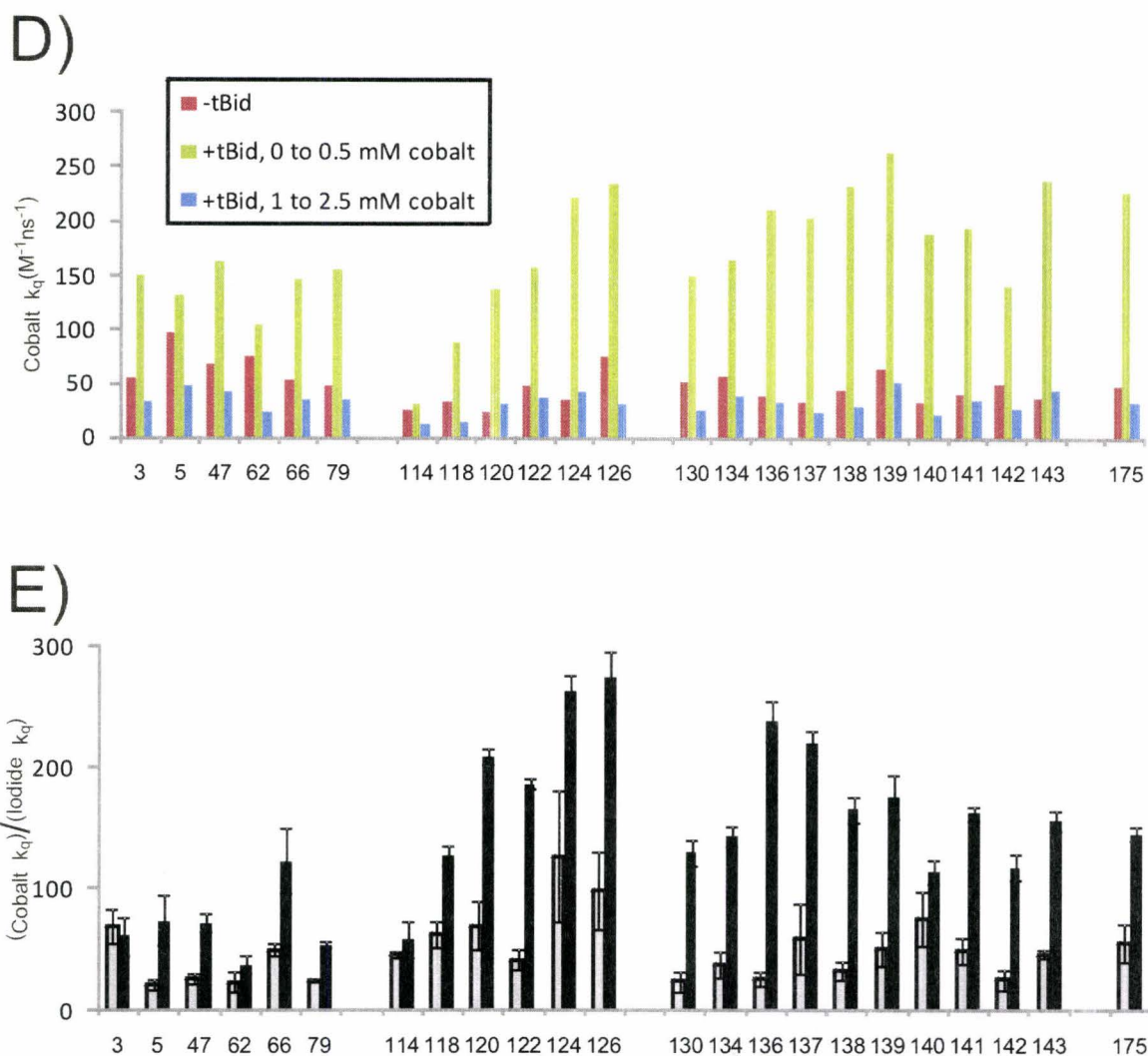


Figure 3.13: Differential ionic quenching of Bax residues

Ai: Iodide titration of 100 nM 122-NBD in the presence of liposomes (125 μ M lipid) with or without incubation with 20 nM tBid for 2 hrs at 37 $^{\circ}$ C. A line of best fit for quenching points is shown. **Aii** shows a cobalt titration of 100 nM 122-NBD in the presence of liposomes with or without incubation with 20 nM tBid. A line of best fit is shown for the sample without tBid, but a line did not fit the data after incubation with tBid. Error bars represent \pm S.D. with $n = 3$.

B: Iodide bimolecular quenching constants for 100 nM NBD labeled Bax mutants. Slope of quenching was divided by the lifetimes shown in Figure 3.12B. Error bars represent \pm S.D. with $n = 3$.

C: Cobalt bimolecular quenching constants for 100 nM NBD labeled Bax mutants. Only the first 0.5 mM CoCl_2 titration was considered for calculations. Slope of quenching was divided by the lifetimes shown in Figure 3.12B. Error bars represent \pm S.D. with $n = 3$.

D: Representative bimolecular quenching constants for cobalt quenching. Red bar shows the quenching without incubation with tBid. The high green bar shows the first titration of cobalt after incubation with 20 nM tBid and liposomes. The blue bar shows the next 4 titration points after the initial titration point of cobalt for Bax that has been incubated with tBid.

E: Ratio of cobalt to iodide bimolecular quenching constants. Since both bimolecular constants were divided by the lifetimes, this division cancels out and this data is independent from recorded fluorescence lifetimes. Error bars represent +/- S.D. with n = 3.

3.12 Doxyl quenching suggests a distinct dynamic membrane spanning topology

Figure 3.14A shows the structures of the doxyl quenchers used to probe the depth of the labeled Bax mutants. By having the nitroxide quencher at different depths, the labeled mutants could be used to examine the topology of Bax. Figure 3.14B shows the effectiveness of the various quenchers for different residues in the pore-forming domain. Although many of the residues were quenched by both deep and shallow doxyl quenchers, there is a pattern that residues on helix 5 were more susceptible to the deeper 16' and 14' quenchers, while residues on helix 6 were most susceptible to the shallow 5' quenchers. This pattern is more apparent in Table 3.5, which shows the quenching values obtained and the standard deviations. The boxes highlighted in grey indicate which doxyl lipid resulted in the maximum quenching of the residues. It is important to note that the quenching was not restricted to a single doxyl quenching lipid, but several residues were quenched well by multiple doxyl quenchers. There still is an overall pattern in between the helices, with the residues on helix 6 being buried shallowly beneath the bilayer and the residues of helix 5 being quenched in a pattern consistent with a membrane spanning helix.

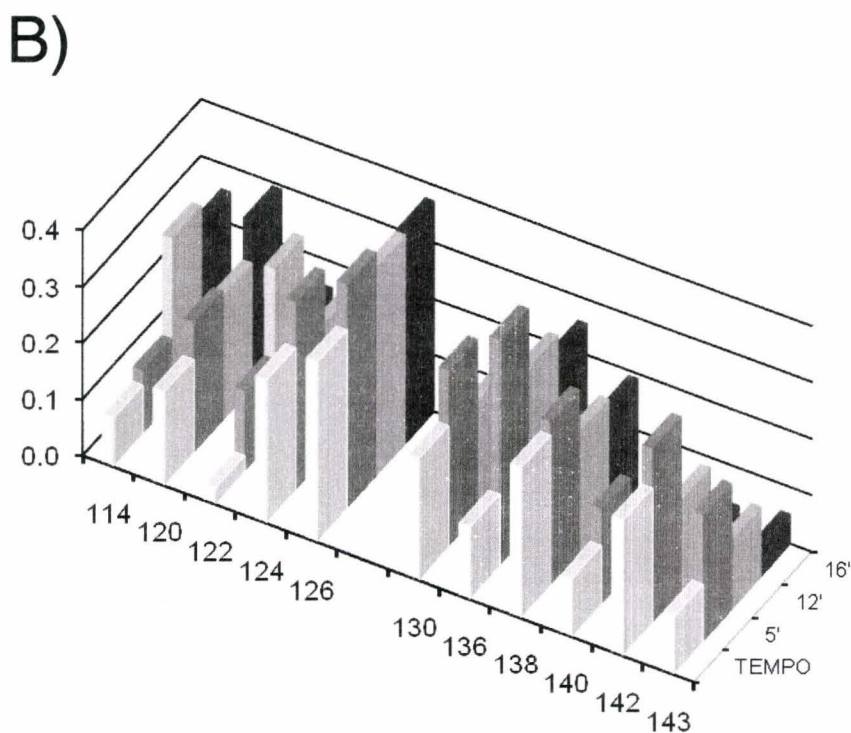
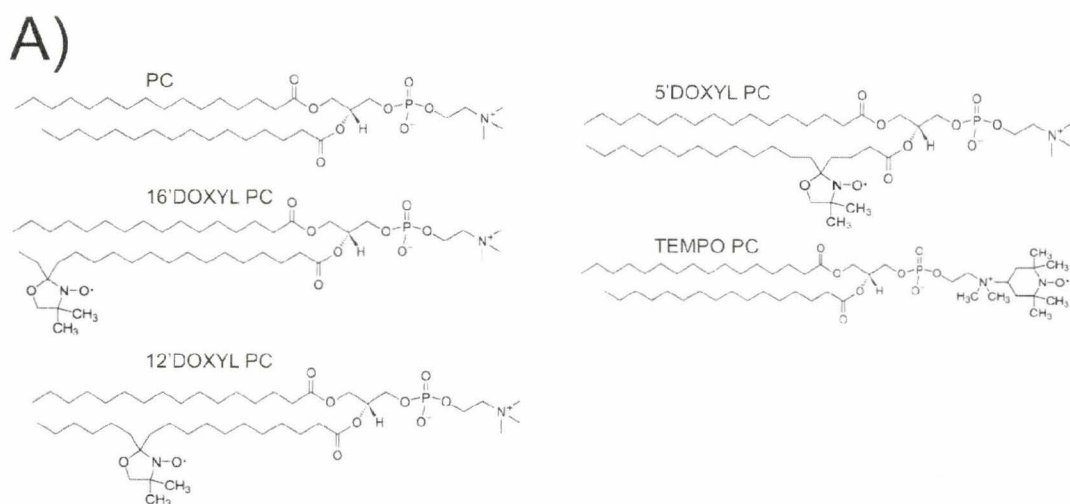


Figure 3.14: Lipid quenching

A: Structures of different nitroxide lipids used. Structures obtained from the supplier website (<http://www.avanti.com>)

B: Lipid quenching of various residues in the pore-forming domain. Liposomes were made with 15 molar percent of nitroxide labeled lipid or unlabeled PC instead of the normal PC used for mitochondria like lipid composition. 100 nM Bax-NBD was then incubated with the liposomes

containing the various quenchers. Quenching was calculated as $[1 - (F_{\text{quench}}/F_{\text{noquench}})]$, where F_{quench} was the background corrected emission in the presence of the lipid quencher and F_{noquench} was the background corrected emission in the absence of the lipid quencher. The obtained values and standard deviations are shown in Table 3.5.

Table 3.5: Quenching of different Bax residues (greatest quencher highlighted in grey, standard deviation shown in brackets with n=3)				
Mutant	TEMPO	5'	12'	16'
79	0.15 (0.023)	0.12 (0.012)	0.13 (0.046)	0.09 (0.07)
114	0.09 (0.02)	0.11 (0.05)	0.29 (0.03)	0.26 (0.03)
120	0.17 (0.037)	0.23 (0.060)	0.22 (0.030)	0.29 (0.001)
122	0.03(0.060)	0.14 (0.044)	0.30 (0.037)	0.16 (0.023)
124	0.25 (0.009)	0.33 (0.002)	0.24 (0.091)	0.19 (0.032)
126	0.32 (0.005)	0.46 (0.019)	0.37 (0.007)	0.37 (0.028)
130	0.21 (0.012)	0.31 (0.107)	0.20 (0.062)	0.14 (0.038)
136	0.13 (0.038)	0.43 (0.136)	0.29 (0.035)	0.26 (0.047)
138	0.26 (0.072)	0.29 (0.024)	0.21 (0.014)	0.19 (0.070)
140	0.10 (0.040)	0.17 (0.030)	0.06 (0.038)	0.01 (0.004)
142	0.24 (0.021)	0.31(0.068)	0.16 (0.049)	0.03 (0.093)
143	0.10 (0.011)	0.22(0.045)	0.12 (0.018)	0.05 (0.001)

4 Discussion and conclusions

4.1 Behaviour of Bax

Several cysteine mutants were successfully purified but were not used in the study since they did not label very well (Table 3.3). These mutants were located towards the N terminus end of helix 5. The NMR structure of Bax (Figure 1.2) shows that this area of the protein is an inaccessible part of the protein and surrounded by other helices and thus it may have been difficult for the dye to access the cysteine residues located there. The space filling model of Bax shows that most residues on helix 5 are buried (Figure 1.3). Other studies using IANBD labeling have used 3M GdCl₃ to denature the protein in order to label difficult to reach residues (Shepard et al., 1998). This may be feasible in the future for Bax, but it is unknown whether or not Bax can be unfolded, labeled then refolded and retain function.

The ANTS/DPX release assay is an established assay (Smolarsky et al., 1977) that has been used previously to verify Bax function (Yethon et al., 2003). However, the overlapping excitation spectra of NBD, DAC and ANTS around 350 nm required that adjustments be made to the wavelength where ANTS emission and excitation is usually measured. Fortunately, there were wavelengths where ANTS could be excited and emit without interference from the other fluorophores (Figure 3.3A).

As seen in Figure 3.3B, in a typical ANTS release, the combination of Bax and tBid would give about 50% release, whereas the two proteins individually would yield less

than 10% each, close to the liposome alone background. The concerted pore-forming effect of tBid and Bax has been documented previously (Terrones et al., 2004). In the absence of tBid, most labeled mutants had less than 20% the synergistic activity of wildtype Bax and tBid. This small but observable amount of background activity implies that tBid is not absolutely necessary to achieve ANTS/DPX release by Bax, although tBid must help initiate or catalyze pore formation. The background activity could be from a subset of Bax that has become activated during the purification or labeling process; or it could come from normal Bax that becomes activated slowly. The ANTS/DPX release assay showed that most of the NBD labeled mutants behaved similarly to wildtype Bax (Figure 3.3C). Like the NBD labeled mutants, DAC labeled proteins also behaved similarly to wildtype unlabeled proteins (Figure 3.3E). This is not entirely surprising, since most of these mutations were in the pore-forming domain, and it has been demonstrated that Bax can retain pore-forming ability even if up to 6 of the charged residues in the pore-forming domain are mutated to alanine (Nouraini et al., 2000). The G94E-tBid-DAC mutant displayed much less activity compared to wildtype tBid and tBid-DAC. This mutation is in the highly conserved GD sequence of the BH3 region of Bid (Figure 1.1) and has previously been shown to inactivate Bid (Wang et al., 1996).

Previously unknown mutations were discovered that changed the functionality of Bax (Figure 3.3D). Cysteine substitution at residue 115 or 116 caused Bax to exhibit limited pore-forming activity with or without NBD labeling. In contrast, cysteine mutations to the adjacent residues, 114 and 118, caused constitutive pore formation even without tBid activation. These residues are at the top of helix 5, approaching the

conserved NWGR sequence of the BH1 domain. This result suggests that this area of the protein is critical for Bax regulation. Since no external energy is required for Bax pore formation, all the necessary energy lies within the Bax protein itself. Perhaps the inactivation mutations of 115C and 116C raise the activation energy of an intermediate state that Bax must go through. Conversely, the 114 and 118 mutations presumably lower the activation barrier normally lowered by the addition of tBid. Two mutations on helix 6, 137C and 141C, also appeared to enhance Bax activity without tBid addition. These residues are one helix rotation apart at the tip of helix 6 and their location is close to the loop between helix 1 and 2 (Figure 1.3). Perhaps Bax is activated if the dislodgement of this loop is facilitated. This loop contains residue 47, which was the only residue assayed to decrease emission intensity. For most of the mutants that displayed abnormal function, this behaviour was already present in the purified single cysteine protein before the attachment of the NBD label (Figure 3.3D).

As seen in Figure 3.6A, besides initiating Bax to cause ANTS/DPX release, tBid also caused the emission of 126C-NBD-Bax to increase as the residue moved into a more hydrophobic environment. This fluorescence increase was accompanied with a movement to liposomes as shown by gel filtration and the formation of CHAPS resistant oligomers. This behaviour for the NBD labeled Bax recapitulates two important *in vivo* characteristics of Bax during apoptosis; movement to membranes and oligomerization. Interestingly, while translocation to liposomes was complete after 15 minutes, at this time point not all the Bax had formed large oligomers (Figure 3.6C). This suggests that oligomerization continued even after Bax migrated to the liposomes.

As shown in Figure 3.4, the fluorophores selected for the pore-forming assay varied in size from 0.5 kDa to 250 kDa, and were spectrally well resolved. Other assays have been used to gain insight on toxin pore size in the past. FITC labeled proteins of different sizes ranging from 0.6 kDa glutathione to 670 kDa thyroglobulin were encapsulated in liposomes and an anti-fluorescein antibody was used to detect release (Heuck et al., 2003). Since the antibody is larger than the fluorophores (in at least one dimension), quenching of the fluorescein by the antibody monitors release of the labeled fluorophores. A disadvantage of this method and most other comparable assays is that liposomes can only have one fluorophore entrapped at a time, since fluorescein emission quenching is the only available measurement. However, this technique has the advantage of being able to monitor pore formation as it occurs, whereas the method presented here requires a lengthy gel filtration step to determine the amount of release. Interestingly, analysis of Perfringolysin O using this technique found that the toxin pores were homogeneous in size. In contrast, as seen in Figure 3.5, liposomes incubated with Bax contained pores of vastly different sizes. There was always the most release for the smallest fluorophores, MPTS, followed by the fluorescein labeled dextran, Allophycocyanin then Betaphycoerythrin. This suggests that there are some liposomes that have Bax pores large enough to release Betaphycoerythrin, while other liposomes contain Bax pores that are not large enough to release the 3 kDa dextran (but can release 0.5 kDa MPTS). To our knowledge, Betaphycoerythrin is the largest protein verified to be released by Bax, although it has been previously shown that Bax can cause the release of extremely large 2 MDa dextrans (Kuwana et al., 2002). In contrast to the data presented here, that work

reported similar amounts of release for 2 MDa dextrans and 10 kDa dextrans. However, another study has shown that Bax lacking the C terminus released ANTS, a 10 kDa dextran and a 70 kDa dextran in decreasing amounts, resulting in some of the liposomes having larger pores than others (Terrones et al., 2004). In that study, full length Bax and tBid gave maximum release for all the entrapped fluorophores, implying the full length Bax is more effective at large pore formation. Another study used kinetic analysis of self quenching fluorescein dextrans to show that the pore size varied along with the number of Bax monomers in the Bax pore (Saito et al., 2000).

The alpha helical diphtheria toxin, similar in structure to Bax, has also been shown to form a pore of variable size (Sharpe and London, 1999). That study used a cascade blue antibody to detect release of liposome contents. At high toxin concentrations, 10 kDa, but not 70 kDa dextrans were released. At lower toxin concentrations only 3 kDa dextrans could be released. It was also determined indirectly that the diphtheria oligomerization occurs in the membrane and not in solution. This is the same result inferred by the Bax to Bax and tBid to Bax studies showing FRET was only detectable when membranes were present (Figure 3.8).

4.2 Characterization of Bax activation by tBid

Since the small, non-ionic NBD probe did not abrogate normal function for most Bax mutants, a donor or acceptor FRET probe for tBid was researched to gain insight into

how Bax is activated. Most of the potential acceptor probes, which had to be at a longer wavelength, were ionic or over 1000 Da. There were several potential sulfhydryl reactive donor probes that were smaller than 500 Da and displayed suitable spectral overlap with IANBD. These included diethylamino-maleimidyl ethyl carbonyl coumarin (MDCC), iodoacetyl amino ethyl amino naphthalene sulfonic acid (IAEDANS), and maleimidylanilino naphthalene sulfonic acid (MIANS). DACM was selected for small size (298 Da), good spectral overlap with NBD, and low background emission at the NBD emission wavelengths. A FRET pair consisting of a different, but structurally similar, succinimidyl ester dye (DMACA-SE) donor and a NBD-phosphatidylethanolamine acceptor has previously been used (Lehto et al., 2002) to study protein lipid interactions. Although the emission and absorption spectra are not the same, the pair was calculated to have a Forster radius of 4 nm, which is comparable to the 4.8 nm determined for DAC and NBD labeled proteins.

The tBid used in this study was generated from murine Bid. The sequences of murine and human Bid are similar (Figure 1.1), although for labeling purposes, murine tBid has the advantage of having one single endogenous cysteine residue, while human tBid does not contain any cysteines. Additionally, human Bid contains three cysteine residues in the p7 fragment (murine Bid only has one) that would further complicate the labeling. Murine tBid has previously been used in our lab to investigate the mechanism of Bcl-2 family members (Yethon et al., 2003; Dlugosz et al., 2006).

Although it has been recognized that tBid translocates to the mitochondria upon cleavage by caspase-8 (Li et al., 1998), there is little information available about when and where tBid activates Bax. Figure 3.8A shows that tBid and Bax interacted when liposomes were present. No FRET was observed when tBid and Bax were combined in solution without liposomes. FRET was also observed between tBid-DAC and Bax-NBD when the Bax was preinserted with the BH3 peptide of Bid. As expected, Bax binding deficient mutant G94E-tBid-DAC displayed less FRET compared to wildtype tBid-DAC, even when the Bax-NBD was preinserted with the BH3 peptide. The FRET observed in membranes between tBid and Bax was therefore not random interaction between two membrane inserted proteins. Like tBid to Bax FRET, Bax to Bax FRET was only observed in the presence of liposomes. It has been suggested that tBid may be the catalyst in a ‘hit and run model’ where tBid does not stably bind Bax or Bak (Wei et al., 2000). CHAPS gel filtration demonstrated that tBid was not part of the Bax complex (Sundararajan and White, 2001). However, the results presented in this FRET study show that tBid did bind to Bax, even in the presence of 50 mM Bid BH3 peptide. However, to explain the difference from previous reported results, CHAPS addition did cause the tBid and Bax FRET to decrease, although some FRET remained. This decrease in FRET shows the weakening of the Bax tBid interaction and may explain why tBid and Bax do not form a complex that will be stable during gel filtration or immunoprecipitation in CHAPS. Furthermore, although the FRET observed between tBid and Bax was not an effect of two proteins simply being in a liposome bilayer together, the nature of the binding is not known. tBid and Bax may specifically associate and dissociate in the

membrane, and an average FRET signal is observed. In this case, FRET would be observed, and a hit and run model for tBid would still be possible.

Because FRET depends on the extinction coefficient of the acceptor, and not the quantum yield, it was possible to simultaneously measure both the membrane insertion of Bax using NBD, and tBid to Bax FRET using DAC, in different excitation and emission channels (Figure 3.9A). To further gain insight into the nature of Bax pore formation, actual pore formation was measured simultaneously at a third wavelength. Since ANTS is compatible with NBD or DAC, but not both simultaneously (Figure 3.3A), a different real time pore formation assay was used. Like ANTS, Tb-DPA release is an established assay that has been used previously to measure pore formation in liposomes (Heuck et al., 2003). It is more reliable to compare data that occurred in the same reaction than to compare data from three separate experiments. One interesting feature shown in Figure 3.10 is that Bax pore formation half time was shorter than that for Bax insertion or oligomerization. However, rates of the reactions showed that Bax insertion reached the maximum rate immediately, while pore formation did not reach the maximum rate until several minutes into the reaction. This suggests Bax insertion and oligomerization continued after pore formation, which is not intuitive. An explanation may be that more Bax was being recruited to an existing pore.

A theoretical model of the order of Bax activation is shown in Figure 4.1. The first step of activation is caspase-8 cleaving Bid. The second step is tBid then proceeding to translocate to the membrane. The translocation of tBid to the mitochondria was observed

in the initial discovery of tBid (Li et al., 1998). tBid translocated to membranes very quickly (Figure 3.10B). The third step is tBid binding to Bax at the membrane. Since tBid moved to liposomes quickly, and tBid and Bax did not interact without liposomes (Figure 3.8A), it is likely that Bax interacts with tBid that has inserted into the liposome. The interaction was stable and specific as determined by FRET (Figure 3.8B), although detergent could weaken the binding. Figure 3.10D shows that Bax insertion preceded oligomerization as judged by FRET between Bax. The fourth step is the formation of small pores. As shown in Figure 3.5, some Bax pores were larger than others, and since the half time of small pore formation occurred more quickly than Bax oligomerization and insertion (Figure 3.10B), it is likely that small pore formation preceded large pore formation. However, this is fairly indirect evidence and the temporal resolution in Figure 3.10B is not convincing. Finally, more Bax is recruited and the pore size grows. In 15 minutes incubation with tBid, Bax translocated to the liposomes, however at this point a large portion of the Bax still had not formed CHAPS resistant oligomers (Figure 3.6C).

It is interesting to note that in the model portrayed in Figure 4.1, there is only one tBid shown on the liposome. However, since all the tBid and Bax are targeting to the liposomes, we can consider the approximate numbers of Bax and tBid on the liposome. Using the estimate that there are 20,000 lipids per 100 nm liposome (Enoch and Strittmatter, 1979) the lipid concentration of 125 μM translates into an effective liposome concentration of about 6 nM. In this scenario, there are about 3 to 4 molecules of tBid on each liposome, and about 15 to 20 molecules of Bax on each liposome. However, based on ANTS/DPX release data shown in Figure 3.3B, only about half the liposomes carry

pores. This suggests that the liposomes do not carry an equal distribution of Bax protein, and the distribution of tBid may also not be equally distributed.

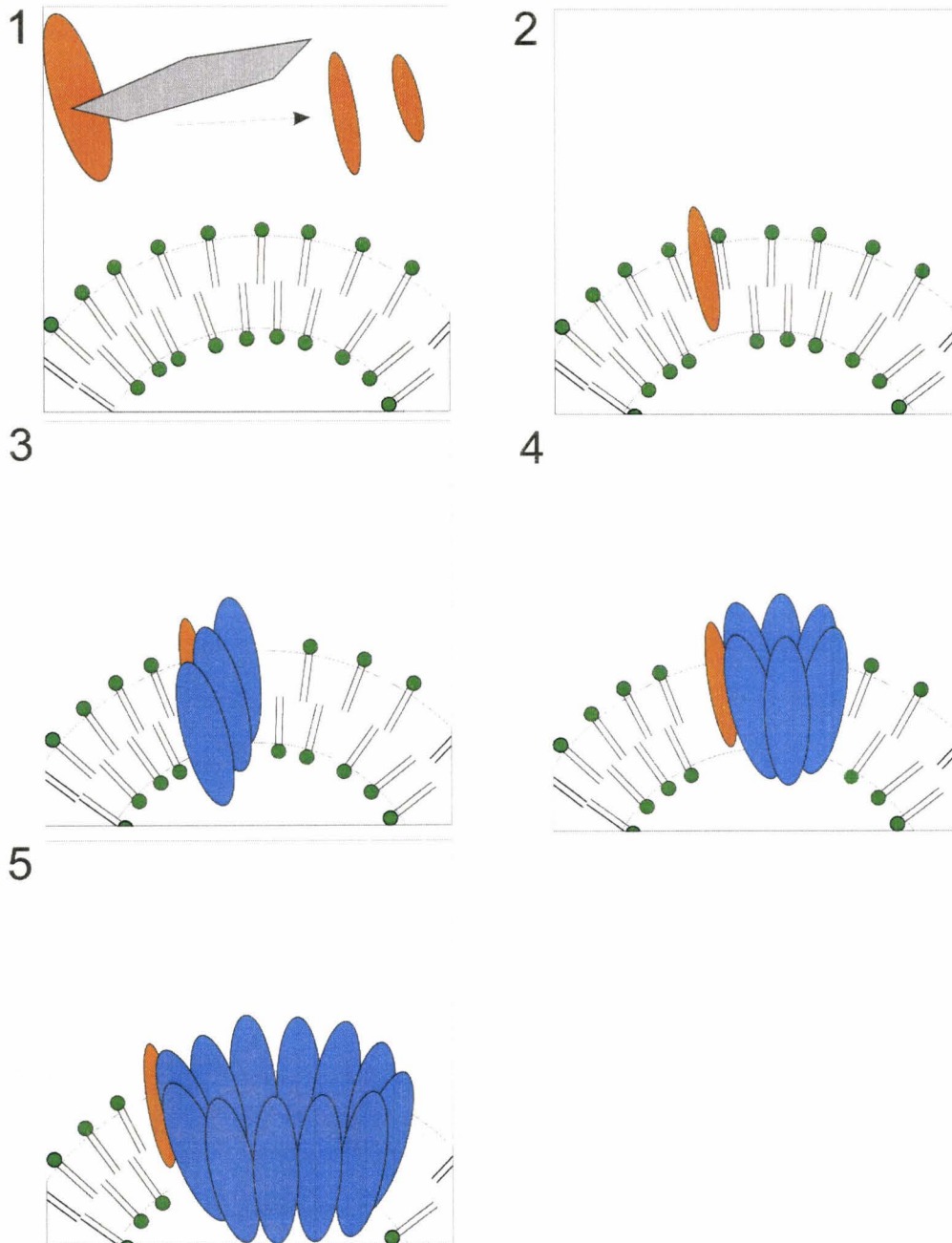


Figure 4.1: Steps in Bax pore formation

- 1. Bid (shown in orange) is cleaved to tBid (also shown in orange) by caspase-8 (shown in grey) after caspases-8 is activated through the Fas pathway**
- 2. tBid then translocates to the mitochondria**
- 3. tBid then interacts with Bax (shown in blue) and Bax inserts into the bilayer before it oligomerizes**
- 4. Bax oligomerizes to form small pores.**
- 5. More Bax is recruited and the pore becomes a larger oligomer. tBid remains in close proximity to Bax**

4.3 Conformational change of Bax

NBD was used to probe conformational changes in Bax. As seen in Figure 3.11B, all the residues in the pore-forming domain increased their intensity during activation. Only one labeled Bax mutant decreased emission; 47C-Bax-NBD, where the cysteine lies in the loop between helix 1 and 2. This residue is also situated close to the pore-forming domain (Figure 1.3). Since NBD emission increases in more hydrophobic environments, it is not surprising that the labeled residues of the pore-forming domain increased their emission as Bax moved to liposomes and oligomerized. It was reassuring that one residue did decrease its emission since this suggests the residues were labeled specifically. Most residues underwent an accompanying emission wavelength blueshift of several nanometers during activation (Figure 3.11D). The residue that had the most blue shifted emission was 114C-Bax-NBD. The NBD probe on this mutant is located centrally on helix 5 (Figure 1.2). The observed increases in intensity obtained (Figure 3.11B) were very similar to the 2 to 4 fold increases seen when a NBD labeled diphtheria toxin was activated to insert and form pores in liposomes (Ladokhin et al., 2004). However, the NBD emission increases were less pronounced than the increases observed for residues in the beta barrel toxin Perfringolysin O, where several labeled mutants increased NBD

fluorescence emission over 6 fold upon activation and one labeled mutant increased NBD emission 25 fold (Shepard et al., 1998).

Fluorescence lifetimes were instructive about the nature of the Bax pore-forming domain. There were two key features about the lifetime data: the residues did not change their lifetime dramatically as they inserted into the bilayer and oligomerized; and there were three groups of lifetimes corresponding to helix 5, helix 6 and the N terminal control residues. As shown in Figure 3.12B, although there is a range in lifetimes from 2 ns to 8 ns, there is not a striking difference in Bax-NBD lifetime between the noninserted monomeric form and the inserted oligomeric form after incubation with tBid. Most residues did not undergo a lifetime change of more than 2 ns. This is not entirely unexpected since it would be energetically favourable that the more hydrophobic areas of the monomeric protein move to a similar region of hydrophobicity in the membrane inserted oligomer, and that the more hydrophilic residues end up in a hydrophilic location of the oligomer. However, the results are in extreme contrast with the results obtained for the Perfringolysin O pore, where several lifetimes of many NBD labeled residues increased 5-10 fold when the protein inserted into membranes. The lifetimes of the membrane inserted Perfringolysin O NBD labeled residues have a lifetime of less than 1 ns if the residue is exposed, and over 6 ns if the residue is inserted into the bilayer (Shepard et al., 1998; Ramachandran et al., 2002). It should be noted that the reported lifetimes in those studies were for only one component, although an intensity weighted average would likely give a similar result. Perfringolysin O undergoes a dramatic change in secondary structure from alpha helix to beta sheet during pore formation, which may

explain the drastic changes in the NBD probe environment. Conversely, evidence suggests that Bax retains its alpha helical structure during activation (Garcia-Saez et al., 2005; Yethon et al., 2003; Xie et al., 1998). The residues that increased lifetime the most were at the base of helix 5. Figure 1.3 shows that this area of the protein is the most accessible part of helix 5. During activation, this part of the helix may swing into a more hydrophobic lipid environment. As shown in the helical wheel plot in Figure 3.12C, in the oligomeric form, the lifetimes of the residues on helix 5 were all greater than 5 ns. These lifetimes were the longest observed, demonstrating that these residues were the least exposed to water, and presumably in contact with the acyl chains of the membrane. The residues that lie N terminal to the pore-forming domain had shorter lifetimes of about 3 ns. The lifetimes of helix 6 were intermediate, ranging from 3 to 5 ns. While the residues of helix 6 were more exposed to water than those of helix 5, this range of lifetimes is longer than expected for an exposed residue. The lifetimes of helix 6 may be explained if they were in an environment that was somewhat exposed both to water and lipid. These results are in agreement with a previous study that showed a peptide corresponding to Bax helix 6 could span the membrane, but only if it was attached to helix 5 (Garcia-Saez et al., 2004). It should be noted that the chi square for the lifetime fit was typically between 1 and 2.5 for a three component fit. A two component fit gave chi square values ten times higher than a three component fit (Table 3.4). Using the same lifetime fluorometer measurement setup, the control of coumarin-6 in absolute ethanol gave a good single exponential fit. This lack of a suitable single or double exponential fit is not unexpected for the NBD data for two reasons. In all solvents, NBD is known to have at

least two lifetimes; and detailed analysis shows that in certain solvents NBD has 3 lifetimes (Lin and Struve, 1991). The non symmetrical emission and excitation of NBD (as seen by the four excitation peaks shown in Figure 3.3A) suggest that this fluorophore undergoes complex excited state geometrical nuclear rearrangement (Lakowicz, 1999, p 8). While there was general agreement between the NBD labeled residues that increased lifetime and those that increased emission intensity, the relationship was certainly not linear. Several NBD labeled residues on helix 6 had lifetimes that decreased, yet the emission intensity increased. The observation of a nonlinear relationship between lifetime and fluorescence intensity changes has been seen before for NBD labeled proteins (Shepard et al., 1998), and may be caused partially by the lack of a single intrinsic lifetime for NBD (Lin and Struve, 1991). Although the lifetimes would imply that helix 5 may span the bilayer, the role of helix 6 is not clear. The pore-forming domain could be either lining an entirely proteinaceous pore where the lipid headgroups are found only at the entrance and exit of the pore, or a toroidal lipidic pore (Figure 4.2A). Indirect evidence showing an outer to inner leaflet lipid rearrangement (Garcia-Saez et al., 2006) suggests that the pore may be lipidic. Quenching data directly supported that model.

When quenching with anionic iodide, most NBD labeled residues became less accessible in membrane inserted oligomeric form, as expected (Figure 3.13B). Interestingly, a couple of very hydrophobic residues, such as 120C-Bax-NBD and 124C-Bax-NBD actually became more accessible to iodide quenching upon activation, however these residues remained relatively resistant to iodide quenching in both inactive and active form compared to the N terminus residues. For the oligomeric Bax, the most

quenchable residues were those found towards the N terminus. Residues on helix 5 were extremely difficult to quench. For the monomeric Bax, residues 130, 138, and 142 stand out as being the residues in the pore-forming domain that were most quenchable by iodide. The structure of Bax shows that these residues on helix 6 are very accessible to water (Figure 1.3). When the protein oligomerized, these residues became more resistant to iodide quenching, indicating this part of the protein moved into protein or lipid contact. The iodide bimolecular quenching constants were not in full agreement with the constants obtained for labeled residues in the Perfringolysin O pore (Shepard et al., 1998). In that study, residues that were exposed to water had iodide bimolecular quenching constants (k_q) of 6 to 10 $M^{-1}ns^{-1}$. The exposed Bax residues towards the N terminus had bimolecular quenching constants of only 2 to 4 $M^{-1}ns^{-1}$. However, this discrepancy can be explained by the much shorter NBD lifetimes of the Perfringolysin residues. Residues on helix 5 of Bax had very similar iodide bimolecular quenching constants as the bilayer inserted residues of Perfringolysin. These residues had quenching constants from about 0.5 to 1 $M^{-1}ns^{-1}$. In general, cobalt was a much more potent quencher of NBD than iodide. This was the first time that NBD labeled protein quenching studies have been performed with cobalt, and the results confirm the observation that cobalt is an effective NBD quencher (Morris et al., 1985). It is interesting to note that the first titer of cobalt was 500 μM , which is in excess of the 125 μM lipid used in the experiment. As seen in Figure 3.13A, the cobalt quenching of Bax incubated with tBid did not follow a linear Stern Volmer quenching, likely because the anionic headgroups of the lipids attracted the cationic quencher, creating a smaller effective volume of higher cobalt concentration that

saturated the membrane. Figures 3.13D and 6.3 show that when Bax inserted and oligomerized in liposomes, the first 500 μM addition of cobalt drastically quenched the NBD labeled residues compared to the subsequent titrations. Remarkably, the residues that showed the greatest susceptibility to cobalt quenching were the residues of the pore-forming domain. Figure 3.13E shows that compared to the N terminal residues before the pore-forming domain, the pore-forming domain was more quenchable by cobalt than iodide. This data suggests the pore-forming domain secures a lipidic pore, as opposed to an entirely proteinaceous pore.

To further verify the role of the pore-forming domain, doxyl quenchers were used to determine the proximity of the labeled residues to quenchers covalently attached to lipids at different depths (Figure 3.14). The residues of helix 5 displayed a quenching pattern consistent with a membrane spanning helix. Interestingly, every assayed mutant on helix 6 displayed the most quenching by the shallowly buried 5' doxyl quencher (Table 3.5). The data also indicated that many of the residues were quenched effectively not just by a single quencher, but at several positions, implying the Bax pore is dynamic.

4.4 A model for the Bax pore-forming domain

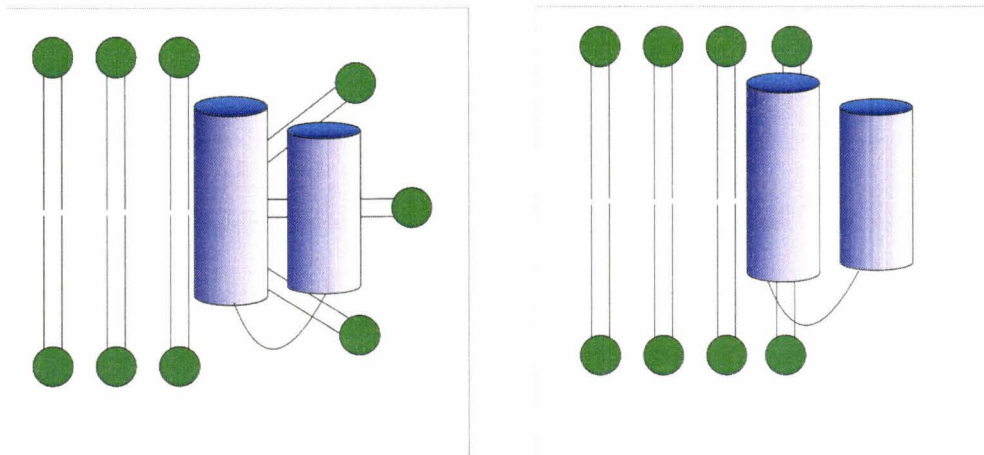
By taking together the data from multiple independent fluorescence techniques, a schematic diagram of the Bax pore may be generated. Figure 4.2A shows a cutaway view of a Bax pore that is forming a lipidic pore (left panel) or alternatively forming a

proteinaceous pore (right panel). Quenching evidence suggests Bax formed lipidic pores. Figure 4.2B shows a Bax pore with only helices 5 and 6 of Bax shown. Helix 6 lies buried just under the headgroups of a toroidal lipidic pore. The environment of helix 6 is dynamic and intermediate, being quenched by doxyl quenchers below the headgroup, but also being quenched by anionic cobalt. Helix 5 on the other hand is more deeply buried, as reflected by longer lifetimes and proneness to quenching by deeper doxyl quenchers. The environment around helix 5 is also dynamic, as residues on this helix did display some quenching from lipid quenchers of multiple depths. The residues were also quenchable by cobalt, although the residues in the middle of this helix were resistant to cobalt quenching. If helix 5 and 6 adopt the position shown in Fig 4.2B, no part of the protein resides on the trans side of the pore (unless another helix besides helix 1 or 9 are transmembrane, which is unlikely based on hydrophobicity). This is unlike the diphtheria toxin, where evidence exists that several of the N terminal helices are on the interior side of the pore (Senzel et al. 2000). The number of Bax monomers comprising the large oligomer is not known. The diphtheria toxin, which appears to make smaller pores than Bax, has been estimated to form oligomers of 20-24 monomers (Bell et al., 1997). Previous attempts have estimated indirectly that Bax forms tetrameric pores (Saito et al., 2000), although a tetramer seems too small to allow the release of large molecules over 100 kDa in size.

This arrangement of helix insertion anchoring a lipidic pore is a new model that sheds light on the mechanism that Bax uses to induce apoptosis. Unlike Bid, where spin labeling studies suggested the helices of Bid are only shallowly inserted (Oh et al., 2005),

the Bax pore-forming domain makes dynamic contact deep into the bilayer. This model may have further implications for our understanding of how other Bcl-2 proteins, such as Bak, function. Furthermore, other alpha helical pore-forming toxins, such as the diphtheria toxin may also use a similar anchoring method to form pores, although previous work using spin labeling has suggested that the diphtheria toxin may form a non-toroidal proteinaceous pore (Oh et al., 1996).

A)



B)

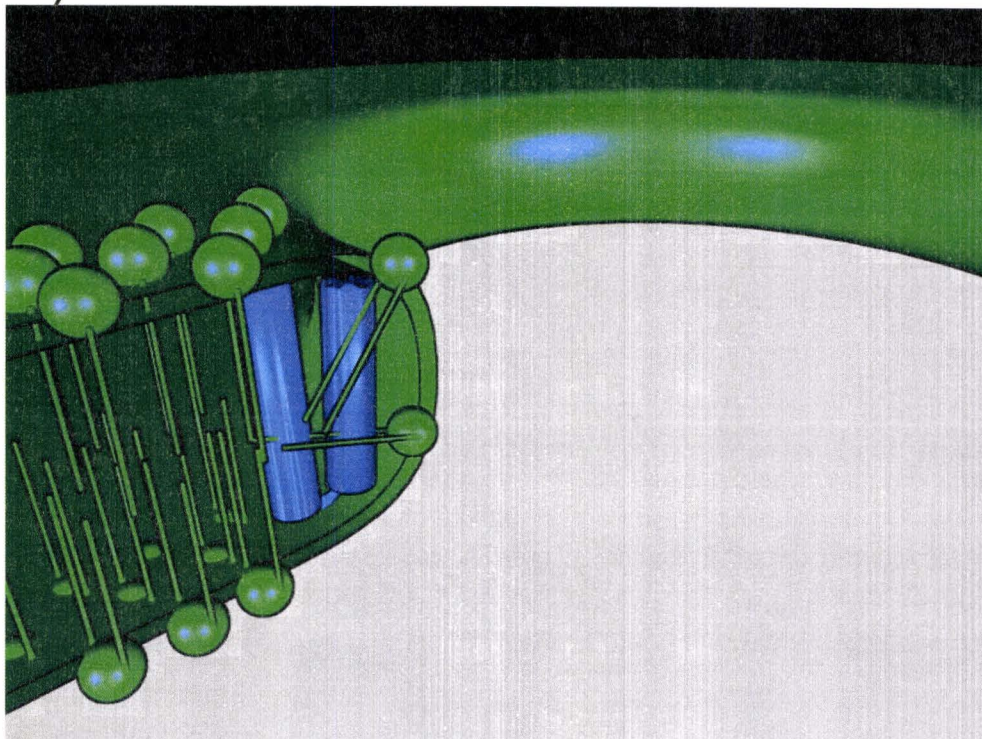


Figure 4.2: Model for topology of the Bax pore-forming domain

A: Sideview of two possible topologies for a lipidic Bax pore (left) and a proteinaceous Bax pore (right). Lipids are shown as green spheres and Bax helix 5 and 6 are shown as blue cylinders.

B: Cutaway model for the possible structure of the pore-forming domain. Image created using the Blender program (available online at <http://www.blender.org>). Blue helices represent Bax helix 5 and 6, with helix 6 closer to the lumen of the pore. The green spheres and their tails represent lipids.

4.5 *Future Direction*

While this study has established a topological model for the pore-forming domain, the role of the other helices and BH regions was not addressed in detail. The lifetimes and quenching data for a couple residues in the amphipathic BH3 region (62C, 66C) suggested that this area of the protein is fairly exposed to water. If the role of the pore-

forming domain is to line a lipidic pore, what parts of the protein must be responsible for oligomerization? Other helices of the protein must be responsible for holding Bax in its cytosolic form until it receives activation from tBid or other Bax. Furthermore, what is the role of the hydrophobic tail anchor of Bax? Residues on this helix become protected from chemical labeling (Annis et al., 2005), but it has been shown that the tail anchor is not required for pore formation. Additional site directed mutagenesis and NBD labeling of more residues can shed more light on the nature of Bax. There are still seven other helices that have unknown function and topology during pore formation. Although this technique can definitely be useful in determining some characteristics of the structure of activated Bax, the difficulty in interpreting the data makes it a temporary replacement for high resolution NMR, crystallographic or EM structural data. Unfortunately, no such data have been reported yet.

There are also several avenues that may be pursued based on the fluorescence assays presented in this thesis. These assays may be used to determine how Bax mutations inhibit the protein. For instance, do all Bax mutants that are unable to permeabilize liposomes and mitochondria behave the same way in terms of helix 5 and 6 insertion and interaction with tBid? tBid-DAC and 126C-Bax-NBD containing further mutations can be used to address this issue. Further work could extend these assays to Bcl-xL to measure how Bcl-xL inhibits Bax and tBid. Furthermore, since this study suggested an order to pore formation by Bax, this system can be used to verify at which point pore-forming inhibitors act. This approach may be more useful if it were extended to determine at which point Bcl-2 and Bcl-xL inhibitors act.

Methods presented in this thesis also could be used for analysis of Bax behaviour in a high throughput screen. Residues have been discovered that undergo large fluorescence increases. Interactions between proteins can be followed with FRET donor emission decreases. These fluorescence parameters could be used to screen compounds that activate Bax or antagonize Bax inhibitors.

5 References

Annis, M. G.; Soucie, E. L.; Dlugosz, P. J.; Cruz-Aguado, J. A.; Penn, L. Z.; Leber, B. & Andrews, D. W.

Bax forms multispanning monomers that oligomerize to permeabilize membranes during apoptosis.

EMBO J, **2005**, *24*, 2096-2103

Antonsson, B.; Conti, F.; Ciavatta, A.; Montessuit, S.; Lewis, S.; Martinou, I.; Bernasconi, L.; Bernard, A.; Mermod, J. J.; Mazzei, G.; Maundrell, K.; Gambale, F.; Sadoul, R. & Martinou, J. C.

Inhibition of Bax channel-forming activity by Bcl-2.

Science, **1997**, *277*, 370-372

Antonsson, B.; Montessuit, S.; Lauper, S.; Eskes, R. & Martinou, J. C.

Bax oligomerization is required for channel-forming activity in liposomes and to trigger cytochrome c release from mitochondria.

Biochem J, **2000**, *345 Pt 2*, 271-278

Antonsson, B.; Montessuit, S.; Sanchez, B. & Martinou, J. C.

Bax is present as a high molecular weight oligomer/complex in the mitochondrial membrane of apoptotic cells.

J Biol Chem, **2001**, *276*, 11615-11623

Astriab-Fisher, A.; Sergueev, D. S.; Fisher, M.; Shaw, B. R. & Juliano, R. L.

Antisense inhibition of P-glycoprotein expression using peptide-oligonucleotide conjugates.

Biochem Pharmacol, **2000**, *60*, 83-90

Bakhshi, A.; Jensen, J. P.; Goldman, P.; Wright, J. J.; McBride, O. W.; Epstein, A. L. & Korsmeyer, S. J.

Cloning the chromosomal breakpoint of t(14;18) human lymphomas: clustering around JH on chromosome 14 and near a transcriptional unit on 18.

Cell, **1985**, *41*, 899-906

Basañez, G.; Zhang, J.; Chau, B. N.; Maksaev, G. I.; Frolov, V. A.; Brandt, T. A.; Burch, J.; Hardwick, J. M. & Zimmerberg, J.

Pro-apoptotic cleavage products of Bcl-xL form cytochrome c-conducting pores in pure lipid membranes.

J Biol Chem, **2001**, *276*, 31083-31091

- Bell, C. E.; Poon, P. H.; Schumaker, V. N. & Eisenberg, D.
Oligomerization of a 45 kilodalton fragment of diphtheria toxin at pH 5.0 to a molecule of 20-24 subunits.
Biochemistry, **1997**, *36*, 15201-15207
- Boatright, K. M. & Salvesen, G. S.
Mechanisms of caspase activation.
Curr Opin Cell Biol, **2003**, *15*, 725-731
- Boise, L. H.; González-García, M.; Postema, C. E.; Ding, L.; Lindsten, T.; Turka, L. A.; Mao, X.; Nuñez, G. & Thompson, C. B.
bcl-x, a bcl-2-related gene that functions as a dominant regulator of apoptotic cell death.
Cell, **1993**, *74*, 597-608
- Cartron, P.; Arokium, H.; Oliver, L.; Meflah, K.; Manon, S. & Vallette, F. M.
Distinct domains control the addressing and the insertion of Bax into mitochondria.
J Biol Chem, **2005**, *280*, 10587-10598
- Cartron, P.; Gallenne, T.; Bougras, G.; Gautier, F.; Manero, F.; Vusio, P.; Meflah, K.; Vallette, F. M. & Juin, P.
The first alpha helix of Bax plays a necessary role in its ligand-induced activation by the BH3-only proteins Bid and PUMA.
Mol Cell, **2004**, *16*, 807-818
- Cartron, P.; Priault, M.; Oliver, L.; Meflah, K.; Manon, S. & Vallette, F. M.
The N-terminal end of Bax contains a mitochondrial-targeting signal.
J Biol Chem, **2003**, *278*, 11633-11641
- Cavard, D.; Sauve, P.; Heitz, F.; Pattus, F.; Martinez, C.; Dijkman, R. & Lazdunski, C.
Hydrodynamic properties of colicin A. Existence of a high-affinity lipid-binding site and oligomerization at acid pH.
Eur J Biochem, **1988**, *172*, 507-512
- Certo, M.; Moore, V. D. G.; Nishino, M.; Wei, G.; Korsmeyer, S.; Armstrong, S. A. & Letai, A.
Mitochondria primed by death signals determine cellular addiction to anti-apoptotic BCL-2 family members.
Cancer Cell, **2006**, *9*, 351-365
- Chami, M.; Prandini, A.; Campanella, M.; Pinton, P.; Szabadkai, G.; Reed, J. C. & Rizzuto, R.
Bcl-2 and Bax exert opposing effects on Ca²⁺ signaling, which do not depend on their

putative pore-forming region.

J Biol Chem, **2004**, *279*, 54581-54589

Cheng, E. H.; Kirsch, D. G.; Clem, R. J.; Ravi, R.; Kastan, M. B.; Bedi, A.; Ueno, K. & Hardwick, J. M.

Conversion of Bcl-2 to a Bax-like death effector by caspases.

Science, **1997**, *278*, 1966-1968

Chipuk, J. E.; Kuwana, T.; Bouchier-Hayes, L.; Droin, N. M.; Newmeyer, D. D.; Schuler, M. & Green, D. R.

Direct activation of Bax by p53 mediates mitochondrial membrane permeabilization and apoptosis.

Science, **2004**, *303*, 1010-1014

Choe, S.; Bennett, M. J.; Fujii, G.; Curmi, P. M.; Kantardjieff, K. A.; Collier, R. J. & Eisenberg, D.

The crystal structure of diphtheria toxin.

Nature, **1992**, *357*, 216-222

Choi, S.; Gonzalvez, F.; Jenkins, G. M.; Slomianny, C.; Chretien, D.; Arnoult, D.; Petit, P. X. & Frohman, M. A.

Cardiolipin deficiency releases cytochrome c from the inner mitochondrial membrane and accelerates stimuli-elicited apoptosis.

Cell Death Differ, **2007**, *14*, 597-606

Cohen, G. M.

Caspases: the executioners of apoptosis.

Biochem J, **1997**, *326 (Pt 1)*, 1-16

Dean, N. M. & Bennett, C. F.

Antisense oligonucleotide-based therapeutics for cancer.

Oncogene, **2003**, *22*, 9087-9096

Dlugosz, P. J.; Billen, L. P.; Annis, M. G.; Zhu, W.; Zhang, Z.; Lin, J.; Leber, B. & Andrews, D. W.

Bcl-2 changes conformation to inhibit Bax oligomerization.

EMBO J, **2006**, *25*, 2287-2296

Du, C.; Fang, M.; Li, Y.; Li, L. & Wang, X.

Smac, a mitochondrial protein that promotes cytochrome c-dependent caspase activation by eliminating IAP inhibition.

Cell, **2000**, *102*, 33-42

Elkins, P.; Bunker, A.; Cramer, W. A. & Stauffacher, C. V.

A mechanism for toxin insertion into membranes is suggested by the crystal structure of the channel-forming domain of colicin E1.

Structure, **1997**, *5*, 443-458

Enoch, H. G. & Strittmatter, P.

Formation and properties of 1000-Å-diameter, single-bilayer phospholipid vesicles.

Proc Natl Acad Sci U S A, **1979**, *76*, 145-149

Epand, R. F.; Martinou, J.; Montessuit, S.; Epand, R. M. & Yip, C. M.

Direct evidence for membrane pore formation by the apoptotic protein Bax.

Biochem Biophys Res Commun, **2002**, *298*, 744-749

Er, E.; Lalier, L.; Cartron, P.; Oliver, L. & Vallette, F. M.

Control of Bax homo-dimerization by its carboxy-terminal.

J Biol Chem, **2007**, *282*, 24938-24947

Eskes, R.; Desagher, S.; Antonsson, B. & Martinou, J. C.

Bid induces the oligomerization and insertion of Bax into the outer mitochondrial membrane.

Mol Cell Biol, **2000**, *20*, 929-935

García-Sáez, A. J.; Mingarro, I.; Pérez-Payá, E. & Salgado, J.

Membrane-insertion fragments of Bcl-xL, Bax, and Bid.

Biochemistry, **2004**, *43*, 10930-10943

García-Sáez, A. J.; Coraiola, M.; Serra, M. D.; Mingarro, I.; Menestrina, G. & Salgado, J.
Peptides derived from apoptotic Bax and Bid reproduce the poration activity of the parent full-length proteins.

Biophys J, **2005**, *88*, 3976-3990

García-Sáez, A. J.; Coraiola, M.; Serra, M. D.; Mingarro, I.; Müller, P. & Salgado, J.
Peptides corresponding to helices 5 and 6 of Bax can independently form large lipid pores.

FEBS J, **2006**, *273*, 971-981

García-Sáez, A. J.; Mingarro, I.; Pérez-Payá, E. & Salgado, J.

Membrane-insertion fragments of Bcl-xL, Bax, and Bid.

Biochemistry, **2004**, *43*, 10930-10943

Geny, B. & Popoff, M. R.

Bacterial protein toxins and lipids: role in toxin targeting and activity.

Biol Cell, **2006**, *98*, 633-651

Gonzalvez, F.; Pariselli, F.; Dupaigne, P.; Budihardjo, I.; Lutter, M.; Antonsson, B.; Diolez, P.; Manon, S.; Martinou, J.; Gubern, M.; Wang, X.; Bernard, S. & Petit, P. X. tBid interaction with cardiolipin primarily orchestrates mitochondrial dysfunctions and subsequently activates Bax and Bak.
Cell Death Differ, **2005**, *12*, 614-626

Hanada, M.; Aimé-Sempé, C.; Sato, T. & Reed, J. C.
Structure-function analysis of Bcl-2 protein. Identification of conserved domains important for homodimerization with Bcl-2 and heterodimerization with Bax.
J Biol Chem, **1995**, *270*, 11962-11969

Hay, S. & Kannourakis, G.
A time to kill: viral manipulation of the cell death program.
J Gen Virol, **2002**, *83*, 1547-1564

Heimlich, G.; McKinnon, A. D.; Bernardo, K.; Brdiczka, D.; Reed, J. C.; Kain, R.; Krönke, M. & Jürgensmeier, J. M.
Bax-induced cytochrome c release from mitochondria depends on alpha-helices-5 and -6.
Biochem J, **2004**, *378*, 247-255

Heuck, A. P.; Tweten, R. K. & Johnson, A. E.
Assembly and topography of the prepore complex in cholesterol-dependent cytolysins.
J Biol Chem, **2003**, *278*, 31218-31225

Hinds, M. G.; Lackmann, M.; Skea, G. L.; Harrison, P. J.; Huang, D. C. S. & Day, C. L.
The structure of Bcl-w reveals a role for the C terminal residues in modulating biological activity.
EMBO J, **2003**, *22*, 1497-1507

Hong, Q.; Gutierrez-Aguirre, I.; Barlic, A.; Malovrh, P.; Kristan, K.; Podlesek, Z.; Macek, P.; Turk, D.; Gonzalez-Manas, J. M.; Lakey, J. H. & Anderluh, G.
Two-step membrane binding by Equinatoxin II, a pore-forming toxin from the sea anemone, involves an exposed aromatic cluster and a flexible helix.
J Biol Chem, **2002**, *277*, 41916-41924

Hsu, Y. T.; Wolter, K. G. & Youle, R. J.
Cytosol-to-membrane redistribution of Bax and Bcl-X(L) during apoptosis.
Proc Natl Acad Sci U S A, **1997**, *94*, 3668-3672

Hsu, Y. T. & Youle, R. J.
Nonionic detergents induce dimerization among members of the Bcl-2 family.
J Biol Chem, **1997**, *272*, 13829-13834

Häcker, G.

The morphology of apoptosis.

Cell Tissue Res, **2000**, *301*, 5-17

Janiak, F.; Leber, B. & Andrews, D. W.

Assembly of Bcl-2 into microsomal and outer mitochondrial membranes.

J Biol Chem, **1994**, *269*, 9842-9849

Jeong, S.; Gaume, B.; Lee, Y.; Hsu, Y.; Ryu, S.; Yoon, S. & Youle, R. J.

Bcl-x(L) sequesters its C terminal membrane anchor in soluble, cytosolic homodimers.

EMBO J, **2004**, *23*, 2146-2155

Jürgensmeier, J. M.; Xie, Z.; Deveraux, Q.; Ellerby, L.; Bredesen, D. & Reed, J. C.

Bax directly induces release of cytochrome c from isolated mitochondria.

Proc Natl Acad Sci U S A, **1998**, *95*, 4997-5002

Kim, H.; Rafiuddin-Shah, M.; Tu, H.; Jeffers, J. R.; Zambetti, G. P.; Hsieh, J. J. & Cheng, E. H.

Hierarchical regulation of mitochondrion-dependent apoptosis by BCL-2 subfamilies.

Nat Cell Biol, **2006**, *8*, 1348-1358

Kluck, R. M.; Bossy-Wetzell, E.; Green, D. R. & Newmeyer, D. D.

The release of cytochrome c from mitochondria: a primary site for Bcl-2 regulation of apoptosis.

Science, **1997**, *275*, 1132-1136

de Kroon, A. I.; Dolis, D.; Mayer, A.; Lill, R. & de Kruijff, B.

Phospholipid composition of highly purified mitochondrial outer membranes of rat liver and *Neurospora crassa*. Is cardiolipin present in the mitochondrial outer membrane?

Biochim Biophys Acta, **1997**, *1325*, 108-116

Kuwana, T.; Mackey, M. R.; Perkins, G.; Ellisman, M. H.; Latterich, M.; Schneider, R.; Green, D. R. & Newmeyer, D. D.

Bid, Bax, and lipids cooperate to form supramolecular openings in the outer mitochondrial membrane.

Cell, **2002**, *111*, 331-342

Lacy, D. B.; Tepp, W.; Cohen, A. C.; DasGupta, B. R. & Stevens, R. C.

Crystal structure of botulinum neurotoxin type A and implications for toxicity.

Nat Struct Biol, **1998**, *5*, 898-902

Lakowicz, J. R.

Principles of Fluorescence Spectroscopy, Second Edition
Kluwer Academic/Plenum Publishers, 1999, New York

Ladokhin, A. S.; Legmann, R.; Collier, R. J. & White, S. H.
Reversible refolding of the diphtheria toxin T-domain on lipid membranes.
Biochemistry, 2004, 43, 7451-7458

Lange, S.; Nüssler, F.; Kauschke, E.; Lutsch, G.; Cooper, E. L. & Herrmann, A.
Interaction of earthworm hemolysin with lipid membranes requires sphingolipids.
J Biol Chem, 1997, 272, 20884-20892

Leber, B.; Lin, J. & Andrews, D. W.
Embedded together: the life and death consequences of interaction of the Bcl-2 family
with membranes.
Apoptosis, 2007, 12, 897-911

Lehto, M. T. & Sharom, F. J.
Proximity of the protein moiety of a GPI-anchored protein to the membrane surface: a
FRET study.
Biochemistry, 2002, 41, 8368-8376

Li, H.; Zhu, H.; Xu, C. J. & Yuan, J.
Cleavage of BID by caspase 8 mediates the mitochondrial damage in the Fas pathway of
apoptosis.
Cell, 1998, 94, 491-501

Li, L. Y.; Luo, X. & Wang, X.
Endonuclease G is an apoptotic DNase when released from mitochondria.
Nature, 2001, 412, 95-99

Lin, S. & Struve, W. S.
Time-resolved fluorescence of nitrobenzoxadiazole-aminohexanoic acid: effect of
intermolecular hydrogen-bonding on non-radiative decay.
Photochem Photobiol, 1991, 54, 361-365

Liu, X.; Kim, C. N.; Yang, J.; Jemmerson, R. & Wang, X.
Induction of apoptotic program in cell-free extracts: requirement for dATP and
cytochrome c.
Cell, 1996, 86, 147-157

Luo, X.; Budihardjo, I.; Zou, H.; Slaughter, C. & Wang, X.
Bid, a Bcl2 interacting protein, mediates cytochrome c release from mitochondria in

response to activation of cell surface death receptors.

Cell, **1998**, *94*, 481-490

Lutter, M.; Fang, M.; Luo, X.; Nishijima, M.; Xie, X. & Wang, X.

Cardiolipin provides specificity for targeting of tBid to mitochondria.

Nat Cell Biol, **2000**, *2*, 754-761

Matsuyama, S.; Schendel, S. L.; Xie, Z. & Reed, J. C.

Cytoprotection by Bcl-2 requires the pore-forming alpha5 and alpha6 helices.

J Biol Chem, **1998**, *273*, 30995-31001

Meijerink, J. P.; Mensink, E. J.; Wang, K.; Sedlak, T. W.; Slöetjes, A. W.; de Witte, T.; Waksman, G. & Korsmeyer, S. J.

Hematopoietic malignancies demonstrate loss-of-function mutations of BAX.

Blood, **1998**, *91*, 2991-2997

Minn, A. J.; Vélez, P.; Schendel, S. L.; Liang, H.; Muchmore, S. W.; Fesik, S. W.; Fill, M. & Thompson, C. B.

Bcl-x(L) forms an ion channel in synthetic lipid membranes.

Nature, **1997**, *385*, 353-357

Miyashita, T. & Reed, J. C.

Tumor suppressor p53 is a direct transcriptional activator of the human bax gene.

Cell, **1995**, *80*, 293-299

Morris, S. J.; Bradley, D. & Blumenthal, R.

The use of cobalt ions as a collisional quencher to probe surface charge and stability of fluorescently labeled bilayer vesicles.

Biochim Biophys Acta, **1985**, *818*, 365-372

Muchmore, S. W.; Sattler, M.; Liang, H.; Meadows, R. P.; Harlan, J. E.; Yoon, H. S.;

Nettesheim, D.; Chang, B. S.; Thompson, C. B.; Wong, S. L.; Ng, S. L. & Fesik, S. W.

X-ray and NMR structure of human Bcl-xL, an inhibitor of programmed cell death.

Nature, **1996**, *381*, 335-341

Musse, A. A. & Merrill, A. R.

The molecular basis for the pH-activation mechanism in the channel-forming bacterial colicin E1.

J Biol Chem, **2003**, *278*, 24491-24499

Musse, A. A.; Wang, J.; Deleon, G. P.; Prentice, G. A.; London, E. & Merrill, A. R.

Scanning the membrane-bound conformation of helix 1 in the colicin E1 channel domain

by site-directed fluorescence labeling.

J Biol Chem, **2006**, *281*, 885-895

Namihisa, T.; Saifuku, K.; Ishii, H.; Watanabe, S. & Sekine, T.

N-(7-dimethylamino-4-methylcoumarinyl)-maleimide (DACM): an alternative label for fluorescence tracing.

J Immunol Methods, **1983**, *56*, 125-134

Nechushtan, A.; Smith, C. L.; Hsu, Y. T. & Youle, R. J.

Conformation of the Bax C-terminus regulates subcellular location and cell death.

EMBO J, **1999**, *18*, 2330-2341

Nouraini, S.; Six, E.; Matsuyama, S.; Krajewski, S. & Reed, J. C.

The putative pore-forming domain of Bax regulates mitochondrial localization and interaction with Bcl-X(L).

Mol Cell Biol, **2000**, *20*, 1604-1615

Ogawa, H.; Taneda, A.; Kanaoka, Y. & Sekine, T.

The histochemical distribution of protein bound sulfhydryl groups in human epidermis by the new staining method.

J Histochem Cytochem, **1979**, *27*, 942-946

Oh, K. J.; Barbuto, S.; Meyer, N.; Kim, R.; Collier, R. J. & Korsmeyer, S. J.

Conformational changes in BID, a pro-apoptotic BCL-2 family member, upon membrane binding. A site-directed spin labeling study.

J Biol Chem, **2005**, *280*, 753-767

Oh, K. J.; Zhan, H.; Cui, C.; Hideg, K.; Collier, R. J. & Hubbell, W. L.

Organization of diphtheria toxin T domain in bilayers: a site-directed spin labeling study.

Science, **1996**, *273*, 810-812

Ohsato, T.; Ishihara, N.; Muta, T.; Umeda, S.; Ikeda, S.; Mihara, K.; Hamasaki, N. & Kang, D.

Mammalian mitochondrial endonuclease G. Digestion of R-loops and localization in intermembrane space.

Eur J Biochem, **2002**, *269*, 5765-5770

Oltvai, Z. N.; Millman, C. L. & Korsmeyer, S. J.

Bcl-2 heterodimerizes in vivo with a conserved homolog, Bax, that accelerates programmed cell death.

Cell, **1993**, *74*, 609-619

Pagliari, L. J.; Kuwana, T.; Bonzon, C.; Newmeyer, D. D.; Tu, S.; Beere, H. M. & Green, D. R.

The multidomain proapoptotic molecules Bax and Bak are directly activated by heat.
Proc Natl Acad Sci U S A, **2005**, *102*, 17975-17980

Parikh, N.; Koshy, C.; Dhayabaran, V.; Perumalsamy, L. R.; Sowdhamini, R. & Sarin, A.
The N-terminus and alpha-5, alpha-6 helices of the pro-apoptotic protein Bax, modulate functional interactions with the anti-apoptotic protein Bcl-xL.
BMC Cell Biol, **2007**, *8*, 16

Petros, A. M.; Olejniczak, E. T. & Fesik, S. W.
Structural biology of the Bcl-2 family of proteins.
Biochim Biophys Acta, **2004**, *1644*, 83-94

Quertenmont, P.; Wattiez, R.; Falmagne, P.; Ruyschaert, J. M. & Cabiliaux, V.
Topology of diphtheria toxin in lipid vesicle membranes: a proteolysis study.
Mol Microbiol, **1996**, *21*, 1283-1296

Ramachandran, R.; Heuck, A. P.; Tweten, R. K. & Johnson, A. E.
Structural insights into the membrane-anchoring mechanism of a cholesterol-dependent cytolysin.
Nat Struct Biol, **2002**, *9*, 823-827

Rampino, N.; Yamamoto, H.; Ionov, Y.; Li, Y.; Sawai, H.; Reed, J. C. & Perucho, M.
Somatic frameshift mutations in the BAX gene in colon cancers of the microsatellite mutator phenotype.
Science, **1997**, *275*, 967-969

Reed, J. C.
Bcl-2 and the regulation of programmed cell death.
J Cell Biol, **1994**, *124*, 1-6

Rosconi, M. P.; Zhao, G. & London, E.
Analyzing topography of membrane-inserted diphtheria toxin T domain using BODIPY-streptavidin: at low pH, helices 8 and 9 form a transmembrane hairpin but helices 5-7 form stable nonclassical inserted segments on the cis side of the bilayer.
Biochemistry, **2004**, *43*, 9127-9139

Rostovtseva, T. K.; Antonsson, B.; Suzuki, M.; Youle, R. J.; Colombini, M. & Bezrukov, S. M.
Bid, but not Bax, regulates VDAC channels.
J Biol Chem, **2004**, *279*, 13575-13583

Roucou, X.; Rostovtseva, T.; Montessuit, S.; Martinou, J. & Antonsson, B.
Bid induces cytochrome c-impermeable Bax channels in liposomes.

Biochem J, **2002**, *363*, 547-552

Ruiz-Carrillo, A. & Renaud, J.

Endonuclease G: a (dG)_n X (dC)_n-specific DNase from higher eukaryotes.

EMBO J, **1987**, *6*, 401-407

Saelens, X.; Festjens, N.; Walle, L. V.; van Gurp, M.; van Loo, G. & Vandenameele, P.
Toxic proteins released from mitochondria in cell death.

Oncogene, **2004**, *23*, 2861-2874

Saito, M.; Korsmeyer, S. J. & Schlesinger, P. H.

BAX-dependent transport of cytochrome c reconstituted in pure liposomes.

Nat Cell Biol, **2000**, *2*, 553-555

Sawada, M.; Sun, W.; Hayes, P.; Leskov, K.; Boothman, D. A. & Matsuyama, S.
Ku70 suppresses the apoptotic translocation of Bax to mitochondria.

Nat Cell Biol, **2003**, *5*, 320-329

Schägger, H. & von Jagow, G.

Tricine-sodium dodecyl sulfate-polyacrylamide gel electrophoresis for the separation of proteins in the range from 1 to 100 kDa.

Anal Biochem, **1987**, *166*, 368-379

Senzel, L.; Gordon, M.; Blaustein, R. O.; Oh, K. J.; Collier, R. J. & Finkelstein, A.
Topography of diphtheria Toxin's T domain in the open channel state.

J Gen Physiol, **2000**, *115*, 421-434

Sharpe, J. C. & London, E.

Diphtheria toxin forms pores of different sizes depending on its concentration in membranes: probable relationship to oligomerization.

J Membr Biol, **1999**, *171*, 209-221

Shepard, L. A.; Heuck, A. P.; Hamman, B. D.; Rossjohn, J.; Parker, M. W.; Ryan, K. R.; Johnson, A. E. & Tweten, R. K.

Identification of a membrane-spanning domain of the thiol-activated pore-forming toxin *Clostridium perfringens* perfringolysin O: an alpha-helical to beta-sheet transition identified by fluorescence spectroscopy.

Biochemistry, **1998**, *37*, 14563-14574

Shimizu, S.; Ide, T.; Yanagida, T. & Tsujimoto, Y.

Electrophysiological study of a novel large pore formed by Bax and the voltage-

dependent anion channel that is permeable to cytochrome c.

J Biol Chem, **2000**, *275*, 12321-12325

Smolarsky, M.; Teitelbaum, D.; Sela, M. & Gitler, C.

A simple fluorescent method to determine complement-mediated liposome immune lysis.

J Immunol Methods, **1977**, *15*, 255-265

Susin, S. A.; Lorenzo, H. K.; Zamzami, N.; Marzo, I.; Snow, B. E.; Brothers, G. M.; Mangion, J.; Jacotot, E.; Costantini, P.; Loeffler, M.; Larochette, N.; Goodlett, D. R.; Aebersold, R.; Siderovski, D. P.; Penninger, J. M. & Kroemer, G.

Molecular characterization of mitochondrial apoptosis-inducing factor.

Nature, **1999**, *397*, 441-446

Sundararajan, R. & White, E.

E1B 19K blocks Bax oligomerization and tumor necrosis factor alpha-mediated apoptosis.

J Virol, **2001**, *75*, 7506-7516

Suzuki, M.; Youle, R. J. & Tjandra, N.

Structure of Bax: coregulation of dimer formation and intracellular localization.

Cell, **2000**, *103*, 645-654

Suzuki, Y.; Imai, Y.; Nakayama, H.; Takahashi, K.; Takio, K. & Takahashi, R.

A serine protease, HtrA2, is released from the mitochondria and interacts with XIAP, inducing cell death.

Mol Cell, **2001**, *8*, 613-621

Terrones, O.; Antonsson, B.; Yamaguchi, H.; Wang, H.; Liu, J.; Lee, R. M.; Herrmann, A. & Basañez, G.

Lipidic pore formation by the concerted action of proapoptotic BAX and tBID.

J Biol Chem, **2004**, *279*, 30081-30091

Tilley, S. J.; Orlova, E. V.; Gilbert, R. J. C.; Andrew, P. W. & Saibil, H. R.

Structural basis of pore formation by the bacterial toxin pneumolysin.

Cell, **2005**, *121*, 247-256

Tilley, S. J. & Saibil, H. R.

The mechanism of pore formation by bacterial toxins.

Curr Opin Struct Biol, **2006**, *16*, 230-236

Tory, M. C. & Merrill, A. R.

Adventures in membrane protein topology. A study of the membrane-bound state of

colicin E1.

J Biol Chem, **1999**, *274*, 24539-24549

Tremblais, K.; Oliver, L.; Juin, P.; Cabellec, T. M. L.; Meflah, K. & Vallette, F. M.
The C-terminus of bax is not a membrane addressing/anchoring signal.

Biochem Biophys Res Commun, **1999**, *260*, 582-591

Tsujimoto, Y.; Finger, L. R.; Yunis, J.; Nowell, P. C. & Croce, C. M.
Cloning of the chromosome breakpoint of neoplastic B cells with the t(14;18)
chromosome translocation.

Science, **1984**, *226*, 1097-1099

Unger, V. M.; Kumar, N. M.; Gilula, N. B. & Yeager, M.

Three-dimensional structure of a recombinant gap junction membrane channel.

Science, **1999**, *283*, 1176-1180

Vaux, D. L.; Cory, S. & Adams, J. M.

Bcl-2 gene promotes haemopoietic cell survival and cooperates with c-myc to
immortalize pre-B cells.

Nature, **1988**, *335*, 440-442

Wang, K.; Gross, A.; Waksman, G. & Korsmeyer, S. J.

Mutagenesis of the BH3 domain of BAX identifies residues critical for dimerization and
killing.

Mol Cell Biol, **1998**, *18*, 6083-6089

Van Gurp, M.; Festjens, N.; van Loo, G.; Saelens, X. & Vandenabeele, P.

Mitochondrial intermembrane proteins in cell death.

Biochem Biophys Res Commun, **2003**, *304*, 487-497

Wang, K.; Yin, X. M.; Chao, D. T.; Milliman, C. L. & Korsmeyer, S. J.

BID: a novel BH3 domain-only death agonist.

Genes Dev, **1996**, *10*, 2859-2869

Wei, M. C.; Lindsten, T.; Mootha, V. K.; Weiler, S.; Gross, A.; Ashiya, M.; Thompson,
C. B. & Korsmeyer, S. J.

tBID, a membrane-targeted death ligand, oligomerizes BAK to release cytochrome c.

Genes Dev, **2000**, *14*, 2060-2071

Wei, M. C.; Zong, W. X.; Cheng, E. H.; Lindsten, T.; Panoutsakopoulou, V.; Ross, A. J.;
Roth, K. A.; MacGregor, G. R.; Thompson, C. B. & Korsmeyer, S. J.

Proapoptotic BAX and BAK: a requisite gateway to mitochondrial dysfunction and death.

Science, **2001**, *292*, 727-730

Willis, S. N.; Fletcher, J. I.; Kaufmann, T.; van Delft, M. F.; Chen, L.; Czabotar, P. E.; Ierino, H.; Lee, E. F.; Fairlie, W. D.; Bouillet, P.; Strasser, A.; Kluck, R. M.; Adams, J. M. & Huang, D. C. S.
Apoptosis initiated when BH3 ligands engage multiple Bcl-2 homologs, not Bax or Bak.
Science, **2007**, *315*, 856-859

Wolter, K. G.; Hsu, Y. T.; Smith, C. L.; Nechushtan, A.; Xi, X. G. & Youle, R. J.
Movement of Bax from the cytosol to mitochondria during apoptosis.
J Cell Biol, **1997**, *139*, 1281-1292

Xiang, J.; Chao, D. T. & Korsmeyer, S. J.
BAX-induced cell death may not require interleukin 1 beta-converting enzyme-like proteases.
Proc Natl Acad Sci U S A, **1996**, *93*, 14559-14563

Xie, Z.; Schendel, S.; Matsuyama, S. & Reed, J. C.
Acidic pH promotes dimerization of Bcl-2 family proteins.
Biochemistry, **1998**, *37*, 6410-6418

Yang, J.; Liu, X.; Bhalla, K.; Kim, C. N.; Ibrado, A. M.; Cai, J.; Peng, T. I.; Jones, D. P. & Wang, X.
Prevention of apoptosis by Bcl-2: release of cytochrome c from mitochondria blocked.
Science, **1997**, *275*, 1129-1132

Yethon, J. A.; Epand, R. F.; Leber, B.; Epand, R. M. & Andrews, D. W.
Interaction with a membrane surface triggers a reversible conformational change in Bax normally associated with induction of apoptosis.
J Biol Chem, **2003**, *278*, 48935-48941

Zalman, L. S. & Wisnieski, B. J.
Mechanism of insertion of diphtheria toxin: peptide entry and pore size determinations.
Proc Natl Acad Sci U S A, **1984**, *81*, 3341-3345

Zha, H.; Aimé-Sempé, C.; Sato, T. & Reed, J. C.
Proapoptotic protein Bax heterodimerizes with Bcl-2 and homodimerizes with Bax via a novel domain (BH3) distinct from BH1 and BH2.
J Biol Chem, **1996**, *271*, 7440-7444

Zha, H. & Reed, J. C.
Heterodimerization-independent functions of cell death regulatory proteins Bax and Bcl-2 in yeast and mammalian cells.
J Biol Chem, **1997**, *272*, 31482-31488

Zhivotovsky, B.; Hanson, K. P. & Orrenius, S.

Back to the future: the role of cytochrome c in cell death.

Cell Death Differ, **1998**, *5*, 459-460

Zou, H.; Li, Y.; Liu, X. & Wang, X.

An APAF-1.cytochrome c multimeric complex is a functional apoptosome that activates procaspase-9.

J Biol Chem, **1999**, *274*, 11549-11556

6 Supplementary material

6.1 *Cleavage by hydroxylamine is preferred over betamercaptoethanol*

To avoid over labeling with IANBD, the use of hydroxylamine was investigated, as this was recommended by a representative of the manufacturer (New England Biolabs). Figure 6.1 shows that cleaving the intein with hydroxyl amine instead of beta-mercaptoethanol reduced non specific labeling. Subsequently, all mutants were repurified using hydroxylamine as the cleaving agent.

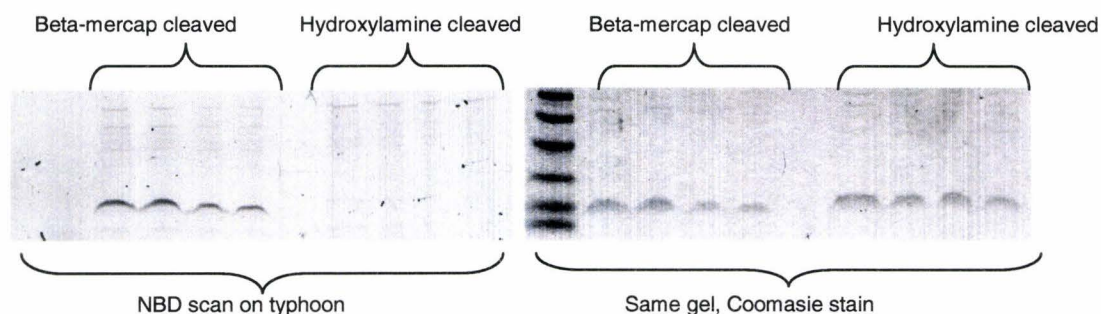
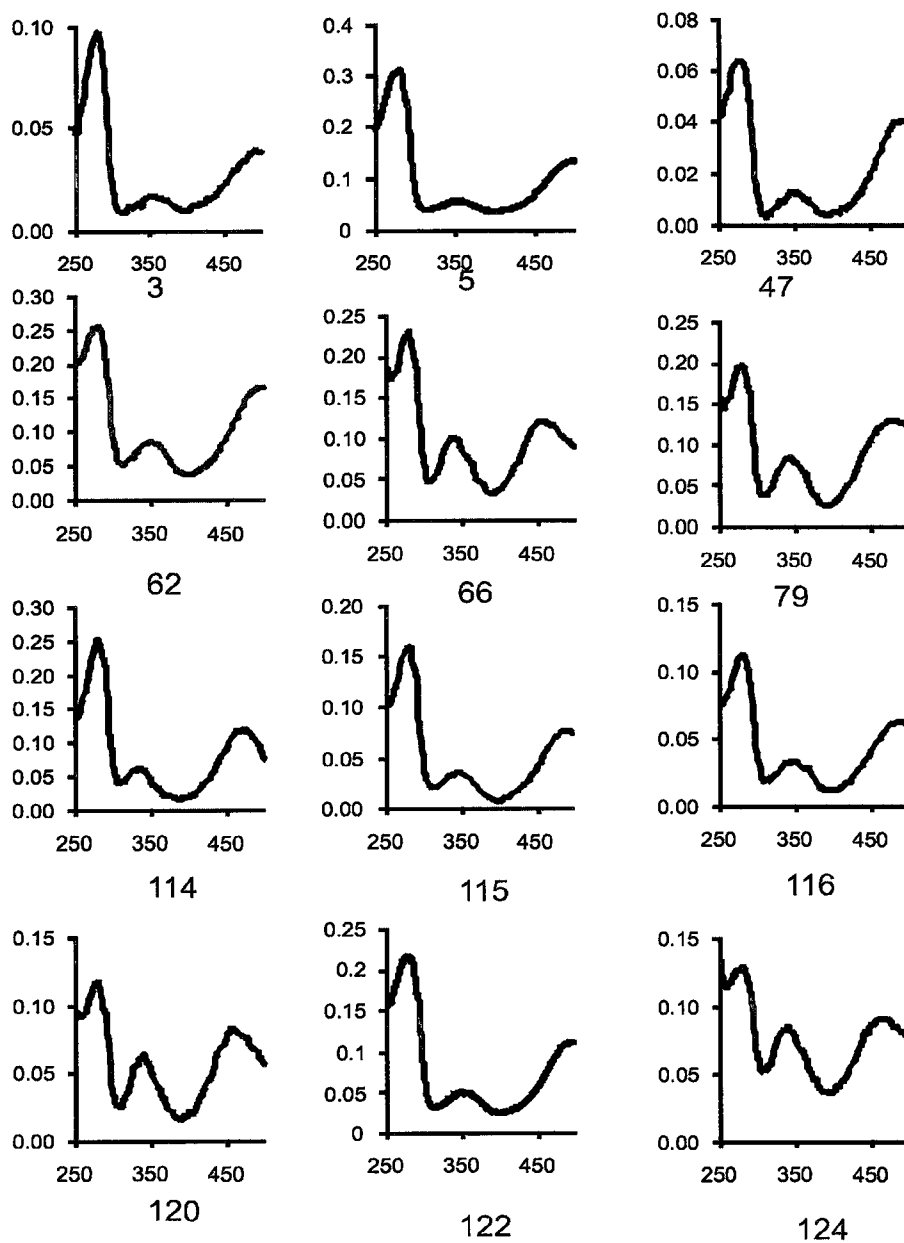


Figure 6.1: Cleavage by hydroxyl amine can reduce non-specific labeling of Bax

Before inducing intein cleavage, cysteine negative Bax (plasmid# 1730) bound to chitin beads was split into two and then was cleaved for 24 hours with 100 mM Beta-mercaptoethanol or 100 mM hydroxylamine. The proteins were then eluted, dialyzed and labeled with 10 fold excess of IANBD. The left panel shows an SDS PAGE gel Typhoon fluorescence scan of 10, 9 8, and 7 uL of labeled protein for both the Beta-mercaptoethanol cleaved Bax and the hydroxylamine cleaved Bax. The hydroxylamine cleaved Bax does not appear on this fluorescence scan. The right panel shows the Coomassie stain of the same gel.

6.2 Absorbance spectra of NBD labeled mutants

Figure 6.1 shows the absorbance spectra of the Bax proteins used in this study.



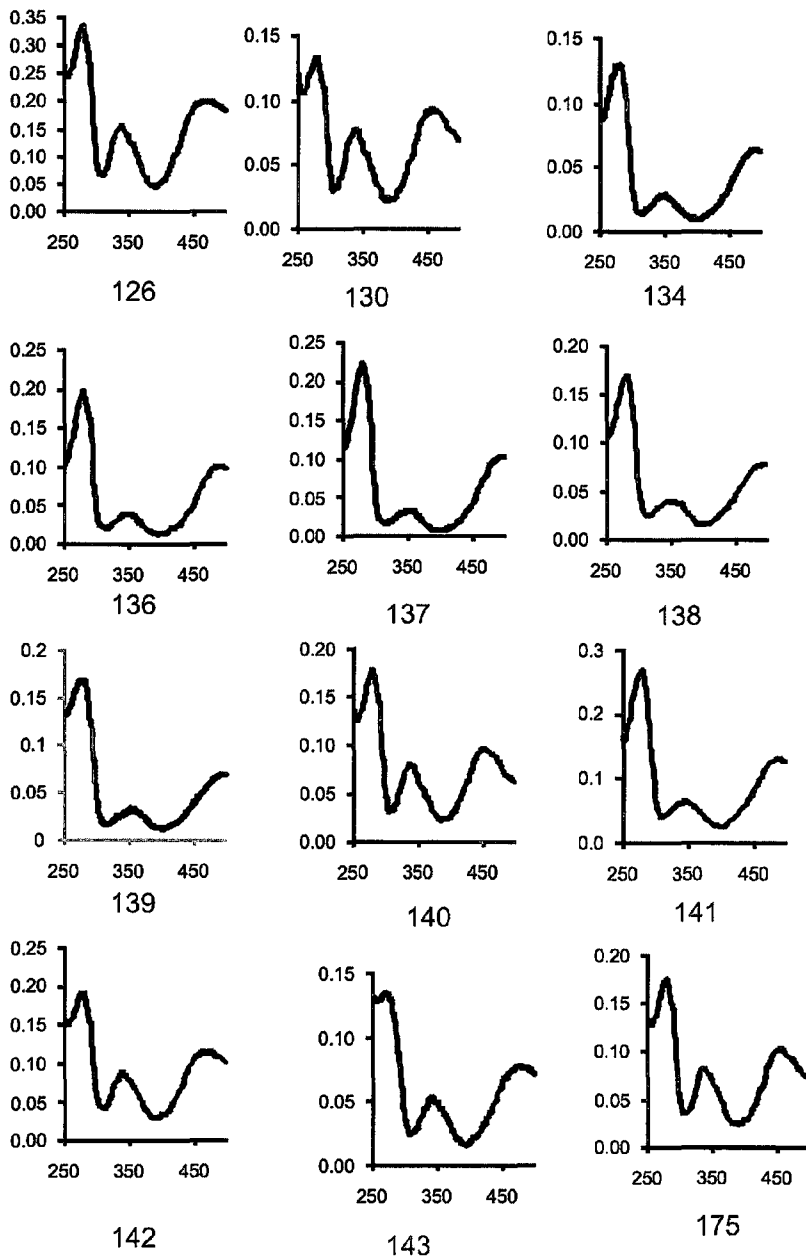
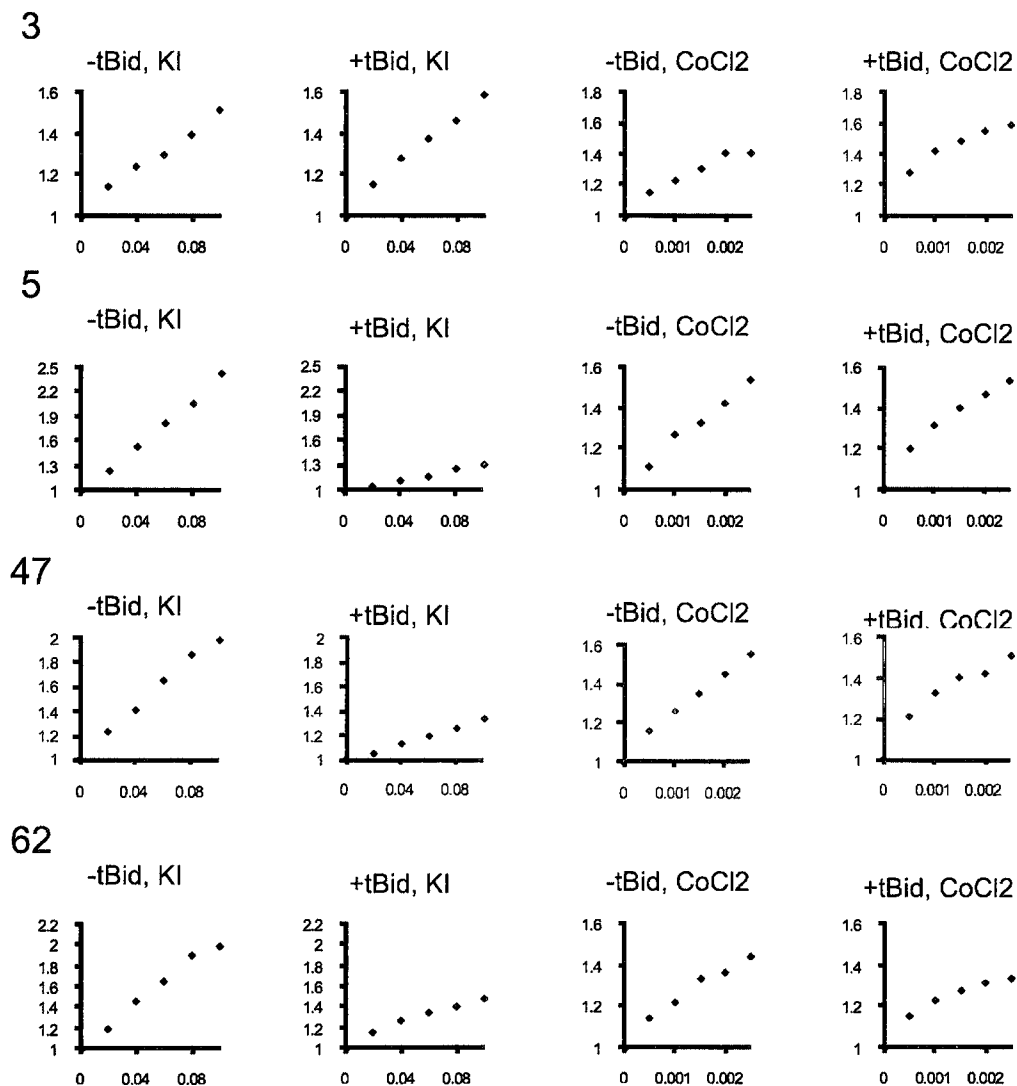


Figure 6.2: Absorbance spectra of labeled Bax mutants

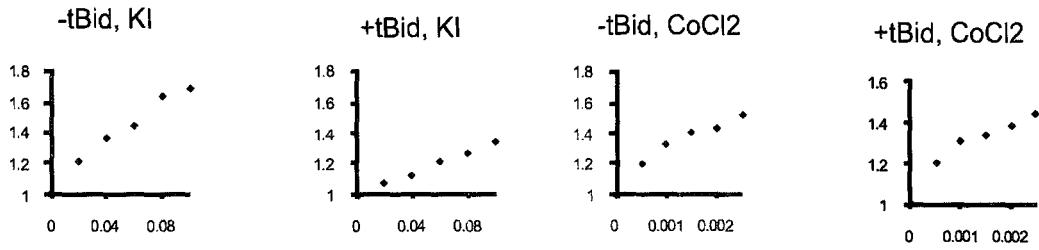
Spectra obtained after labeling and removing free dye from sample. The x axis shows the wavelength in nm and the y axis shows the absorbance. The pathlength was 0.8 cm. All spectra had a buffer blank (10% glycerol, 0.2 M NaCl, 0.2 mM EDTA, 10 mM HEPES pH7) subtracted.

6.3 Ionic quenching titrations

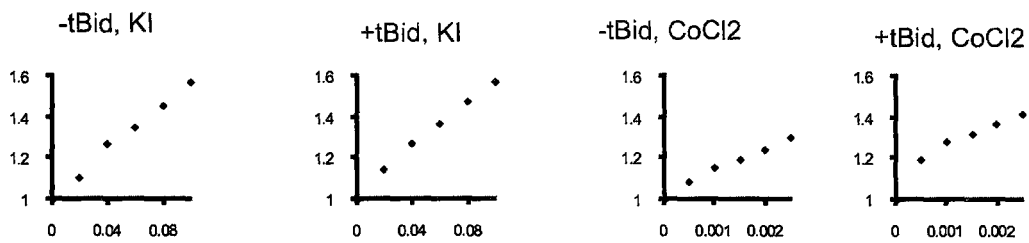
Figure 6.2 shows representative iodide and cobalt quenching curves for the NBD labeled Bax mutants assayed with or without incubation with tBid.



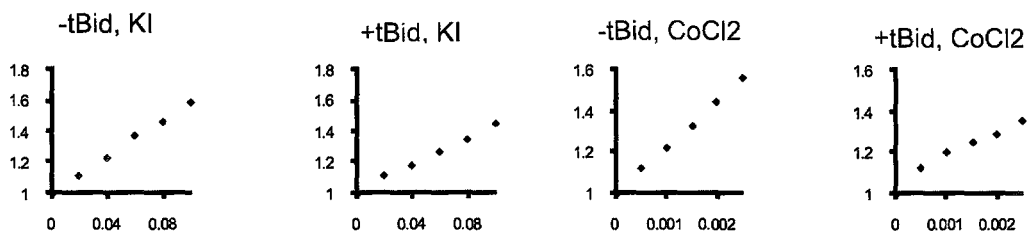
66



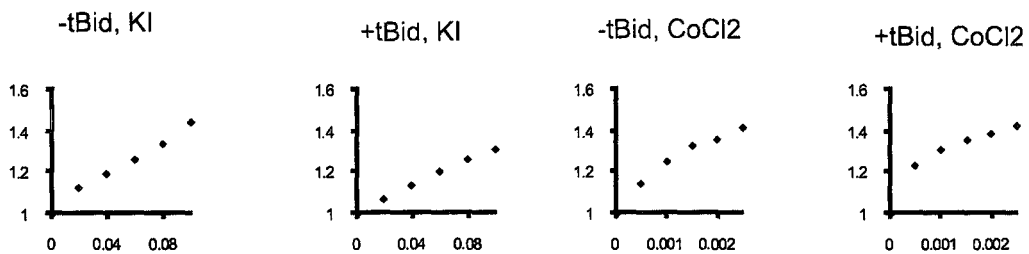
79



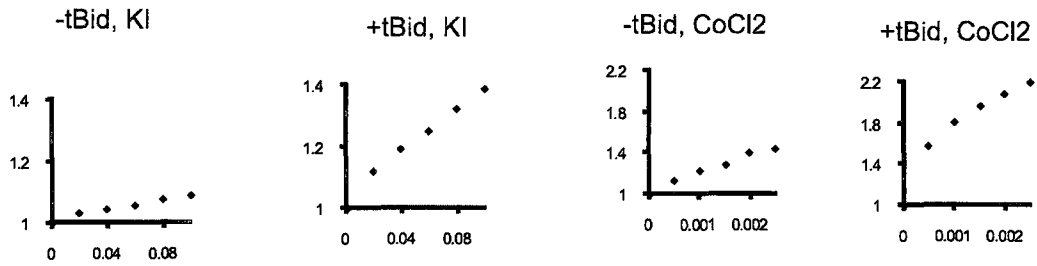
114



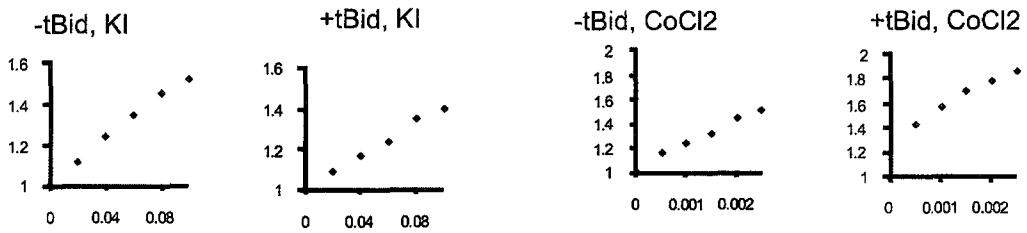
118



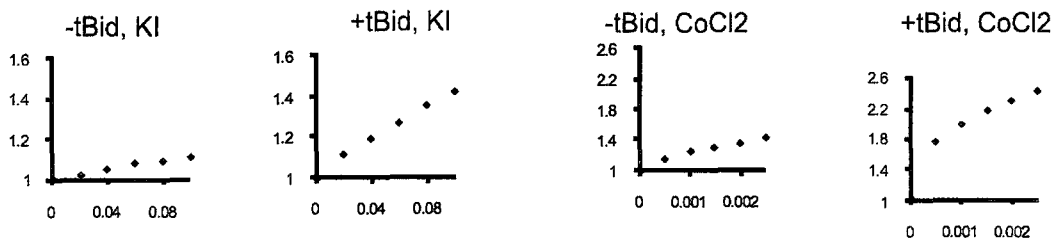
120



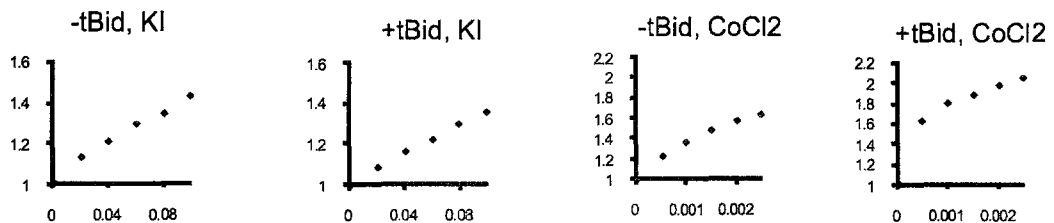
122



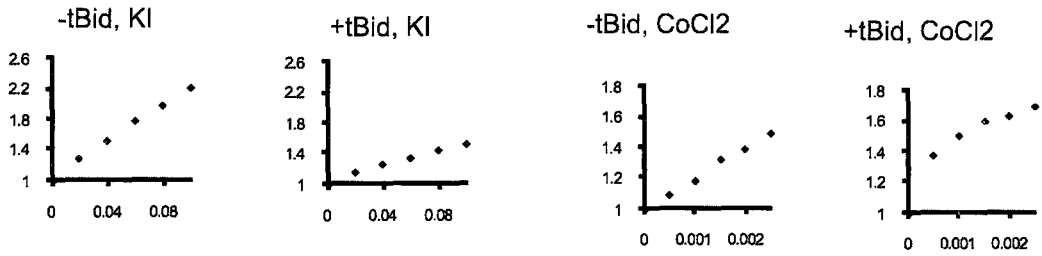
124



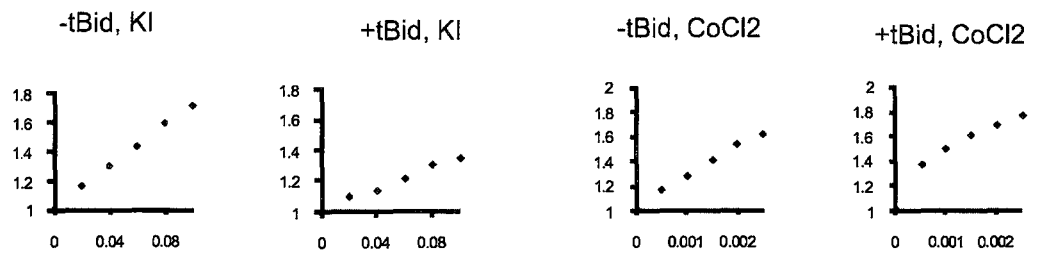
126



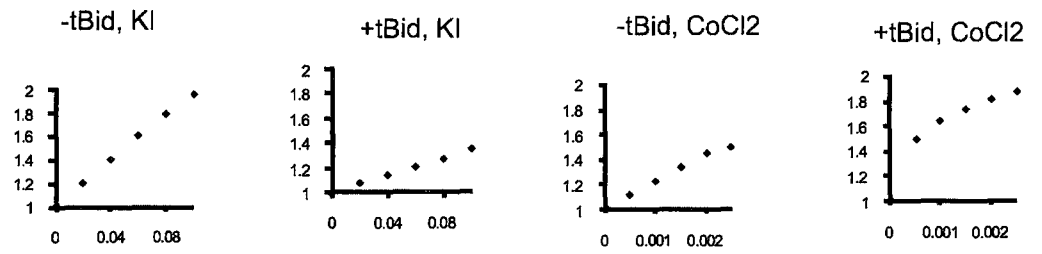
130



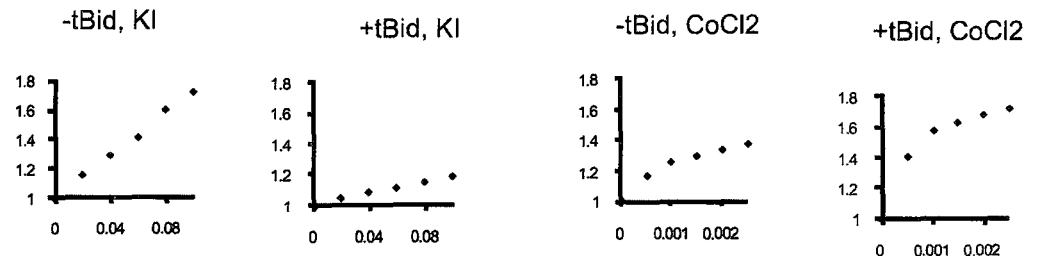
134



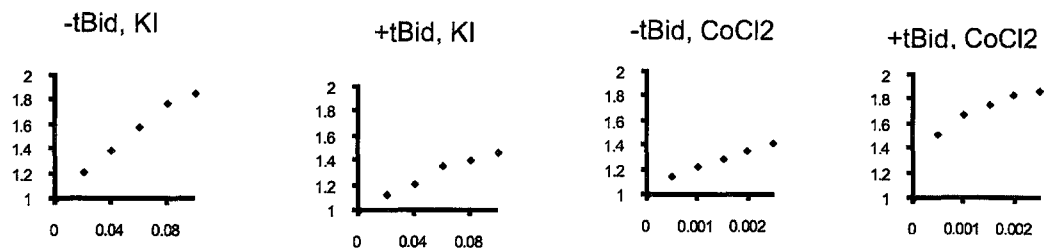
136



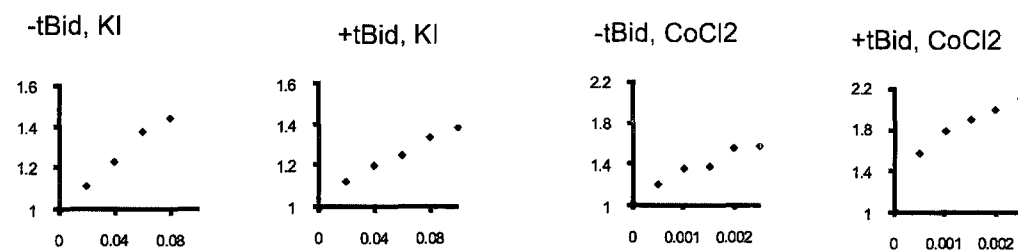
137



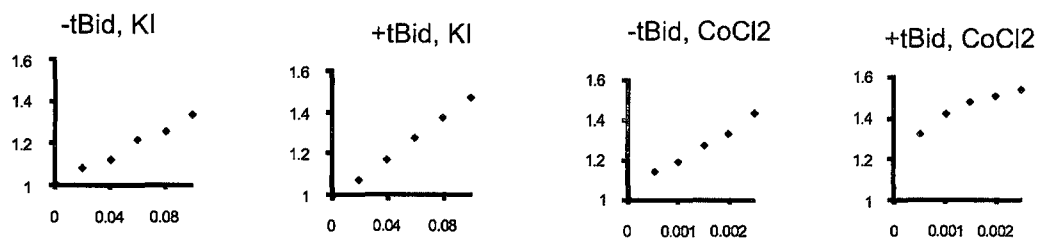
138



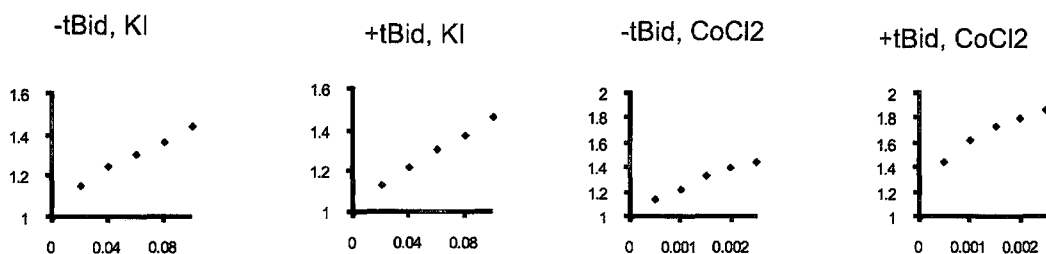
139



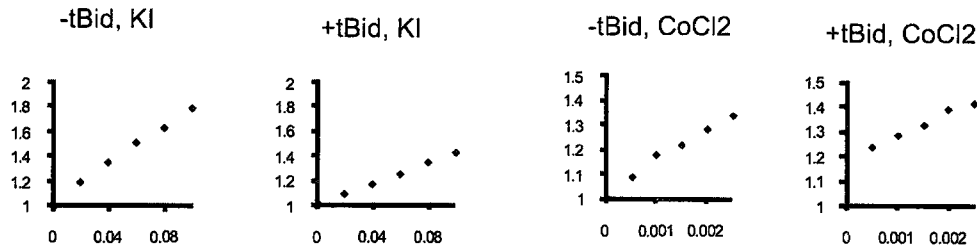
140



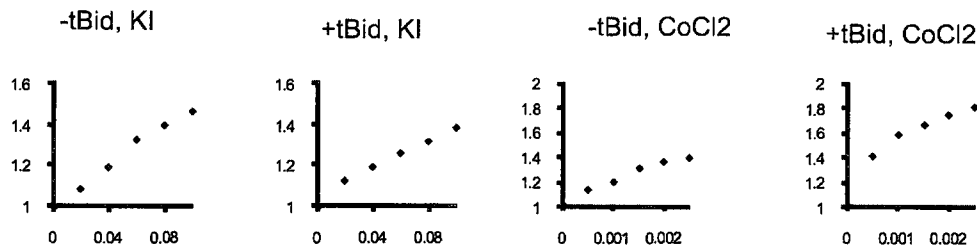
141



142



143



175

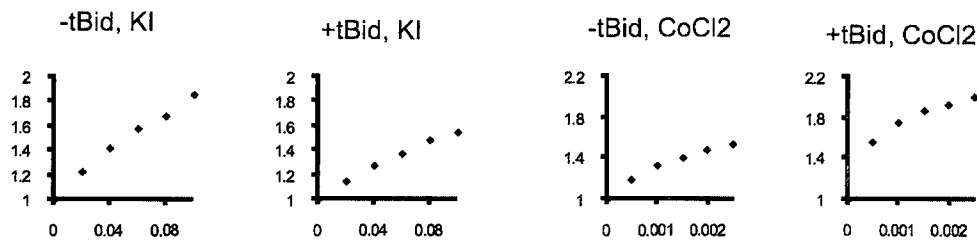


Figure 6.3: Quenching titrations for KI and CoCl₂.

Quenching is shown for 100 nM NBD labeled Bax mutants either incubated with 20 nM tBid (indicated by +tBid) or without. The x axis shows the molar concentration of KI or CoCl₂ added to the mix and the y axis shows F_0/F , where F_0 is the background corrected initial emission of the NBD labeled mutant and F is the background corrected emission in the presence of quencher.

6.4 *Tb-DPA liposomes can be lysed with 0.5% CHAPS*

When initially using Tb-DPA containing liposomes, it became apparent that Triton-X100, the detergent used to lyse ANTS/DPX containing liposomes, attenuated Tb-DPA fluorescence, even in the absence of EDTA in the external medium. Figure 6.4 shows that addition of CHAPS did not disrupt the Tb-DPA complex. CHAPS was subsequently used to lyse Tb-DPA containing liposomes.

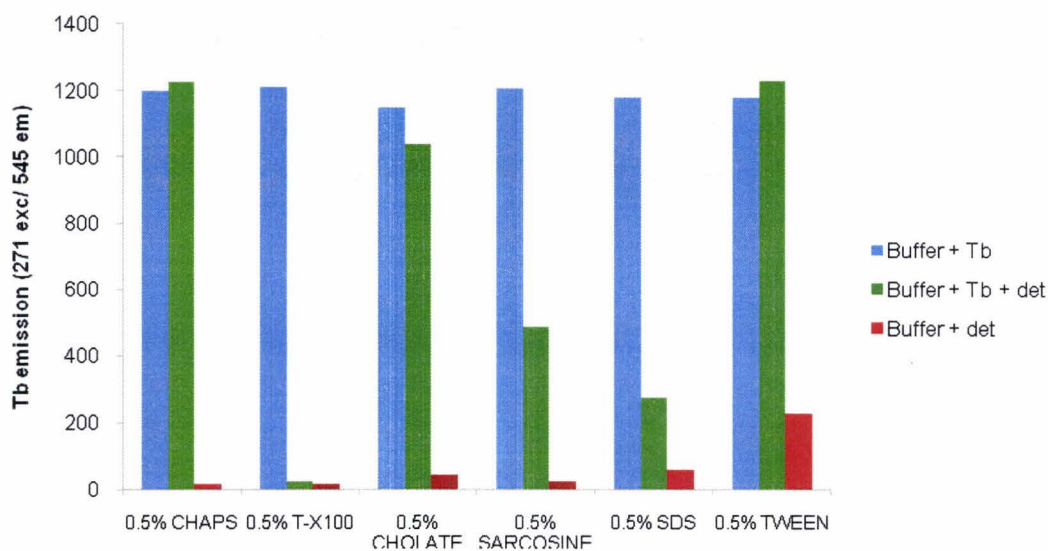


Figure 6.4: 0.5% CHAPS is suitable for lysing Tb-DPA containing liposomes

The fluorescence of 100 μ M Tb and 300 μ M DPA were measured in a buffer of 0.2 M KCl, 1 mM MgCl₂ and 10 mM HEPES pH 7, exciting at 280 nm and measuring emission at 490 nm. After initial emission measurement (blue), detergents were added and the fluorescence was measured again (green). The fluorescence of the Tb-DPA should not decrease if the detergent did not affect the complex. The fluorescence background of the detergent alone is shown in red.

6.5 Data fitting for lifetimes

Table 6.1 shows the three component fit for the NBD labeled Bax mutants. The average lifetime is shown as the intensity weighted mean. The + and – signs indicate whether or not that mutant had been incubated with 20 nM tBid for 2 hours at 37° C. The average lifetime shown is the intensity weighted mean lifetime.

Table 6.1: Three component fit parameters for lifetimes								
Residue	comp1 (ns)	comp1 %	comp2 (ns)	comp2 %	comp3 (ns)	comp3 %	Average (ns)	χ^2
3-	0.0722	15	0.949	40	5.45	45	2.84	1.57
3+	0.235	21	1.32	33	5.67	46	3.08	2.21
5-	0.192	27	0.968	43	5.07	30	1.96	2.82
5+	0.258	22	2.08	39	5.7	39	3.08	2.46
47-	0.33	18	2.05	44	5.78	38	3.13	1.67
47+	0.24	25	1.32	37	5.54	38	2.63	2.2
62-	0.99	42	16.5	30	5.3	28	1.96	3.28
62+	0.29	30	1.91	41	7.29	29	3	1.55
66-	0.28	26	1.81	34	7.44	40	3.7	2.12
66+	0.23	34	1.62	40	7.54	26	2.69	2.29
79-	0.229	26	1.35	47	6.61	27	2.45	2.07
79+	0.293	27	1.57	43	5.93	30	2.56	1.94
<hr/>								
114-	0.0124	1	1.65	6	9.4	93	8.81	0.731
114+	0.438	4	2.89	12	9.2	84	8.06	1.33
118-	0.314	15	2.25	31	7.67	54	4.86	2.33
118+	0.38	12	2.27	28	7.67	60	5.28	2.26
120-	0.29	13	2.4	24	10.4	63	7.21	1.84
120+	0.28	7	2.72	20	10.5	70	8.24	0.679
122-	0.267	9	2.51	46	6.7	45	4.18	0.834
122+	0.191	5	2.34	30	7.09	65	5.31	1.35
124-	0.28	14	2	32	7.3	55	4.66	1.29
124+	0.41	6	2.49	26	8.39	69	6.42	0.89
126-	0.24	19	1.46	36	5.99	45	3.29	1.81
126+	0.31	12	2.4	29	7.82	59	5.34	1.67
<hr/>								
130-	0.296	13	1.98	38	6.14	49	3.83	1.09
130+	0.35	13	1.99	33	7.54	55	4.82	2.64
134-	0.329	12	2.25	34	6.38	54	4.28	1.48
134+	0.268	8	2.44	40	6.72	52	4.49	0.36
136-	0.41	11	2.4	36	8.16	53	5.2	0.91

136+	0.241	7	2.49	41	6.87	52	4.63	0.865
137-	0.37	10	1.98	30	6.14	60	4.31	1.53
137+	0.31	12	2.15	41	6.37	47	3.93	0.655
138-	0.255	13	1.92	40	5.77	46	3.49	1.96
138+	0.445	12	2.7	42	7.02	46	4.44	0.875
139-	0.281	21	1.6	40	7.22	39	3.53	1.95
139+	0.139	7	1.73	36	6.36	57	4.27	1.4
140-	0.265	17	2.19	32	8.23	51	4.95	0.966
140+	0.265	27	2.04	38	7.38	35	3.41	1.59
141-	0.325	13	1.93	38	6.89	49	4.19	1.98
141+	0.51	11	2.5	39	6.86	50	4.46	0.622
142-	0.276	30	1.61	39	6.53	32	2.78	1.78
142+	0.257	26	1.78	34	6.68	40	3.35	1.61
143-	0.28	23	1.9	39	8.48	38	4.02	1.83
143+	0.344	21	2.16	46	7.22	33	3.46	0.7
175-	0.341	20	2.55	37	7.96	43	4.45	1.7
175+	0.394	15	2.47	36	8.13	49	4.97	1.72